

Center for Pathobiochemistry and Genetics
Medical University of Vienna

Institute of Medical Genetics
(Head: Univ. Prof. Mag. Dr. Markus Hengstschläger)

**Identification of signaling pathways activated by
cancer-associated fibroblasts leading to Akt
activation in colon cancer cells**

Master thesis submitted for the fulfilment of the requirements for the degree of
MASTER OF SCIENCE

University of Veterinary Medicine Vienna

Submitted by
Claudia Weindorfer, BSc

Vienna, January 2020

External Supervisor:

Assoc. Prof. PD Mag. Dr. Helmut Dolznig

Internal Supervisor:

Dr. rer. nat. Sabine Macho-Maschler

Reviewer:

Dr. rer. nat. Sabine Lagger

Acknowledgements

This thesis becomes reality with the kind support and help of many individuals. I would like to express my sincere thanks to all of them.

First, I would like to thank my supervisor Assoc. Prof. PD Mag. Dr. Helmut Dolznig for his guidance, encouragement and patience. Thank you for your motivation and immense knowledge. It was a pleasure to work in your lab.

I am very grateful to Dr. rer. nat. Sabine Macho-Maschler for her keen interest on my research. Her suggestions with kindness, enthusiasm and dynamism helped me to a great extent.

Thanks to all my lab colleagues, especially Daniela Unterleuthner, MSc and Simone Stang, BSc, for your daily advices and for the funny times we had.

Finally, I would like to say thank you to my family and friends. This is dedicated to you, even though you will probably never read it.

With Love, always.

Abstract

With 10.2 % of all cancer types, colorectal cancer (CRC) is the third most common cancer in both sexes and accounts for 900,000 deaths per year worldwide. These numbers show the urgency of effective treatment strategies for this cancer type. In the past, most research studies focused on cancer cells themselves and how they can be targeted to treat cancer. Over the last 20 years, this perspective has considerably changed and studies additionally focused on the tumor microenvironment – also called the tumor stroma. There is now compelling evidence that the tumor stroma is critically involved in cancer initiation and progression. The tumor microenvironment is composed of extracellular matrix and many different cell types with cancer-associated fibroblasts (CAFs) being the most abundant cells. These cells can promote cancer progression by interacting with cancer cells directly or by modulating other stromal cells and components. In previous studies, we found that especially CAF-derived insulin-like growth factor (IGF)-2 is an important factor in CRC carcinogenesis. We could show that stroma-derived IGF-2 signals via the IGF-1 receptor (IGF-1-R) and leads to increased p-Akt levels in CRC cells which is an accepted risk factor for CRC development and progression. However, these studies also demonstrated that IGF-2 is only partially responsible for Akt activation by CAFs indicating that other stromal factors than IGF-2 are present in the CAF secretome and mediate Akt activation. Thus, the aim of this study was to identify these other CAF-derived factors next to IGF-2 or additional pathways other than the IGF-1-R signaling which are responsible for full Akt activation. Inhibition of these CAF-induced signaling pathways might serve as future therapeutic route to target pro-tumorigenic CAF/colon cancer cell interactions. Therefore, a medium throughput screen with a 378 small molecules kinase inhibitor library was assessed to pinpoint potential inhibitors which downregulate CAF-dependent p-Akt upregulation in HCT116 colon cancer cells. As expected by the previous IGF-2 results, we found several promising IGF-1receptor/insulin receptor inhibitors but also c-Met and JAK inhibitors which substantially inhibited Akt phosphorylation. These inhibitors were further validated and hits with the best Akt inhibitory effect and target selectivity for each of the three kinases (OSI-906, JNJ-38877605 and Fedratinib) were examined in further experiments. Phenotypic assays were performed to test the impact of the inhibitors on CAF-activated colon cancer cell proliferation, migration and invasion. Indeed, the inhibitors significantly impaired these cellular functions *in vitro*. With these results, we might contribute to the identification of novel therapeutic targets to interfere with the pro-tumorigenic effects of the tumor stroma/cancer cell interaction.

Kurzfassung

Das kolorektale Karzinom (KRK) ist der dritthäufigste Krebstyp bei Frauen und Männern und ist weltweit für 900.000 Todesfälle pro Jahr verantwortlich. Die Häufigkeit dieser Erkrankung zeigt die Dringlichkeit effektive Therapiemöglichkeiten zu finden. Obwohl sich frühere Studien eher auf die Krebszellen selbst fokussierten, ist es in den letzten 20 Jahren zu einem Umdenken gekommen. Es wurde gezeigt, dass die Tumor Mikroumgebung – auch Tumor Stroma genannt – einen großen Teil zur Krebsentstehung und -fortschreitung beiträgt. Die Tumor Mikroumgebung besteht aus der extrazellulären Matrix und vielen verschiedenen Zelltypen, wobei Tumor-assoziierte Fibroblasten (TAFs) die am häufigsten vorkommenden Zellen sind. TAFs können den Krebsverlauf zugunsten der Krebszellen beeinflussen indem sie mit Krebszellen direkt interagieren oder andere Stromakomponenten regulieren. In vorhergehenden Studien konnten wir bereits zeigen, dass der von TAFs sezernierte Insulin-like growth factor (IGF)-2 wesentlich zur kolorektalen Karzinogenese beiträgt. Dabei bindet stromales IGF-2 an den IGF-1 Rezeptor und führt zu erhöhten p-Akt Mengen in KRK Zellen was ein allgemein anerkannter Risikofaktor für die Entstehung und das Fortschreiten eines KRK ist. Allerdings führte eine Blockierung des IGF-1 Rezeptors oder die direkte Inhibierung von IGF-2 zu keiner vollständigen p-Akt Inhibition, sondern lediglich zu einer verminderten Aktivierung. Daher war das Ziel dieser Arbeit weitere von TAFs sekretierte Faktoren oder von TAFs induzierte Signalwege zu finden, die zu einer vollständigen Akt Aktivierung führen und deren Inhibierung eine mögliche, zukünftige Krebstherapie darstellt.

Zu diesem Zweck wurde ein Durchsatz-Screening mit 378 verschiedenen Kinase Inhibitoren durchgeführt um Inhibitoren zu finden, die TAF induzierte p-Akt Aktivierung in HCT116 KRK Zellen herabregulieren. Wie durch die vorausgegangene Studie erwartet, wurden mehrere IGF-1 Rezeptoren/Insulin Inhibitoren aber auch c-Met und JAK Inhibitoren gefunden, die p-Akt wirksam inhibieren konnten. Diese Inhibitoren wurden in verschiedenen Experimenten validiert und der wirksamste jeder Kategorie mit der höchsten Selektivität (OSI-906, JNJ-38877605 und Fedratinib) wurde in weiteren Experimenten eingesetzt. In phenotypischen Experimenten wurde der Einfluss der Inhibitoren auf die Zellproliferation, -migration und -invasion von TAF-aktivierten Krebszellen getestet. Wir konnten mit diesen Experimenten zeigen, dass die Inhibitoren diese Zellfunktionen *in vitro* signifikant beeinträchtigen. Diese Resultate können zur Identifikation von neuen therapeutischen Angriffspunkten beitragen, die die Kommunikation zwischen TAFs und KRK Zellen beeinträchtigen und somit das Voranschreiten der Krebserkrankungen verhindern.

List of abbreviations

7-AAD	7-aminoactinomycin D
α -SMA	Alpha-smooth muscle actin
apCAFs	Antigen presenting cancer-associated fibroblasts
BM	Bone marrow
CAFs	Cancer-associated fibroblasts
CM	Conditioned medium
CRC	Colorectal cancer
DMEM	Dulbecco's modified eagle medium
DMSO	Dimethyl sulfoxide
(D)PBS	(Dulbecco's) phosphate-buffered saline
ECM	Extracellular matrix
EdU	5-Ethynyl-2'-deoxyuridine
EMT	Epithelial to mesenchymal transition
EpCAM	Epithelial cell adhesion molecule
FAP	Fibroblast-activation protein
FCS	Fetal calf serum
FGF-2	Fibroblast growth factor 2
FOXO	Forkhead box O
FSP-1	Fibroblast-specific protein-1
HGF	Hepatocyte growth factor
HSCs	Hematopoietic stem cells
IC ₅₀	Half maximal inhibitory concentration
iCAFs	Inflammatory cancer-associated fibroblasts
ICW	In-Cell Western
IGF	Insulin-like growth factor
IGF-1-R	Insulin-like growth factor 1 receptor
IL	Interleukin
Ins-R	Insulin receptor
JAK	Janus kinase
LOI	Loss of imprinting
MAPK	Mitogen-activated protein kinase
MFIs	Mean fluorescence intensities

MHC	Major histocompatibility complex
MMPs	Matrix-metalloproteinases
MSCs	Mesenchymal stem cells
mTORC	Mammalian target of rapamycin complex
myCAFs	Myfibroblastic cancer-associated fibroblasts
p-Akt	Phospho-Akt
PDGFRs	Platelet-derived growth factor receptors
PDK1	3-phosphoinositide-dependent protein kinase 1
PI3K	Phosphoinositide-3-kinase
PIP ₂	Phosphatidylinositol (3,4)-biphosphat
PIP ₃	Phosphatidylinositol (3,4,5)-triphosphat
rh	Recombinant human
RT	Room temperature
RTK	Receptor tyrosine kinase
scRNA-seq	Single-cell RNA-sequencing
siRNA	Small interfering RNA
STAT	Signal transducer and activator of transcription proteins
sTRAILs	Secretable tumor-necrosis factor-related apoptosis-inducing ligands
TE	Trypsin-EDTA
TGF- β	Transforming growth factor beta
TME	Tumor microenvironment
TNM	Tumor-node-metastasis
VEGF	Vascular endothelial growth factor

Table of content

1.	INTRODUCTION	1
1.1.	Colorectal cancer	2
1.2.	Tumor microenvironment	6
1.3.	Cancer-associated fibroblasts	7
1.3.5.	Characteristics of cancer-associated fibroblasts	7
1.3.6.	Origin and activation of cancer-associated fibroblasts	8
1.3.7.	Heterogeneity and markers of cancer-associated fibroblasts	10
1.3.8.	The crosstalk between tumor cells and cancer-associated fibroblasts	12
1.3.9.	Cancer-associated fibroblasts as targets of anti-cancer therapy	15
2.	HYPOTHESES AND AIMS OF THE STUDY	18
3.	METHODS	19
3.1.	Cell culture	19
3.1.1.	Changing medium	19
3.1.2.	Cell passaging	20
3.1.3.	Harvesting of conditioned medium	20
3.1.4.	Cell freezing	20
3.1.5.	Thawing cells	21
3.1.6.	Cell counting	21
3.1.7.	Starvation	22
3.2.	Kinase inhibitor screen	22
3.3.	In-Cell Western assay	23
3.3.1.	Cell fixation and permeabilization	23
3.3.2.	Blocking and staining	23
3.3.3.	Plate scanning and data acquisition	24
3.4.	Near-infrared Western blot	25
3.4.1.	Lysate preparation	25
3.4.2.	Protein concentration measurement	25
3.4.3.	Gel preparation	26
3.4.4.	Protein separation	26
3.4.5.	Transferring the protein from to gel to the membrane (blotting)	26
3.4.6.	Blocking and staining of Western blot membranes	27
3.4.7.	Membrane scanning and data acquisition	27

3.5. Spheroid formation	28
3.6. 7-AAD/EdU cell cycle analysis (proliferation assay)	28
3.6.1. EdU incorporation and trypsinization of cells	28
3.6.2. Cell fixation, permeabilization and Click-iT™ EdU reaction.....	29
3.6.3. Staining cells for their DNA content	29
3.6.4. Flow cytometry analysis and data acquisition.....	29
3.7. Transwell migration assay	30
3.7.1. Cell fixation and detachment of non-migrated cells	30
3.7.2. Staining cells for visualization with DAPI	31
3.7.3. Microscopic analysis and data acquisition	31
3.8. Spheroid outgrowth assay	31
3.8.1. Embedding spheroids in collagen gels	32
3.8.2. Microscopic analysis, data acquisition and statistical analysis	32
3.9. Statistical analysis and graphical representation	33
4. RESULTS	35
4.1. Comparing the impact of cancer-associated fibroblast-conditioned medium and DMEM 1 % FCS on p-Akt levels in HCT116 cells	35
4.2. Kinase inhibitor screening	36
4.3. Validation of the kinase inhibitor screening in HCT116, DLD-1 and LS174T cells	38
4.4. Determining the on-target specificity of OSI-906 and JNJ-38877605 in HCT116 cells	41
4.5. The impact of recombinant human IGF-2 and HGF on p-Akt levels in HCT116 cells	43
4.6. Determination of dose responses	45
4.7. Testing the impact of JAK inhibitors on p-Akt levels in HCT116 cells	47
4.8. Impact of OSI-906, JNJ-38877605 and Fedratinib on cell proliferation in HCT116 cells	49
4.9. Impact of OSI-906, JNJ-38877605 and Fedratinib on cell migration in HCT116 cells	51
4.10. Impact of OSI-906, JNJ-38877605 and Fedratinib on cell invasion in HCT116 cells	53

5.	DISCUSSION	55
5.1.	Activation of IGF-1-R, c-Met and JAK2 by cancer-associated fibroblast-derived factors are responsible for full Akt activation in HCT116 colon cancer cells	57
5.2.	Inhibition of the IGF-1-R/Ins-R, c-Met and JAK-2 in HCT116 colon cancer cells showed impaired proliferation, migration and invasion	60
6.	CONCLUSION.....	63
	BIBLIOGRAPHY	64
	LIST OF FIGURES	77
	APPENDIX	78
	Buffers and Solutions	88
	List of reagents.....	91

1. INTRODUCTION

Cancer is one of the major health issues of the 21st century. In 2018, about 18 million new cancer cases were reported with 9.5 million deaths worldwide. These numbers show the need to better understand the biology of cancer (Bray et al. 2018). Colorectal cancer (CRC) is one of the most frequent cancer types and since 1975, more than 200,000 publications dealing with CRC were published (Sperr 2016). In the past, most research studies focused more on cancer cells themselves and how they can be targeted to treat cancer. Over the last 20 years, this perspective considerably changed and research additionally concentrated on the tumor microenvironment (TME) – also called the tumor stroma. There is now compelling evidence that the tumor stroma is critically involved in cancer initiation, progression and therapy resistance. The TME plays an important role in tumor surveillance but also protects cancer cells by establishing a pro-tumorigenic environment. It supports the resistance of cancer cells to cancer cell targeting therapies by impairing an efficient drug delivery (Valkenburg et al. 2018, Yamauchi et al. 2018). The tumor stroma is composed of many different cell types including immune cells, blood vessel cells or fibroblasts and the extracellular matrix (ECM). Cancer-associated fibroblasts (CAFs) are the most abundant cells in the stroma and they can make up more than 70 % of the TME in certain tumors (Yu and Tannock 2012). CAFs can promote cancer progression by interacting with cancer cells directly or by modulating other stromal cells or components (Liu et al. 2019).

In previous studies, we found that especially CAF-derived insulin-like growth factor (IGF)-2 is an important factor in CRC progression. We could show that stroma-derived IGF-2 signals via the IGF-1 receptor (IGF-1-R) and results in increased phospho-Akt (p-Akt) levels leading to an enhanced phosphoinositide-3-kinase (PI3K)/Akt signaling in CRC cells. An aberrant activation of the PI3K/Akt pathway is a risk factor for CRC development and progression. However, by blocking the IGF-1-R/Insulin receptor (Ins-R) with a small molecule inhibitor or neutralizing IGF-2, we could show that IGF-2 is only partially responsible for CAF-induced Akt activation indicating that other stromal factors in the CAF secretome mediate Akt activation (Unger et al. 2017). Thus, the aim of this study was to identify other CAF-derived factors next to IGF-2 or other signaling pathways besides IGF-1-R/Ins-R signaling induced by CAFs which are responsible for full Akt activation.

1.1. Colorectal cancer

CRC is the most frequent malignant disease of the gastrointestinal tract worldwide (Kolligs 2016). With 10.2 % of all cancer types, CRC is the third most common cancer in both sexes after lung cancer, prostate cancer and female breast cancer. Globally, more than 1.8 million new CRC cases and almost 900,000 deaths were reported in 2018. In this context, men are more often affected than women regarding the incidence as well as the mortality of CRC cases (Bray et al. 2018).

In general, two types of CRC are described depending on the origin of the mutation: Sporadic CRC forms, which is the most common CRC type accounting for 70 % of all cases, and hereditary CRC (Keum and Giovannucci 2019). The mutations leading to CRC can be classified into three categories namely chromosomal instability, microsatellite instability and the CpG island methylator phenotype. These molecular mechanisms of mutation can lead to severe changes in important signaling cascades found for example in the PI3K/Akt, Janus kinase (JAK)/signal transducer and activator of transcription proteins (STAT), Wnt, transforming growth factor beta (TGF- β) or p53 pathways. Genes, which are often mutated in CRC, are e.g. *PIK3CA*, *JAK1* and *JAK2*, *STAT1-6*, *APC*, *RAS*, *cMYC*, *KRAS*, *BRAF*, *PTEN*, *SMAD2* and *SMAD4* (Slattery et al. 2013, Yamagishi et al. 2016, Mármol et al. 2017). Some of these mutated genes such as *KRAS* or *BRAF* are used as predictive biomarkers in CRC (Boussios et al. 2019).

As the PI3K/Akt and JAK/STAT signaling pathways are relevant for our findings they will be described in more detail. The PI3K/Akt signaling pathway is a highly conserved multistep process. Upon ligand binding, membrane bound receptors activate PI3K. Subsequently, activated PI3K triggers the conversion of phosphatidylinositol (3,4)-bisphosphate (PIP₂) to phosphatidylinositol (3,4,5)-trisphosphate (PIP₃). PIP₃ serves as a docking site for Akt, recruiting it to the cell membrane and enabling its phosphorylation by the 3-phosphoinositide-dependent protein kinase 1 (PDK1) at Thr308 which leads to a partial activation. This activation status is sufficient to activate the mammalian target of rapamycin complex (mTORC) 1 which regulates protein synthesis and cellular proliferation. Phosphorylation of Akt at Ser473 by the mTORC2 stimulates full enzymatic activity. Fully activated Akt can further phosphorylate several downstream targets and mediate cellular functions involved in cell growth, proliferation, differentiation and survival (Hemmings and Restuccia 2012) (Figure1).

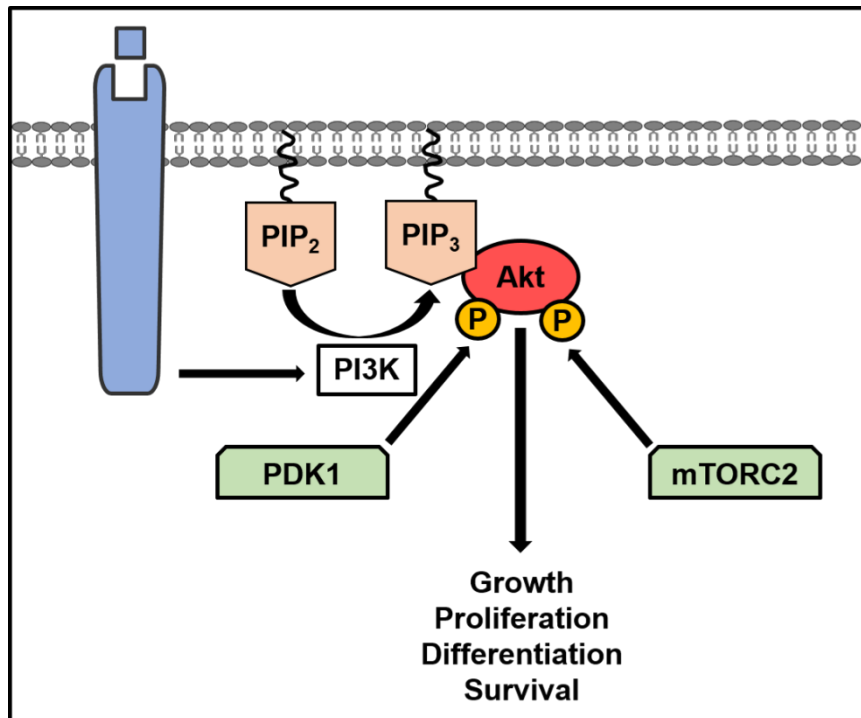


Fig. 1: Schematic illustration of the PI3K/Akt pathway. Upon ligand binding and receptor activation, PI3K associates with the receptor and induces the production of PIP₃ via the phosphorylation of PIP₂. PIP₃ serves as a docking site for Akt at the plasma membrane where PDK1 phosphorylates Akt at Thr308 leading to a partial activation. Phosphorylation of Akt at Ser473 by mTORC2 stimulates full enzymatic activity and results in increased cell growth, proliferation, differentiation and survival.

The JAK/STAT signaling pathway is one of the most important signaling pathways downstream of cytokine receptors and is involved in cell proliferation, differentiation, migration and apoptosis. The binding of ligands to their receptors leads to a dimerization of intracellular receptor units and receptor bound JAKs get in close proximity to another. JAKs phosphorylate each other and subsequently the receptors units. STATs can bind to the activated receptor units and are phosphorylated by JAKs. These phosphorylated STAT proteins form hetero- or homodimers and translocate to the nucleus where they induce the transcription of their target genes (Imada and Leonard 2000). Furthermore, JAKs and STATs can regulate other pathways by the induction of e.g. Ras or PI3K indicating the pivotal role of the JAK/STAT pathway in intracellular crosstalks (Lee and Rhee 2017, Bousoik and Montazeri Aliabadi 2018) (Figure 2).

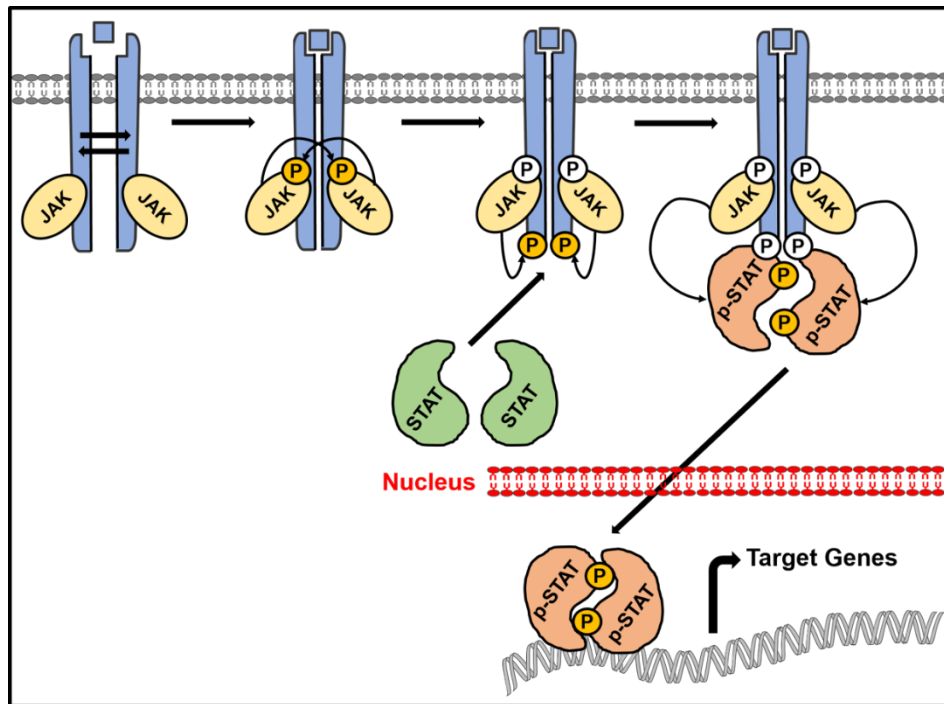


Fig. 2: Schematic illustration of the JAK/STAT pathway. Cytokine binding induces receptor dimerization and the activation of the associated JAKs which phosphorylate themselves and the receptor. STATs can bind to the phosphorylated receptor and get phosphorylated by JAKs. Phosphorylated STATs dimerize and translocate to the nucleus to regulate target gene transcription.

As already mentioned, sporadic cancers are more common than hereditary forms. In this context, it is reasonable that the possibility of developing CRC is associated with several environmental risk factors such as an unhealthy diet and lifestyle (Hughes et al. 2017). A prospective study from 2019 showed that the consumption of red and processed meat of more than 76 g per day is associated with an increased risk of developing CRC. In contrast to that, a fiber-rich diet can reduce the risk of being diagnosed with colon cancer (Bradbury et al. 2019). Another important factor, which is related to CRC and connected to the dietary behavior, is obesity. It was shown that an increase of each unit of the BMI enhances the risk of CRC development by 2–3 % (Kuipers et al. 2015). Conversely, it is assumed that physical activity can prevent 15 % of all colon cancer cases. Even after the diagnosis exercise can improve the disease outcome and decrease the recurrence of CRC (Oruç and Kaplan 2019). In addition to dietary factors and obesity, smoking is a commonly accepted cause of all types of cancer including CRC. Smokers have a two- to threefold increased risk to suffer from CRC in their lifetime in contrast to non-smokers (Marley and Nan 2016). Furthermore, alcohol consumption is linked to the development of CRC. Regular drinkers are associated with a 13 % increased risk to suffer from CRC compared to occasional or non-drinkers (Wang et al. 2015b). Taken

all risk factors together, it is obvious that they are omnipresent in the Western world. This is the reason why the highest incidence of CRC can be found in the USA, Australia, New Zealand and in several Western European countries (Arnold et al. 2017). Moreover, a lot of those countries offer CRC population-screening programs for men and women over 50 years. These screenings include a fecal occult blood test and a colonoscopy and allow the detection of even early CRC stages (Binefa et al. 2014). Consequently, the detection rate of CRC in these countries is much higher and thus displays increased incidence levels compared to countries which do not provide CRC screening tests. At the same time these tests enable a more effective treatment of early cancer stages and thereby reduce CRC mortality (Buskermolen et al. 2019).

There are two different cancer staging models in CRC: The older Dukes staging system and the tumor-node-metastasis (TNM)-system. The TNM-system is more robust and more frequently used. The goal of both is the same as they are used to make a disease prognosis and to plan the treatment approach (Ahmed Farag et al. 2016). Based on the TNM categories CRC is divided into four different stages. Stage one tumors are associated with a five-year survival rate of 94 %. The five-year survival rate of stage two tumors drops to 82 % and further decreases to 67 % in stage three tumor patients. Metastatic or stage 4 tumors have the worst prognosis with a survival rate of only 11 % in five years (Sagaert et al. 2018). In addition to the classic staging systems, molecular staging becomes increasingly important as patients with certain mutations such as *KRAS* exon 2 or *BRAF*^{V600E} mutations did not benefit from standard of care treatments (Punt et al. 2017). Nevertheless, most primary colon cancers are treated by surgery. In early stages of CRC an excision of the affected colon parts including ligated arteries and veins is sufficient for an excellent oncological outcome. In some cases, a segmental colectomy can be necessary (DE ROSA et al. 2015). Adjuvant therapy, meaning chemotherapy or radiotherapy, is mostly given to younger patients as they in general can deal better with therapy associated toxicity (Kim 2015).

Taken together, CRC cancer is a very common disease nowadays and responsible for many deaths each year. It is a heterogeneous cancer type which is characterized by a plethora of different cancer cells mutations. Nevertheless, focus is put on the TME nowadays with respect to cancer progression and therapy.

1.2. Tumor microenvironment

Already in 1863, Rudolph Virchow studied the interaction of tumors with their surrounding environment by observing the infiltration of leukocytes into solid tumors (Schmidt and Weber 2006). Steven Paget published the “seed and soil” theory of metastasis in 1889 and he proposed that tumors do not metastasize into certain organs randomly but rather prefer organs which provide a proper environment for the tumor cells (Akhtar et al. 2019). Modern TME research started in the 1970s when angiogenesis and the immune system of tumors were studied as independent fields (Devroede et al. 1971, Auerbach et al. 1975, Langer et al. 1980).

Nowadays it is well known that a tumor does not only consist of tumor cells. The tumor niche also includes other cells and non-cellular components which form the TME, also called tumor stroma. Notably, the TME is a double-edged sword. On the one hand, when it is in a healthy state, it has anti-tumor properties and protects against tumorigenesis and -progression. On the other hand, it can also support tumor growth and metastasis (Wang et al. 2017).

The tumor stroma consists of many different cell types but also contains components of the ECM. The ECM, defined as non-cellular tissue part, is a highly dynamic construct and is composed of water, minerals, proteoglycans and fibrous proteins such as collagens. It has an important role in cell-cell communication, cell adhesion or cell proliferation as some ECM molecules can bind growth factors and control their release and presentation to cancer cells (Walker et al. 2018). These characteristics clearly show that a dysfunction or a change in the composition of the ECM can support cancer progression. Of note, the ECM is produced and continuously restructured by stromal cells in close interaction with epithelial cells (Lu et al. 2011). It was shown that also cancer cells are a source of ECM molecules. They mostly produce ECM-modifying enzymes such as the collagen and elastin cross-linking enzyme lysyl oxidase which induces ECM stiffening and thereby integrin ligation. Cells are linked to the ECM via integrins which can translate extracellular mechanical signals into intracellular biochemical processes. This so called mechanotransduction can activate several signaling pathways in cancer cells such as the PI3K/Akt or mitogen-activated protein kinase (MAPK) pathways which aberrant activations promote cancer cell growth, proliferation, and migration. Hence, cancer cells modulate the ECM directly or exploit other stromal cells to produce ECM molecules to promote tumor progression by establishing a pro-tumorigenic environment (Poltavets et al. 2018).

Cells, which frequently can be found in the tumor stroma, are fibroblasts, endothelial cells, pericytes, adipocytes or all kind of immune cells. They all interact with tumor cells in pro- or

anti-tumorigenic ways. For example, endothelial cells provide nutrients for tumor cells or enable metastatic spreading of tumor cells to distant organs. Immune cells can support pro-tumorigenic phenotypes by playing a role e.g. in epithelial to mesenchymal transition (EMT) or support tumorigenesis by expressing inflammatory cytokines. In contrast to that, cells of the immune system also can combat tumor cells by different immunological mechanisms (Valkenburg et al. 2018, Wang et al. 2019). Among all these stromal cell types, the most abundant ones are CAFs. Although, CAFs are well-studied tumor promoting cells, many functions of CAFs in tumor development remain unclear (Liao et al. 2019). As important cells regarding their pro-tumorigenic properties, CAFs are more detailed discussed in the next chapters.

1.3. Cancer-associated fibroblasts

CAFs were already investigated in in the 1980s. Delinassios *et al.* observed differences between normal fibroblasts and fibroblasts derived from the tumor stroma (Delinassios et al. 1983). Additionally, they demonstrated in *in vitro* experiments that tumor stroma-derived fibroblasts had cytotoxic effects on co-cultured tumor cells (Delinassios 1987). On the contrary, other studies showed that fibroblasts derived from the tumor stroma showed pro-tumorigenic effects on cancer cells (Yan et al. 1993, Ellis et al. 1994). Nowadays, studies on CAFs indicate that these cells predominantly have tumor promoting properties (Maman and Witz 2018).

1.3.5. Characteristics of cancer-associated fibroblasts

CAFs mostly evolve from resident fibroblasts present in the normal stroma of the tissue from which the tumor arises. These tissue resident fibroblasts are quiet or resting cells (LeBleu and Kalluri 2018). In physiological conditions, fibroblasts are spindle-shaped cells and the main source of ECM components. Additionally, they secrete ECM-degrading enzymes thereby dynamically influencing the structure and composition of the ECM (Santi et al. 2018). Fibroblasts also control the recruitment of immune cells via e.g. Toll-like receptors or secreted inflammatory factors. Furthermore, tissue resident fibroblasts participate in the construction of the basement membrane (Alkasalias et al. 2018). During inflammation and wound healing, fibroblasts get activated and often acquire myofibroblast properties in order to support wound closure and release a plethora of cytokines and growth factors to induce immune responses. After resolution of the inflammation and completion of the wound healing process, these

activated fibroblasts undergo apoptosis and are cleared from the site of injury (Bainbridge 2013, Augsten 2014).

CAFs have similar characteristics as normal fibroblasts but they are constantly activated. They continuously proliferate and undergo metabolic adaptations to support tumor cells by e.g. inducing EMT in cancer cells to acquire invasive phenotypes or producing tumor promoting factors (LeBleu and Kalluri 2018). They are larger than normal fibroblasts with indented nuclei and a more branched cytoplasm due to their increased metabolic activity (De Wever et al. 2008). CAFs are permanently active which leads for example to an increased production of ECM molecules and thereby to massive remodeling processes of the tumor stroma and to an aberrant continuous release of cytokines and growth factors. Thereby, cancer cells can promote the activation of CAFs to produce high levels of pro-tumorigenic factors (Liu et al. 2019).

1.3.6. Origin and activation of cancer-associated fibroblasts

The origins of CAFs are intensively discussed in research. Several studies reported that CAFs arise from resident fibroblasts. Mitra *et al.* showed that cancer cells can directly change the miRNA expression profile in fibroblasts. The authors were able to transform tissue resident normal fibroblasts into CAFs by transfecting miRNAs or their inhibitors. They could observe that the transfection of anti-miR-31, anti-miR-214 and pre-miR-155 leads to a reprogramming of the cells and to a conversion into CAFs (Mitra et al. 2012). Furthermore, reactive oxygen species induce fibroblast reprogramming. The “Warburg effect”, which particularly can be found in early carcinogenesis, leads to increased reactive oxygen levels and triggers the transition from normal fibroblasts to CAFs (Avagliano et al. 2018). In contrast to the classical “Warburg effect”, where cancer cells tend to favor aerobic glycolysis rather than oxidative phosphorylation, the “reverse Warburg effect” describes that this metabolic adaptation occurs in CAFs. Thereby, cancer cells induce the “Warburg effect” in stromal fibroblasts which differentiate into CAFs and secrete lactate and pyruvate. These molecules are then taken up by cancer cells for energy production. Hence, cancer cells transform the normal stroma into a pro-tumorigenic and energy-rich microenvironment (Pavlidis et al. 2009). Another way to trigger fibroblast activation are growth factors and cytokines. Especially factors such as TGF- β , hepatocyte growth factor (HGF), platelet-derived growth factor (PDGF) and fibroblast growth factor 2 (FGF-2), mostly derived from cancer cells, induce the activated fibroblast phenotype (Kuzet and Gaggioli 2016).

CAFs can also arise from bone marrow (BM)-derived stem cells such as BM-derived mesenchymal stem cells (MSCs) or BM-derived hematopoietic stem cells (HSCs). Both stem cell types can transform into CAFs via several mechanisms. Already in 2008, an *in vitro* study, where BM-derived MSCs were exposed to tumor-conditioned medium (CM), could show the transition from BM-derived MSCs to a CAF-like phenotype (Mishra et al. 2008). A few years later, Quante *et al.* demonstrated that at least 20 % of CAFs originate from BM-derived MSC by performing BM reconstitution studies in mice with gastric dysplasia. They transplanted BM from alpha-smooth muscle actin (α -SMA)-red fluorescence protein transgenic mice in irradiated mouse models for gastric cancer. As α -SMA is a prominent marker for CAFs, they isolated CAFs from the gastric tumors and determined the contribution of BM-derived cells to the CAF population (Quante et al. 2011). In addition, about 8 % of all CAFs express markers from BM-derived HSC. Hence, CAFs seem to arise at least partly from BM-derived HSC (McDonald et al. 2015).

The EMT is a highly discussed topic regarding the origin of CAFs. EMT is associated with the transition from an epithelial to a mesenchymal phenotype. Physiologically, EMT can be found during embryogenesis or wound healing (Dongre and Weinberg 2019). In the past, a lot of studies proposed that CAFs originate via EMT from epithelial cancer cells (William Petersen et al. 2001, Iwano et al. 2002). However, some studies show that EMT is not a mechanism leading to the emergence of CAFs (Dvořánková et al. 2015, Wang et al. 2015a). The assumption that CAFs do not arise from epithelial cancer cells is supported by the finding that CAFs in general do not show the same oncogenic drivers as present in tumor cells (Campbell et al. 2009). These controversial findings show that further research is needed in order to demonstrate the involvement of EMT in CAF development.

Finally, another hypothesis suggested that CAFs arise from adipocytes which dedifferentiate into fibroblast-like cells during carcinogenesis. It was shown that breast cancer cells are capable to induce the transition of mature adipocytes into cells with a fibroblast phenotype called adipocyte-derived fibroblasts (Bochet et al. 2013). Additionally, a pancreatic cancer study demonstrated that adipose tissue-derived stromal cells are recruited to the tumor side. These cells shared several features with CAFs such as a high α -SMA expression and tumor promoting properties like an increased production of ECM molecules suggesting that adipose tissue cells could be precursors of CAFs (Okumura et al. 2019).

In summary, different sources of CAFs are described in the literature and this topic is still under debate. Undoubtedly, resident tissue fibroblasts are the main source of CAFs. Nevertheless,

the heterogeneity of CAFs suggests that also other cell types such as adipocytes or BM-derived stem cells are potential candidates as precursors of CAF subtypes (Figure 3).

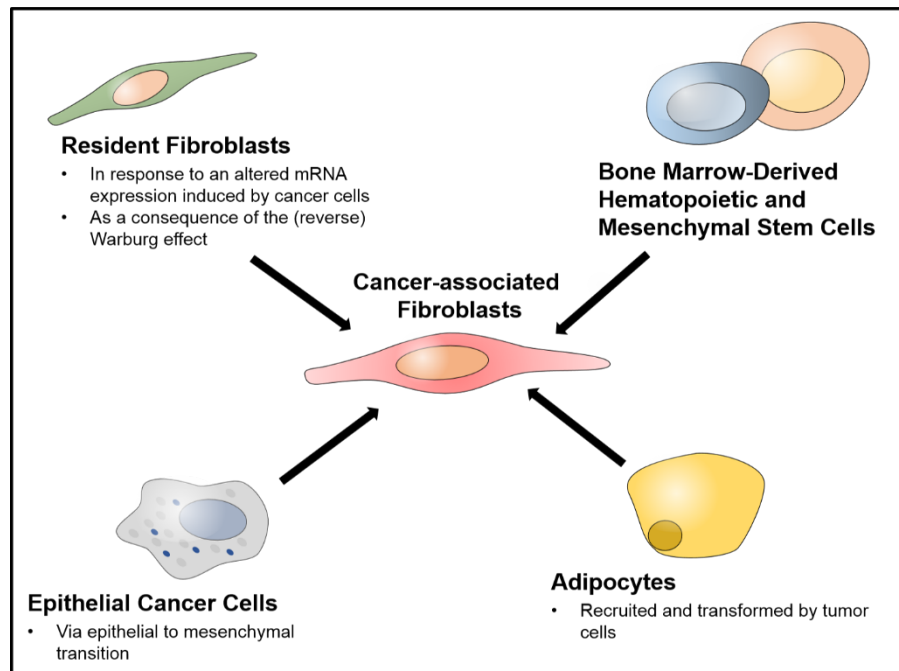


Fig. 3: *Potential origins of cancer-associated fibroblasts.* CAFs arise from many different cell types as resident fibroblasts, bone marrow-derived stem cells, adipocytes or endothelial cells.

1.3.7. Heterogeneity and markers of cancer-associated fibroblasts

As mentioned above, CAFs can arise from different cell types and are a highly heterogeneous cell population. They express many different markers which are also found on other cell types. These non-specific markers make their identification complicated and challenging.

The two most common markers, which are expressed by many activated normal fibroblasts as well as by CAFs, are α -SMA and fibroblast-specific protein-1 (FSP-1) (Costa et al. 2018). α -SMA plays an important role in cell motility, structure and integrity. These features are needed especially during wound healing (Micallef et al. 2012). However, an overexpression of α -SMA is associated with a poor prognosis in CRC patients (Tsuji et al. 2007). FSP-1 is a protein which is involved in tissue degrading, cell motility and angiogenesis (Björk et al. 2013). In addition to α -SMA, it is often used to confirm the CAF phenotype (Sandberg et al. 2019, Son et al. 2019). Nevertheless, recent studies claim that this marker is not reliable and not exclusively expressed by CAFs. In liver cancer, it was shown that fibroblasts did not express FSP-1 at all. Instead, cells co-expressing F4/80, a marker of the myeloid-monocytic cell

lineage, and FSP-1 were found. These findings show that FSP-1 should not be used as the single marker for CAFs at least in liver cancer (Österreicher et al. 2011). Moreover, a CRC study showed that α -SMA and FSP-1 describe two completely different subsets of CAFs and thereby cannot be used as reliable general markers for CAFs (Li et al. 2017).

Kahounová *et al.* claimed that the fibroblast-activation protein (FAP) is the most specific marker comparing different surface epitopes of fibroblasts (Kahounová et al. 2018). FAP is extensively expressed in the tumor stroma. It is highly upregulated in almost all carcinomas and correlates with a higher tumor grade and a worse overall survival. Nevertheless, many different cell types of the TME seem to express FAP making it unsuitable as a specific marker of CAFs (Puré and Blomberg 2018).

The platelet-derived growth factor receptors (PDGFRs) are also used markers for CAFs although they are also found on other cells such as astrocytes or pericytes (Funa and Sasahara 2014). Even though PDGFRs are not specific to CAFs, they can be found on the entire fibroblast population. Therefore, this marker is predominantly used in combinations with other CAF markers to identify CAF populations (Nurmik et al. 2019).

Other cell markers which are connected to CAFs are vimentin, transgelin or podoplanin. However, these molecules are very broadly expressed in many cell populations. Additionally, negative markers of CAFs such as the epithelial cell adhesion molecule (EpCAM), smoothelin, CD45 or CD34 are used to exclude non-fibroblastic cell populations (Nurmik et al. 2019).

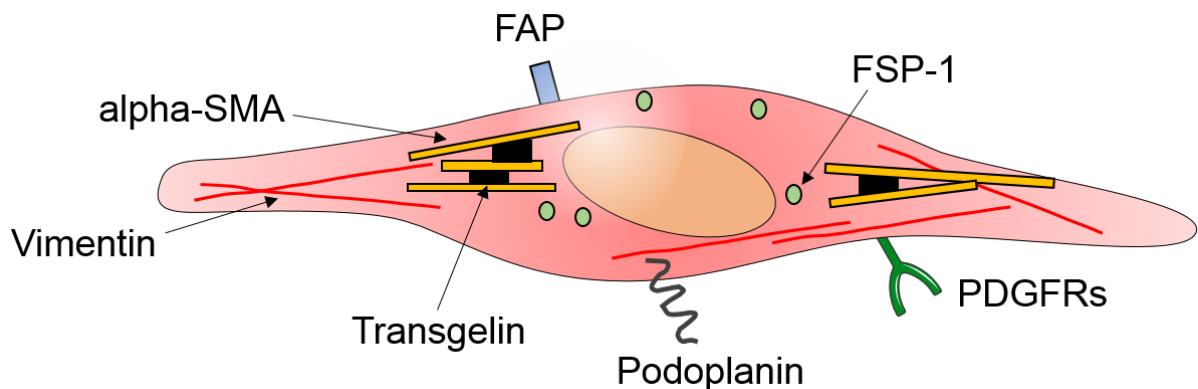


Fig. 4: *Markers of cancer-associated fibroblasts.* CAFs are a very heterogeneous cell population characterized by many different markers with α -SMA and FSP-1 being the most prominent ones.

Another technological innovation, which allows to define CAF subpopulations by investigating the transcriptome of individual cells, is single-cell RNA-sequencing (scRNA-seq). This technology again confirms the high heterogeneity of CAFs (Bartoschek et al. 2018a). In recent studies, scRNA-seq experiments were performed to characterize the TME of pancreatic tumors. Thereby, CAF subclasses such as myofibroblastic CAFs (myCAF), characterized by a high α -SMA expression, and inflammatory CAFs (iCAF), which secrete increased levels of cytokines and lose myofibroblastic features, were identified. It was shown that iCAFs are a significant source of interleukin (IL)-6 and IL-11. These cytokines lead to an activation of the JAK/STAT pathway and mainly activate STAT3 in cancer cells. myCAF lack the expression of inflammatory cytokines but a third subclass of CAFs could be found within this population namely antigen presenting CAFs (apCAF). apCAF express major histocompatibility complex (MHC) class II molecules but they lack the costimulatory molecules needed for T-cell activation. Hence, it is assumed that the MHC class II receptor is used to decoy T-cells in order to deactivate them (Öhlund et al. 2017, Elyada et al. 2019). Similar studies proved the high heterogeneity of CAFs in CRC, breast cancer and lung cancer (Li et al. 2017, Bartoschek et al. 2018b, Lambrechts et al. 2018).

Taken together, CAFs are a highly heterogeneous cell population expressing many different cell markers. These characteristics make it hard to identify and specify them also in regard to various CAF subtypes. The best and most used strategy to discriminate between CAFs and other cells of the tumor stroma is to combine experimentally verified markers. Nevertheless, finding the best combination of markers to identify CAFs is still under investigation. In addition, next generation sequencing could further add still unknown subtypes of CAFs to the TME.

1.3.8. The crosstalk between tumor cells and cancer-associated fibroblasts

CAFs and tumor cells interact with each other in many different ways. This so-called tumor stroma crosstalk is mediated through signals derived from one cell type impacting on the recipient cell. The consequences of these interactions between two or more cell types present in the TME can be pro- or anti-tumorigenic. However, this communication axis is a promising therapeutic target regarding future therapeutic approaches (Bu et al. 2019).

The most studied cytokine released from CAFs is TGF- β . When TGF- β binds to its receptor on cancer cells, SMAD or non-SMAD pathways are activated. In pre-malignant stages, TGF- β derived from stromal cells has tumor-suppressive properties as it induces cell-cycle arrest or apoptosis in epithelial cells or early carcinoma cells. In CRC, it was shown that different

mutations in the TGF- β pathway are often present in cancer cells causing for example the inactivation of the TGF- β receptor or the downstream SMAD signaling proteins. These alterations make CRC unresponsive to the anti-tumor effects of TGF- β (Fearon 2011). Additionally, in cancer cells, activation of the TGF- β pathway promotes EMT, invasion and metastasis (Colak and ten Dijke 2017). In CAFs, it was shown that CM from CRC cells induced the activation of the TGF- β signaling pathway in fibroblasts leading to enhanced expression of α -SMA. Thereby, cancer cells can control the activation of fibroblasts (Hawinkels et al. 2014). Another important CAF-derived factor is the hepatocyte growth factor (HGF). Ding *et al.* showed that CAF-released HGF promoted proliferation, migration and invasion in gastric cancer cells which did not have an amplification of the *MET* gene. Upon binding of HGF to the receptor tyrosine kinase (RTK) c-Met, many different pathways such as the PI3K/Akt or the JAK/STAT pathway are activated explaining the multifaceted biological effect of this paracrine factor. By upregulating the expression of the IL-6 receptor, HGF indirectly activates the JAK/STAT pathway which increases the expression of c-Met in a positive feedback loop (Ding et al. 2018a). Tumor cells in turn secrete factors to upregulate the production of HGF in CAFs which demonstrates the dynamic tumor-CAF interaction (Konstorum and Lowengrub 2018).

Moreover, CAFs support cancer progression by activating the PI3K/Akt signaling pathway in cancer cells. As mentioned above, this pathway is important in cancer pathogenesis as it is associated with reduced apoptosis, enhanced cell growth and increased proliferation of cancer cells. Akt is a central component of this signaling cascade as it can activate many other downstream targets (Danielsen et al. 2015). By phosphorylating and thereby inhibiting pro-apoptotic proteins such as Bad, Akt directly regulates cell survival. Akt can inhibit cell cycle arrest and promote cellular proliferation by the phosphorylation of the tumor suppressor p21. The most important role of Akt in cell proliferation is related to mTORC1 which activates the translation of proteins and thereby contributes to cell growth. Furthermore, Akt can interfere in cancer development and progression by preventing the translocation of forkhead box O (FOXO) transcription factors into the nucleus where they induce the transcription of several target genes involved in the suppression of growth, proliferation and survival (Hoxhaj and Manning 2019, Revathidevi and Munirajan 2019).

Different ligands can activate RTKs which activate PI3K/Akt signaling (Danielsen et al. 2015). An important molecule, which is responsible for Akt activation in carcinoma cells, is IGF-2. IGF-2 is mainly expressed in early embryonic and fetal development. After binding to the IGF-1-R, it can activate the PI3K/Akt and the MAPK pathway (Bergman et al. 2013).

Overexpression of IGF-2 could be observed in many subsets of CRC and seems to have a high oncogenic potential (Zhong et al. 2017). IGFs are key regulators of all colon cancer stages as they are associated with the initiation, progression and metastasis of CRC (Brouwer-Visser and Huang 2015). Tumor cells are an accepted source of IGF-2. Secreted by cancer cells, IGF-2 promotes carcinogenesis in an autocrine or paracrine fashion (Bergman et al. 2013). A study from Xu *et al.* demonstrated that IGF-2 activated fibroblasts are induced to produce molecules as the vascular endothelial growth factor (VEGF) which promoted tumor malignancy by inducing endothelial cell sprouting and enhancing the invasion of tumor cells (Xu et al. 2017). Several mechanisms are responsible for increased IGF-2 activities in cancer cells with epigenetic changes being the most prominent ones. In CRC, mostly loss of imprinting (LOI), which describes a biallelic gene expression, is responsible for the overexpression of IGF-2. Tian *et al.* compared the imprinting status of *IGF2* between CRC samples and normal colons and demonstrated that 63 % of all CRC samples showed an LOI of *IGF2* whereas only 22 % of normal colon samples were found with an LOI. Thereby, the LOI of *IGF2* is linked to a hypomethylation of H19 (Tian et al. 2012). Besides the deregulation of imprinted gene expression, loss of transcriptional repressors, activation of transcription factors or altered binding proteins can lead to an increased IGF-2 signaling (Kasprzak and Adamek 2019). In addition to cancer cells, CAFs express IGF-2 as an increased mRNA expression could be found in the tumor stroma. Unger *et al.* demonstrated that CAF-derived IGF-2 contributed to Akt activation in CRC cells. Furthermore, IGF-2 from CAFs lead to a reorganization of the ECM indicating an autocrine effect as CAFs are the main source of ECM(-degrading) molecules. Additionally, ECM remodeling supported the invasion of tumor cells in organotypic co-culture assays from CAFs and CRC cells. *In vivo* experiments of subcutaneous colon cancer xenografts co-injected with CAFs lacking IGF-2 expression by small interfering RNA (siRNA) knockdown revealed similar results as they showed decreased tumor growth and invasion. Furthermore, relapse and survival analysis of human CRC datasets demonstrated that high *IGF2* gene expression levels correlated with a reduced overall and relapse-free survival (Unger et al. 2017).

Many more factors derived from CAFs or acting on CAFs are described in the literature but it is far beyond the scope of this thesis to describe all of them in detail. In summary, it is a widespread theme in carcinomas that CAFs and cancer cells communicate via paracrine factors in a feedback loops promoting cancer initiation and progression.

1.3.9. Cancer-associated fibroblasts as targets of anti-cancer therapy

The TME does not only contribute to tumor initiation and progression it is also associated with therapy resistance. In general, there are two different types of TME-mediated therapy resistance. Inherent also named intrinsic resistance exists prior to therapy and is the result of cancer cell-TME interactions. This pre-existing TME resistance includes impaired drug delivery through an abnormal tumor vasculature or protective niches such as the perivascular niche which represents a supportive microenvironment within the TME for cancer cells (Ritchie and Nör 2013, Klemm and Joyce 2015). This is in contrast to acquired resistance which evolves by selection pressure mechanisms through drug- or radiotherapy (Holohan et al. 2013). As fibroblasts are the most abundant cells in the TME, many researchers focused on this cell type of the tumor stroma to avoid cancer therapy resistance (Kadel et al. 2019). However, many open questions remain to be addressed in the future concerning the mechanism of acquired, stroma-induced therapy resistance.

Beside the coherence of CAFs and therapy resistance, CAFs also directly contribute to cancer progression. Hence, they are potential targets for an anti-cancer therapy and different targeting strategies can be found in literature. One therapeutic approach depletes CAFs directly via cell surface markers. However, transgenic mice with the ability to delete α -SMA positive fibroblasts in pancreatic cancer showed a decreased survival which could also be seen in patients with less myofibroblasts in their TME. Therefore, targeting CAFs via unspecific markers such as α -SMA underscores the need for caution as this can stimulate cancer progression. Alternatively, different tumor entities might react differently to CAF depletion (Özdemir et al. 2014). Although FAP is a more specific marker for CAFs and might be a better target, several studies reported severe side effects after depleting FAP expressing cells (Roberts et al. 2013, Lo et al. 2015). In contrast to that, a recent study introduced a novel therapy with promising tumor inhibitory effects and less side effects. Watanabe *et al.* targeted FAP positive CAFs by using the near-infrared photoimmunotherapy. This novel therapy uses monoclonal antibodies which are conjugated to a photosensitizer. This photosensitizer only shows cytotoxic effects on cells when the antibody is bound to the cell membrane and is irradiated with near-infrared light. Mice treated with this cell-selective therapy showed decreased tumor growth without any adverse effects. Nevertheless, this therapy is still in its very early stages and needs to be further evaluated (Watanabe et al. 2019). Altogether, additional exclusive fibroblast-specific markers are required to obtain a more precise CAF targeting strategy with less side effects.

Another possibility to use CAFs as a target in therapy is to normalize the activated status of CAFs. As already described, CAFs are constitutively activated fibroblasts. By forcing them back into a quiescence state, CAFs could acquire tumor-suppressive properties. *In vitro* studies already demonstrated that this phenotypic conversion is possible by using gold nanoparticles which enhance lipid synthesis and utilization in fibroblasts. This altered metabolism of lipids seems to be important to maintain the quiescent fibroblast phenotype (Hossen et al. 2019). In addition, it was shown that pancreatic stellate cells, which are the equivalent to CAFs in the pancreatic TME, returned to a quiescent phenotype after treatment with a vitamin D receptor ligand. It was shown that vitamin D receptor ligands reduced tissue fibrosis and inflammation in a murine mouse pancreatitis model. Additionally, a decreased expression of α -SMA in CAFs could be observed which is associated with an inactive CAF phenotype. Thereby, the vitamin D receptor might act as a master transcriptional regulator of targets including the cytokine or ECM component production. (Sherman et al. 2014).

In addition, targeting cytokines or regulatory factors that are crucial to CAFs or cancer cells might be possible therapeutic targets. As mentioned above, the JAK/STAT pathway is hyperactivated in many cancer types and is associated with a poor prognosis. In addition to other molecules, IL-6 is secreted by cells of the TME including CAFs. It binds to the IL-6 receptor and activates the JAK/STAT signaling cascade. Antibodies targeting either IL-6 or the IL-6 receptor are already in phase I-II clinical studies and show promising results (Johnson et al. 2018). Huang *et al.* went one step further and demonstrated that inhibition of the murine TGF- β receptor reduces IL-6 production from CAFs which resulted in a decreased STAT3 activation in cancer cells (Huang et al. 2018). Another approach to target CAF-derived factors driving cancer progression is to block the PDGF receptor signaling in CAFs. It was shown that blocking this signaling pathway lead to a reduced FGF-2 and FGF-7 production and thereby to an impaired tumor angiogenesis and tumor cell proliferation (Jain et al. 2008).

Fibroblasts are the main source of ECM proteins and are responsible for TME stiffness and desmoplastic reactions. Targeting ECM molecules by enzymatic ablation or inhibitory antibodies and impairing their production might be another tumor-suppressive approach. Possible candidates to target are for example fibronectin, tenascin C or matrix metalloproteinases (Chen and Song 2019). Important pathways involved in ECM production are TGF- β 1 and the canonical hedgehog signaling. Targeting CAFs with inhibitors of these pathways may offer a novel therapeutic strategy (Garamszegi et al. 2010, Valenti et al. 2017). Mpekris *et al.* demonstrated that inhibiting the sonic-hedgehog pathway reduced the

proliferative capacities of CAFs and displayed effects on TME remodeling which promotes drug delivery and thereby improves the efficacy of chemotherapy (Mpekris et al. 2017). TGF- β inhibition as an anti-cancer therapy is problematic due to its dual role in cancer progression. As already mentioned, TGF- β suppresses tumor development in early cancer stages and *in vivo* models demonstrated that a downregulation of the TGF- β signaling resulted in decreased survival. Hence, TGF- β therapies need to obtain the tumor suppressive features of TGF- β signaling and repress its tumor promoting properties at the same time (Sangaletti et al. 2017). Finally, CAFs could also function as vehicle to deliver anti-tumor therapeutics. Miao *et al.* generated nanoparticles which were taken up by fibroblasts *in situ*. These nanoparticles are lipid-coated protamine DNA complexes which were used to encapsulate secretable tumor-necrosis factor-related apoptosis-inducing ligands (sTRAILs) plasmids. Fibroblasts, which had taken up the nanoparticles, became tumor-suppressive cells by producing secreted TRAILs. This cytotoxic cytokine induces apoptosis selectively in tumor cells. Additionally, the engineered fibroblasts were reverted into a quiescent state (Miao et al. 2017).

Taken together, CAFs are a promising target for anti-cancer therapy with many different applications. CAF-targeted therapy is a rapidly developing topic in research. Nevertheless, studying the CAF biology in more detail is needed to identify CAF subpopulations and their roles in the TME. In addition, inefficient therapies with severe side effects underscore the need for precision in targeting CAFs (Prakash 2016).

2. HYPOTHESES AND AIMS OF THE STUDY

CAFs are the most abundant cells in the tumor stroma and have an important role in tumor initiation, progression and metastasis but also in therapy resistance (Pezzella et al. 2019). Several studies demonstrated the involvement of various signaling cascades in the crosstalk of CAFs and tumor cells in different cancer types (Alguacil-Núñez et al. 2018, Monteiro Araujo et al. 2018, Awaji et al. 2019). However, many pro-tumorigenic interactions of CAFs with colon cancer cells are not fully understood.

In a previous study, we showed the involvement of CAF-derived IGF-2 in colon cancer progression. By binding to the IGF-1 receptor, IGF-2 activates the PI3K/Akt signaling pathway which mediates pro-survival cell functions by suppression of apoptosis and regulates other cellular features like proliferation, differentiation or motility. We showed a significant reduction of Akt phosphorylation at Ser473 when blocking the IGF-1-R/Ins-R by a small molecule inhibitor or by neutralizing IGF-2 with specific antibodies. However, the inhibition of Akt phosphorylation in these experiments was only partial. 30–50% of p-Akt levels remained detectable under these conditions. Hence, we hypothesized that the remaining elevated p-Akt activity in colon cancer cells upon interaction with CAFs was due to other CAF-derived stromal factors than IGF-2 (Unger et al. 2017).

The aim of this study was to find additional pathways other than the IGF-1-R/Ins-R signaling in colon cancer cells and/or secreted factors other than IGF-2 from colon CAFs, which activate Akt signaling in cancer cells thereby leading to an increased survival, proliferation, invasiveness or drug resistance of the tumor cells. Therefore, we posed the following research question:

- Which upstream signaling cascades other than IGF-1-R signaling activated by CAF-secreted factors lead to the activation of the PI3K/Akt pathway in colon cancer cells?

To address this, we employed a cellular screening approach with an inhibitor library purchased from Selleckchem, composed of 378 different small molecule inhibitors and targeting 60 different kinases. Specifically, we used this library to identify inhibitors which displayed Akt inhibition in colon cancer cells stimulated with CAF-CM. Furthermore, we wanted to investigate the impact of the identified kinase inhibitors on the cancer cells phenotype. Thus, with this study we aim to contribute to the identification of novel therapeutic targets which interfere with the pro-tumorigenic effects of the tumor stroma/cancer cell interaction.

3. METHODS

3.1. Cell culture

DLD-1, HCT116 and LS174T colon carcinoma cell lines were purchased from American Type Culture Collection (ATCC, LGC Standards GmbH, Wesel, Germany), authenticated by short tandem repeat profiling and tested to be mycoplasma free. They were cultured in 10 cm culture dishes in 8 ml Dulbecco's modified eagle medium (DMEM) supplemented with 10 % heat inactivated fetal calf serum (FCS) and 2 mM L-glutamine which is referred to as DMEM 10 % FCS in this study. Primary CAFs (CAF3 17790), which were previously isolated from human colon carcinomas, were used and propagated in 10 cm culture dishes in 8 ml microvascular endothelial cell growth medium.

Cell culture procedures were performed in a laminar flow hood (MSC-Advantage™ Class II Biological Safety Cabinet, Thermo Fisher Scientific™, Waltham, MA, USA). Before and during work, the cell culture hood was cleaned with 70 % ethanol. Additionally, all items placed in the hood were disinfected with 70 % ethanol. Pipettes, pipette tips and all other autoclaveable items were autoclaved at 121 °C for 20 minutes with a top-loading autoclave (Varioklav, Thermo Fisher Scientific™, Waltham, MA, USA). Each pipette tip was used only once to avoid cross contaminations. Accidental spills or splashes were cleaned immediately with 70 % ethanol. After working in the laminar flow hood, ultraviolet light was turned on for one hour to sterilize the air and work surfaces.

The culture dishes were incubated at 37 °C, 5 % CO₂ and 95 % humidity in an incubator (BBD 6220 CO₂ Incubator, Thermo Fisher Scientific™, Waltham, MA, USA). Cells were checked microscopically daily with an inverted microscope (IX51, Thermo Fisher Scientific™, Waltham, MA, USA) to ensure they are healthy and growing as expected.

3.1.1. Changing medium

During expansion of the cells, medium changes were performed every second to third day depending on the cell type and growth density to remove dead cells or cell material, to replenish nutrients as well as to keep the pH value stable. Therefore, culture medium was warmed up in a bead bath (M714, Lab Armor, LLC, Cornelius, OR, USA) to 37° C. Colon carcinoma cells were washed with Dulbecco's phosphate-buffered saline (DPBS) prior to the

addition of pre-warmed culture medium. CAF3 17790 medium was only partially replaced (1:2) to avoid removing autocrine factors.

3.1.2. Cell passaging

Cell culture medium was discarded and cells were washed with DPBS twice to get rid of dead cells and to remove FCS from the medium as FCS inhibits the enzymatic activity of trypsin. 500–1,000 µl of 0.25 % trypsin-EDTA (TE) were added to a 10 cm tissue culture plate which was tilted gently to make sure TE contacts with each cell. Afterwards, culture dishes were incubated in the incubator for two to five minutes depending on the cells' adherence capability. As soon as 70–80 % of all cells have detached the fourfold amount of DMEM 10 % FCS was added for TE inactivation. Subsequently, cell suspension was transferred into a Falcon tube and centrifuged for three minutes at 200 x g (Centrifuge 5810 R, Eppendorf AG, Hamburg, Germany) at room temperature (RT). Supernatants were discarded and the cell pellet was resuspended in medium. Afterwards, cells were split 1:3 to 1:5 onto new cell culture dishes depending on the experiment.

3.1.3. Harvesting of conditioned medium

CAF3 17790 cells were grown to confluence in 10 cm dishes, washed twice with DPBS and 8 ml DMEM containing 1 % FCS and 1 % L-glutamine were added for 48 hours. Then, supernatants were harvested with a sterile single-use syringe (B. Braun Melsungen AG, Melsungen, Germany) and sterile filtered with a syringe filter with 0.2 µm pore size (Sarstedt AG & Co, Nümbrecht, Germany). Sterile CAF-CM was stored at -80 °C. After collecting enough CAF-CM, it was pooled and sterile filtered for a second time with a vacuum filtration unit with a pore size of 0.2 µm (Filtropur, Sarstedt AG & Co, Nümbrecht, Germany). The medium was tested to induce Akt activation in three different colon cancer cell lines (DLD-1, HCT116 and LS174T) by near-infrared Western blot detection (see chapter 3.3.). Finally, CM was aliquoted and stored at -80 °C.

3.1.4. Cell freezing

Colon carcinoma cells were grown to confluence. On the contrary, CAF3 17790 cells were grown to 70–80 % confluence to keep cells in a proliferative state. The cells were trypsinized, cell suspension collected in a 15 ml Falcon tube and centrifuged at 200 x g.

After centrifugation, cells were slowly resuspended in 3 ml of freezing medium, which is constituted of 90 % FCS and 10 % dimethyl sulfoxide (DMSO). 1 ml of the resuspension was aliquoted in sterile cryotubes representing a split of 1:3. CAF3 17790 were frozen without splitting the cells. Subsequently, tubes were stored on ice for 20 minutes as DMSO is cytotoxic at RT. Afterwards, tubes were frozen overnight at -80 °C in a styrofoam box with 1 cm wall thickness, which guarantees an optimal drop in temperature of 1 °C/min to -80 °C. On the next day, tubes were transferred to a -196 °C liquid nitrogen vessel (Arpege 170, Air Liquide S.A., Paris, France) for long term storage.

3.1.5. Thawing cells

7 ml of appropriate culture medium were put into 10 cm culture dishes and pre-warmed at 37 °C in the incubator. Cryotubes were thawed quickly by hand warmth to complete thawing. Cell suspension was transferred into a Falcon tube with 5 ml of DMEM 10 % FCS and centrifuged for three minutes at 200 x g at RT to get rid of DMSO from the freezing medium. 1 ml of pre-warmed culture medium was used to resuspend the cells. Cell suspension was added to the pre-warmed medium in the culture dish and cells were spread evenly by gently rotating the culture dish. Medium was changed when cells were attached to remove remaining DMSO and dead cells.

3.1.6. Cell counting

Cells were counted in suspension using a glass hemacytometer (Bright-Line Hemacytometer, Hausser Scientific Company, Horsham, PA, USA). Hematocytometer and coverslip were cleaned with 70 % ethanol before usage. Small waterdrops were placed on the edges of the coverslip which was then placed over the counting surface. To ensure proper adhesion, Newton's refraction rings must be seen. 10 µl of cell suspension were loaded in the V-shaped well of the chamber. Cells within the outer 1 mm² corner squares were counted, whereas cells touching the inner boundary lines were excluded from counting. The average cell count from four corner squares was calculated and multiplied by 10⁴ which represents the number of cells per milliliter.

3.1.7. Starvation

To synchronize the cell cycle and exclude activation by the growth medium which might affect cell treatment, cells were starved after they reached a confluence of about 80–90 %. Therefore, cells were washed twice with DPBS to remove growth medium remains. DMEM plain, which does not contain any FCS or L-glutamine, was added and cells were starved for 24 hours.

3.2. Kinase inhibitor screen

Cells were grown to confluence and washed twice with DPBS. After trypsinization cells were counted. 4×10^4 cells in 150 μ l DMEM 10 % FCS, were transferred into each well of a clear-bottomed 96-well microtiter plate using a multichannel pipette (Axygen, Corning Incorporated Life Sciences, Tewksbury, MA, USA) and incubated for 48 hours. Then, culture medium was removed and cells were starved in 100 μ l DMEM plain. After 24 hours starving medium was removed and 100 μ l DMEM plain containing 2 μ M of a kinase inhibitor from the library or DMSO with the same dilution scheme as the kinase inhibitors (DMSO control) were added to separate wells in triplicates. Each 96-well plate was carried out with the following control wells:

- Starved cells: Cells which were not treated with any inhibitor and not stimulated with CAF-CM containing a DMSO control.
- Positive control for Akt activation: Cells which were not treated with any inhibitor but stimulated with CAF-CM containing a DMSO control.
- Positive control for Akt inhibition: Cells which were treated with 1 μ M of the Akt inhibitor MK-2206 and stimulated with CAF-CM.
- Isotype control well: Cells which were treated the same way as the positive control.

Cells were treated with the inhibitors for one hour at 37 °C. Next, 100 μ l of CAF-CM were added, which represents a 1:2 ratio in total, and incubated for another 15 minutes at 37° C in order to induce Akt signaling in the tumor cells.

p-Akt and total Akt levels were measured by performing an In-Cell Western (ICW) assay which is described in the next chapter.

3.3. In-Cell Western assay

Prior to each ICW experiment, cells were starved, treated and stimulated by CAF-CM as described in chapter 3.2. using varying inhibitor concentrations. The same controls were implemented in each experimental setup.

3.3.1. Cell fixation and permeabilization

Supernatants were discarded and cells were fixed with 100 µl of 4 % formaldehyde solution for ten minutes at RT. Then, cells were pre-chilled on ice for one minute. After fixation, formaldehyde was removed. To remove remaining formaldehyde, cells were washed with 50 µl DPBS. For permeabilization, 200 µl of ice-cold 90 % methanol were added and plates were stored at -20 °C for at least 24 hours.

3.3.2. Blocking and staining

On the next day, cells were washed with 100 µl DPBS on a rotator (Rocking Platform, VWR International, Radnor, PA, USA) twice to remove methanol. Blocking was performed with 150 µl blocking buffer for 1.5 hours at RT with moderate shaking on a rotator. Primary total Akt (mouse) and p-Akt (Ser473, rabbit) antibodies were mixed with blocking buffer in the following dilution scheme: Total Akt 1:300, p-Akt 1:100. Total Akt levels were determined for normalization issues. 50 µl of antibody solution were added to each well excluding isotype control wells. For isotype controls, mouse IgG1 and rabbit IgG were diluted in blocking buffer in the same concentrations as primary antibodies and 50 µl were added to the isotype control wells. Next, plates were incubated overnight at 4 °C with gentle shaking on a rotator. After incubation, cells were washed five times with 200 µl tween washing solution for five minutes at RT on a rotator. From now on, all steps were performed with minimal light exposure. Secondary antibodies IRDye® 680RD goat anti-mouse IgG and IRDye® 800CW goat anti-rabbit IgG were mixed with the blocking buffer with a dilution of 1:800 for both antibodies. To lower the background fluorescence, Tween-20 was added to a final concentration of 0.2 %. 50 µl of secondary antibody solution were added to all wells and plates were incubated for one hour at RT on a rotator. Cells were washed five times with 200 µl tween washing solution. After the last washing step, tween washing solution was removed completely with a multichannel pipette. The bottom surfaces of the 96-well plates were cleaned with 70 % ethanol to remove eventual stains which might interfere with the measurement.

3.3.3. Plate scanning and data acquisition

Plates were scanned with the Odyssey® CLx scanning system (LI-COR Biosciences, Lincoln, NE, USA) using the Image Studio™ Software (Version 4.0, LI-COR Biosciences, Lincoln, NE, USA). For scanning the plates, ICW settings were chosen, the resolution was set at 169 µm and the focus offset was adjusted to 3 mm. Image channels with the wavelengths 700 nm and 800 nm were used for detection of total Akt and p-Akt signals. In order to obtain the best conditions for further analysis, the highest scan quality was chosen. The mean fluorescence intensities (MFIs) of total Akt and p-Akt were measured whereas each channel was analyzed separately (Figure 5). Isotype control mean MFIs were subtracted from each result and p-Akt MFIs were divided by total Akt MFIs to normalize the acquired data using Microsoft Excel (Version 15.30, Microsoft Corporation, Redmond, WA, USA).

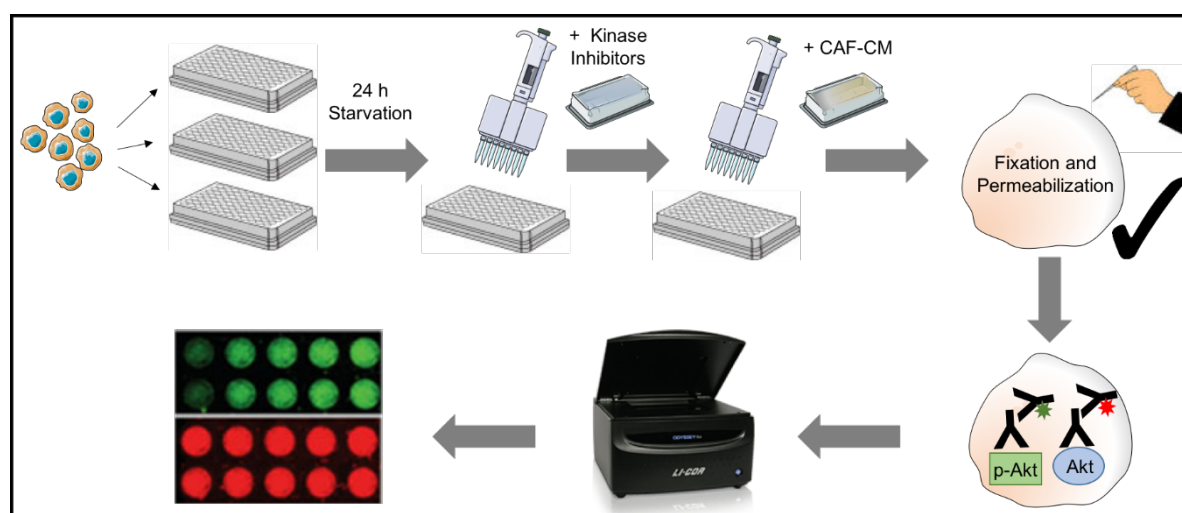


Fig. 5: Workflow In-Cell Western Assay. First cells were seeded in 96-well plates and grown for 48 hours. After 24 hours of starving, kinase inhibitors were added and incubated for one hour. Afterwards, CAF-CM was added for another 15 minutes. Cells were fixed and permeabilized prior to the addition of primary and secondary antibodies. Imaging was carried out with Odyssey® Imager. Some graphics were used from Servier Medical Art (<http://www.servier.com/Powerpoint-image-bank>).

3.4. Near-infrared Western blot

6×10^5 cells were cultured in 6-well plates and grown to 80–90 % confluence. Then, cells were starved with 2 ml DMEM plain for 24 hours. After starvation, DMEM plain was removed and cells were treated with 1 ml DMEM plain containing kinase inhibitors or the respective DMSO control for one hour. In order to activate the PI3K/Akt pathway in the tumor cells, CAF-CM was added in a 1:2 ratio and cells were stimulated for 15 minutes.

As control, untreated cells, which were further starved with DMEM plain and not stimulated with CAF-CM, were used. Additionally, the same volume of DMSO as the kinase inhibitor solution was added (DMSO control). Cells stimulated with CAF-CM containing a DMSO control were used as positive control for Akt activation. Cells treated with 1 μ M MK-2206 and stimulated with CAF-CM were used as positive control for efficient Akt inhibition.

3.4.1. Lysate preparation

After treatment and stimulation, cells were washed twice with ice-cold 1xPBS. 1xPBS was removed completely by using a water jet pump. 30–50 μ l lysis buffer were added depending on the cells' adherence capacity and cells were scraped off with a cell scraper (TPP Techno Plastic Products AG, Trasadingen, Swiss) and collected in safe-lock microtubes. Then, lysates were vortexed thoroughly, snap frozen in liquid nitrogen and re-thawed for three times. Next, lysates remained on ice for 20 minutes. Samples were vortexed again and centrifuged for 20 minutes at 20,000 x g at 4 °C (Centrifuge 5417 R, Eppendorf AG, Hamburg, Germany). Supernatants were aspirated, collected in separate tubes and stored at -80° C.

3.4.2. Protein concentration measurement

Samples were thawed on ice. Protein concentrations were measured by performing a Bradford protein assay with a photometer (BioPhotometer 6131, Eppendorf AG, Hamburg, Germany). Bradford reagent was mixed with distilled water in a ratio of 1:5 and filtered afterwards with a grade 1573 filter paper with a pore size of 12 μ m (GE Healthcare, Chicago, IL, USA). 1 ml of Bradford solution and 1 μ l of lysates were mixed together and incubated for five minutes at RT. After blank measurement with the lysis buffer, the protein concentration of each sample was measured.

3.4.3. Gel preparation

A 10 % polyacrylamide gel and a 5 % stacking gel were chosen as these concentrations were suitable for separation of all proteins of our interest. The separating gel was prepared and filled between two glass plates with spacers to get a gel of 0.75 mm thickness. 500 μ l isopropyl alcohol were added on top to get a horizontal straight gel boundary. After gel was solidified, isopropanol was removed before the stacking gel was poured. A ten or 15 tooth comb was placed into the gel depending on the number of samples. Gel casting was performed using the Mini-PROTEAN Tetra Cell System (Bio-Rad Laboratories, Inc., Hercules, CA, USA).

3.4.4. Protein separation

30 μ g of total protein were mixed with 6 μ l sample loading buffer and filled up with lysis buffer to a final volume of 18 μ l. After vortexing, samples were incubated at 95 °C for five minutes in a thermomixer (Thermomixer comfort, Eppendorf AG, Hamburg, Germany) to denature proteins. Next, tubes were vortexed again and cooled down on ice before they were centrifuged briefly to spin down drops from the inside of the tubes. A protein ladder containing ten proteins spanning 10–180 kDa was used as a size standard. Combs were removed from the gel and 7 μ l of the protein ladder and 18 μ l of the sample mix were loaded into the wells of the stacking gel. Polyacrylamide gel electrophoresis was performed in electrophoresis buffer for 15 minutes at 90 V, 2,000 mA and 300 W until all proteins were focused in one band in the stacking gel. Afterwards, electrophoresis was performed for approximately one and a half hours at 110 V until the dye front left the separating gel completely. Electrophoresis was performed in a Mini-Trans-Blot Cell System.

3.4.5. Transferring the protein from to gel to the membrane (blotting)

Blotting was done in Harlow buffer for one hour at 300 V, 350 mA and 300 W in the presence of a cooling unit to absorb the heat generated during the transfer. Whatman papers (GE Healthcare, Chicago, IL, USA) and a nitrocellulose membrane with a pore size of 0.22 μ m (LI-COR Biosciences, Lincoln, NE, USA) were soaked in Harlow buffer for ten minutes. Gel and membrane were placed together followed by three soaked Whatman papers which were placed on both sides of the gel and the membrane. A sponge was used on both sides next to the Whatman papers to squeeze the membrane and the gel together. After blotting, membranes were washed with distilled water on an orbital shaker (Rocking Platform, VWR

International, Radnor, PA, USA) for 10 minutes. Blotting was performed in a Mini-Trans-Blot Cell System.

3.4.6. Blocking and staining of Western blot membranes

After blotting, membranes were dried between two Whatman papers for at least ten minutes. For blocking, membranes were incubated in Odyssey® blocking buffer for one hour on an orbital shaker.

Next, primary antibodies were diluted in Odyssey® blocking buffer containing 0.2 % Tween-20 according to the manufacturer's instructions. Membranes were put into a 50 ml Falcon tube together with the antibody solution and incubated overnight at 4°C on a tube roller mixer (RM10W-80V, CAT, M. Zipperer GmbH, Ballrechten-Dottingen, Germany). To get rid of the primary antibody solutions on the next day, membranes were washed with 1xTBS containing 0.1 % Tween-20 four times for five minutes on an orbital shaker. From now on, all steps were performed with minimal light exposure. IRDye® 800CW (anti-rabbit) and IRDye® 680RD (anti-mouse) were used as secondary antibodies. Secondary antibodies were diluted 1:20,000 in Odyssey® blocking buffer containing 0.2 % Tween-20. Membranes were put in a black Western blot incubation box (LI-COR Biosciences, Lincoln, NE, USA) together with the antibody solution and incubated for one hour at RT with gentle shaking on a rotator. Membranes were washed with 1xTBS containing 0.1 % Tween-20 four times for five minutes in a black Western blot incubation box on an orbital shaker.

3.4.7. Membrane scanning and data acquisition

Pictures of the membranes were taken using the Odyssey® CLx scanner together with the Image Studio™ Software. Membranes were placed on the scanning surface with the sample surface down. The sides of the membranes were parallel to the X/Y scan axes which makes it easier to analyze the samples. A silicon mat was put on the membranes and bubbles were removed by gently sweeping over the mat. Membranes were scanned with highest quality using the Western blot settings with a resolution of 337 µm and a focus offset of 0.0 mm. As two fluorescence signals were detected simultaneously, both channels (700 nm and 800 nm) were needed for detection. The MFIs of the bands and the background were measured whereas each channel was evaluated separately. Finally, the background signals were subtracted from the band signals to obtain consistent data using Microsoft Excel.

3.5. Spheroid formation

For spheroid formation, u-bottom shaped, untreated 96-well plates were used. First, a bulk mixture of HCT116 cells, DMEM containing 5 % FCS and 1 % L-Glutamin and 20 % methylcellulose was prepared. For easier calculation and in order to avoid an insufficient amount of methylcellulose-cell suspension for 96-well plates we calculated with 100 wells per plate. Therefore, 2 ml of methylcellulose were filled into a Falcon tube. Because of the viscous consistence of the methylcellulose it was poured dropwise into the tube. Then, 2×10^5 HCT116 cells, making 2×10^3 cells per well, were added to the bulk mixture. Next, DMEM 5 % FCS was added to a final volume of 10 ml. After mixing the suspension properly, it was filled into a v-shaped reservoir (Eppendorf AG, Hamburg, Germany) and 100 μ l were transferred to each well using a multichannel pipette. Afterwards, 96-well plates were centrifuged at 300 x g for 10 minutes and incubated at 37 °C. After 72 hours, spheroids have formed and were treated according to the experiment.

3.6. 7-AAD/EdU cell cycle analysis (proliferation assay)

Spheroids of one 96-well plate were collected in a 15 ml tube and centrifuged at 100 x g for three minutes. Supernatants were discarded and spheroids were washed with DPBS. After another centrifugation at 100 x g for three minutes, supernatants were discarded, spheroids were resuspended in 1.5 ml DMEM 1% FCS and kinase inhibitors or the same volume of DMSO (DMSO control) were added. In order to stimulate Akt activation in the cancer cells, 1.5 ml CAF-CM were added to each well excluding the starved cells control. Spheroids were incubated for 24 hours at 37 °C.

As control, untreated cells, which were further starved with DMEM plain and not stimulated with CAF-CM, were used. Additionally, same volume of DMSO as the kinase inhibitors was added to the control. Cells stimulated with CAF-CM containing a DMSO control were used as positive control for Akt activation. Cells treated with 1 μ M MK-2206 and stimulated with CAF-CM were used as positive control for Akt inhibition.

3.6.1. EdU incorporation and trypsinization of cells

As spheroids tend to stick together, they were first separated by pipetting up and down carefully. 5-ethynyl-2'-deoxyuridine (EdU) was added to a final concentration of 10 μ M to each well except the EdU exclusion well. After 30 minutes, spheroids were transferred into 15 ml

Falcon tubes and centrifuged at 100 x g for three minutes. Supernatants were discarded and spheroids were washed with 1xPBS. After another centrifugation at 100 x g for three minutes, supernatants were discarded, 1,000 µl of TE were added and Falcon tubes were incubated at 37 °C. When spheroids dispersed into a single cell suspension, trypsinization was stopped by adding 5 ml of DMEM 10 % FCS. Falcon tubes were centrifuged at 200 x g for three minutes and supernatants were discarded. 750 µl of FACS buffer were added and cells were transferred to 1.5 ml Eppendorf tubes.

3.6.2. Cell fixation, permeabilization and Click-iT™ EdU reaction

Tubes were centrifuged at 200 x g for five minutes and supernatants were removed. The washing step with the FACS buffer was repeated once. Afterwards, the FACS buffer was removed, 750 µl ice cold 100 % methanol were added and samples were incubated for at least ten minutes at -20 °C. To get rid of the methanol, tubes were centrifuged at 200 x g for five minutes and supernatants were removed. Cells were washed twice with the FACS buffer which was removed after the last washing step. From now on, all steps were performed with minimal light exposure. 125 µl of the 1xClick-iT™ reaction cocktail (Click-iT™ EdU Alexa Fluor™488 Flow Cytometry Assay Kit, Invitrogen, Waltham, MA, USA) were added. Samples were incubated for 30 minutes at RT.

3.6.3. Staining cells for their DNA content

Tubes were centrifuged at 200 x g for 5 minutes and supernatants were removed. Samples were washed again with 750 µl FACS buffer. FACS buffer was removed and 125 µl of FACS buffer were added again followed by 2.5 µl RNase and 1 µl of 7-aminoactinomycin D (7-AAD). Samples were vortexed carefully and incubated for 30 minutes at RT. Next, they were centrifuged at 200 x g for five minutes and supernatants were removed. 400 µl of FACS buffer were added and cell suspension was filtered using 5 ml tubes with cell strainer caps with a 35 µm nylon mesh to avoid clogging of the flow cytometer by remaining cell clumps from the spheroids.

3.6.4. Flow cytometry analysis and data acquisition

To analyze EdU incorporation and total DNA by 7-AAD staining, cells were measured with a CytoFLEX S flow cytometer (Beckman Coulter Inc., Brea, CA, USA). Raw data analysis was

performed in Flow Jo (Version 10, Tree Star Inc., Ashland, OR, USA). Dead cells and doublets were excluded from analysis. Controls without EdU were included in data analysis as well. To calculate the percentage of cells in G1, G2/M and S phase, percentages of cells in gates were summed up and each gate was divided by the sum of all gates using Microsoft Excel.

3.7. Transwell migration assay

6.5 mm transwell inserts with a pore size of 8 μm (Corning Inc., Corning, NY, USA) were preincubated with medium for one hour at 37 °C. Therefore, 600 μl CAF-CM were added per well already containing kinase inhibitors and 100 μl DMEM plain were added per insert. Then, inserts were put into the wells.

Cells were pretreated with kinase inhibitors as follows: 2×10^5 cells were resuspended in 100 μl DMEM plain containing the inhibitors or DMSO as a control in a 1.5 ml tube and incubated for 30 minutes at 37 °C. For each condition, two approaches were assessed.

After preincubation, transwell inserts were first removed from the wells and put into an empty well to remove the medium. 100 μl of cell suspension containing the inhibitors or DMSO were added to the inserts. Inserts were put back into the wells which already contained the CAF-CM/kinase inhibitors or DMSO mixture. Cells were incubated for 20 hours at 37 °C.

Cells stimulated with CAF-CM containing DMSO were used as positive control for Akt activation. Cells treated with 1 μM MK-2206 and stimulated with CAF-CM were used as positive control for Akt inhibition. Control wells for background determination did not contain any cells and were treated the same way as the positive control.

3.7.1. Cell fixation and detachment of non-migrated cells

Inserts were removed from the wells and put into an empty well where the medium was removed. 200 μl of Histofix per insert and 600 μl of Histofix per well were added and cells were incubated for ten minutes at RT. Inserts were removed from the well before Histofix was removed. Inserts were washed three times using two beakers filled with 1xPBS. Therefore, inserts were shortly dipped twice in the first beaker and once in the second beaker. Remaining 1xPBS was removed as well as in any way possible. To remove non-migrated cells on the inside of the insert, 1xPBS-soaked cotton swabs were gently twisted over the surface without destroying the membrane.

3.7.2. Staining cells for visualization with DAPI

From now on, all steps were performed with minimal light exposure. 100 µl DAPI with a concentration of 2 µg/ml were added to each insert and 600 µl DAPI with the same concentration as used for the inserts were added to each well. Inserts were put back to the wells and the membrane was incubated for ten minutes at RT without light exposure. Inserts were removed from the well, put into an empty well. DAPI was removed carefully without destroying the membrane of the inserts.

Before pictures were taken, 1xPBS-soaked cotton swabs were gently twisted over the surface of the inner membrane of the transwell as already done before to ensure that no non-migrated cells were left on the inner membrane of the transwell.

3.7.3. Microscopic analysis and data acquisition

Pictures were taken using an inverted microscope equipped with a color camera (XC50, Olympus Corporation, Tokyo, Japan) and a digital image software (cellSens Standard, Olympus Corporation, Tokyo, Japan) using the fluorescence illumination and a DAPI filter (BP 350/50–BP 460/50). Microscopy camera was set on DAPI mode and exposure time was set to 500 ms. Five pictures of each membrane were taken in a cross-shaped manner.

To evaluate the migration capacity ImageJ (Version 1.x, <https://imagej.net/Welcome>) was used. Membrane pictures were converted into 32 bit black and white pictures. The whole picture was selected and mean grey values were measured. To obtain the correct fluorescence signals of migrated cells only, mean background signals were subtracted from each value using Microsoft Excel.

3.8. Spheroid outgrowth assay

Spheroids of 32 wells of a u-bottom shaped, untreated 96-well plate were collected in a 15 ml tube and centrifuged at 100 x g for three minutes. Supernatants were discarded and spheroids were resuspended in 1 ml 1xPBS. Resuspended spheroids were then transferred into 1.5 ml Eppendorf tubes and centrifuged at 100 x g for three minutes again. Supernatants were removed thoroughly, leaving less than 5 µl of 1xPBS remaining on the cell pellet.

3.8.1. Embedding spheroids in collagen gels

Next, collagen gels were prepared on ice whereas 300 μ l of gel were needed per silicone form and per condition. Therefore, a collagen gel bulk mixture was prepared containing 2 mg/ml collagen type I, 10xPBS diluted to 1xPBS and DMEM with 5 %FCS. In a final step, about 7 μ l 1 M NaOH per ml were added to the bulk mixture. Quickly, the tube was shaken well until the color of the mixture turned salmon-pink which indicates the right pH value for our purpose. To get rid of bubbles in the gel emerged from shaking the mixture, the tube was centrifuged in a precooled centrifuge at 250 x g for ten seconds.

For gel pouring, sterile silicone forms with a diameter of 1.5 cm and a height of 1 mm were placed in culture plate lids. Prior to that, silicone forms were cut out of a sealing gasket for gel dryers (Model 583 Transparent Sealing Gasket, Bio-Rad Laboratories, Inc., Hercules, CA, USA) and autoclaved. Spheroids were carefully resuspended in 300 μ l collagen gel without forming bubbles. The gel containing the spheroids was then poured into the silicon forms and evenly distributed with a pipette tip. Ring-shaped meshes, prepared from the nylon mesh inserts of syringe filters with a 120 μ m mesh size (Medicon, Becton, Dickinson and Company, Franklin Lakes, NJ, USA) were added to the gel and submerged. Gels were incubated at RT for 30 minutes without moving that all spheroids descend to the bottom.

After gels were solidified, silicon forms were removed from the gels. Therefore, they were sprinkled with DMEM 5 % FCS and then detached using forceps. The formed gel cylinders were transferred into 24-well plates and cultured in CAF-CM diluted 1:2 in DMEM 5 % FCS containing kinase inhibitors or DMSO. After 48 hours, medium/CAF-CM mix and inhibitors or DMSO were renewed.

Cells stimulated with CAF-CM containing a DMSO control were used as positive control for Akt activation. Cells treated with 1 μ M MK-2206 and stimulated with CAF-CM were used as positive control for efficient Akt inhibition.

3.8.2. Microscopic analysis, data acquisition and statistical analysis

Pictures were taken after 24 hours (10x objective) and after 96 hours (4x objective) with an inverted microscope equipped with a color camera and a digital image software. The exposure time was set to 11.68 ms and the gain was set to 5.3 dB. Each picture contained a scale bar (10x objective – 200 μ m; 4x objective – 100 μ m).

Evaluation of the outgrowth of the spheroids was performed using ImageJ. To set the scale, the scale bar in the picture was used to measure a known distance. The scale bar was traced with the straight-line tool and the length of the scale bar as well as the unit of the length were adjusted. The settings were applied to all pictures. For each image, two areas were measured using the freehand-tool to trace the structures. First, the outgrowth structures of each spheroid containing the spheroids themselves were traced followed by the spheroids without the outgrowths (Figure 6). The area of the spheroids was subtracted from the area of the outgrowths containing the spheroids using Microsoft Excel to obtain the area of the invasive structures.

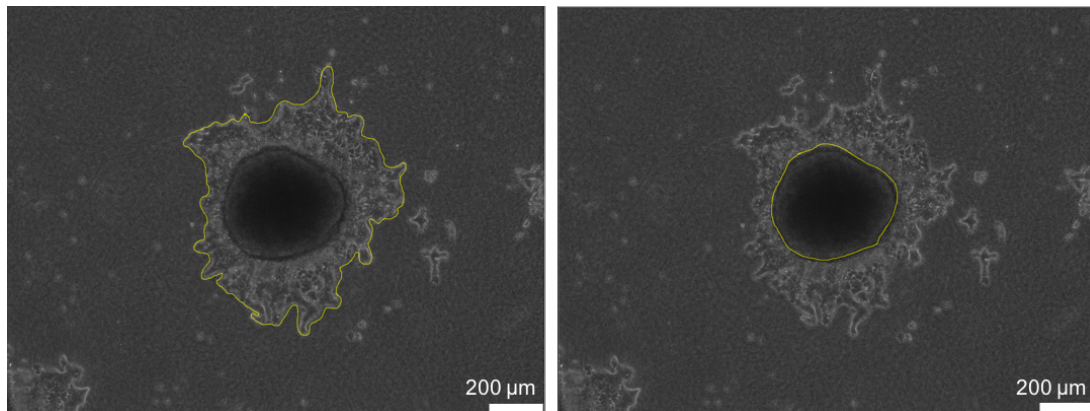


Fig. 6: Scheme for the determination of the outgrowth area of spheroids used in the spheroid outgrowth assay. First, the areas of the outgrowth and the spheroids were measured (left, yellow line) followed by the measurement of the spheroid alone (right, yellow circular structure) using ImageJ. To obtain the area of the invasive structures alone, the area of the right picture was subtracted from the area of the left picture.

3.9. Statistical analysis and graphical representation

For statistical analysis GraphPad Prism (Version 6, GraphPad Software, San Diego, CA, USA) was used. Comparison between two different groups were calculated using a t-test for independent samples (two tailed, unpaired), statistical significance was given with p-values ≤ 0.05 . Prior to that, data were checked for Gaussian distribution. If the data was not normally distributed, a Mann-Whitney U test was performed instead of a t-test.

Graphical representation was done using GraphPad Prism. The data was graphically displayed in box plots and bar charts with error bars. Thus, box plots represent the interquartile range which contains 50 % of the data between the upper and the lower quartile. The line, which divides the box in two parts indicates the median. The upper and the lower whiskers represent

values outside the middle 50 % while the end of the whiskers display the maximum and the minimum of the data. Bar charts represent mean numbers of varying values and error bars represent the standard error of the mean. When only one value was available, bar charts didn't contain error bars.

4. RESULTS

4.1. Comparing the impact of cancer-associated fibroblast-conditioned medium and DMEM 1 % FCS on p-Akt levels in HCT116 cells

As the CAF-CM used in this study contains 1 % FCS derived from the culture medium, we wanted to test whether the serum has an impact on p-Akt levels in our colon cancer cells. Therefore, we stimulated starved (plain DMEM, 24 hours) HCT116 cells with CAF-CM and DMEM 1 % FCS, respectively, for 15 minutes and detected p-Akt levels by performing an ICW assay. MFIs of p-Akt signals were normalized to total Akt levels detected by a total Akt antibody. Starved cells were used as control and cells treated with the Akt inhibitor MK-2206 served as positive control for efficient Akt inhibition.

We couldn't see significant differences regarding p-Akt levels in cells stimulated with DMEM 1 % FCS and starved cells. In contrast, cells stimulated with CAF-CM showed significantly increased p-Akt levels which almost doubled when compared with p-Akt levels of starved cells or cells stimulated with DMEM 1 % FCS ($p < 0.0001$). Cells treated with MK-2206 displayed the lowest p-Akt levels of all treatment approaches (Figure 7).

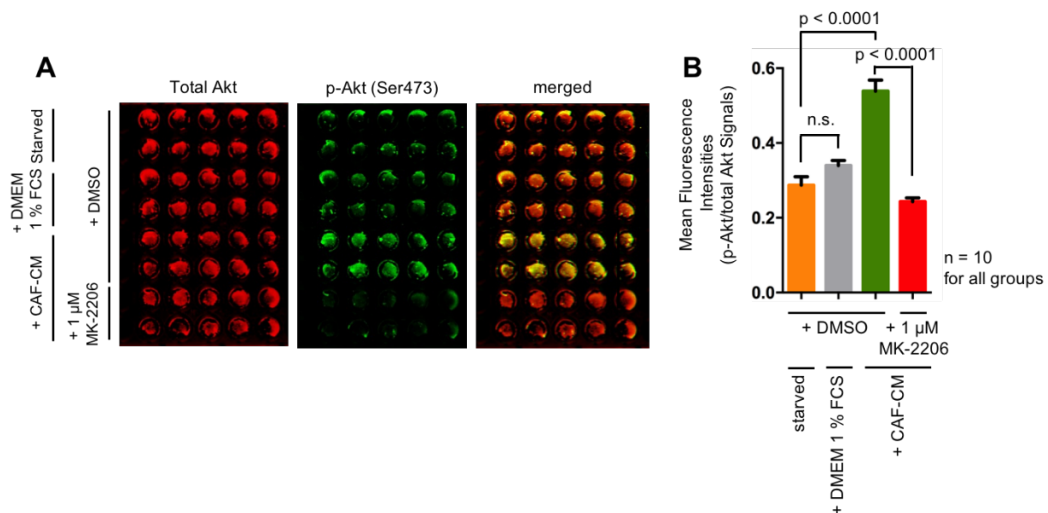


Fig. 7: The impact of CAF-CM and DMEM 1 % FCS on p-Akt levels in HCT116 colon cancer cells. HCT116 cells were starved for 24 hours and treated with the Akt inhibitor MK-2206 for one hour. Cells were stimulated with CAF-CM or DMEM 1 % FCS for 15 minutes. Ten replicates were carried out per condition ($n = 10$). Subsequently, an ICW assay was performed detecting p-Akt (Ser473) and total Akt levels. Starved cells were used as control and cells treated with MK-2206 were used as positive control for effective Akt inhibition. **A:** Representative wells of the ICW assay showing p-Akt (Ser473), total Akt and merged channels. **B:** Graphical illustration of the ICW assay. Bar graphs represent the normalized MFIs (p-Akt/total Akt) of the ICW assay, error bars display the standard error of the mean. p-values were calculated using a t-test for independent samples (two-tailed, unpaired).

4.2. Kinase inhibitor screening

To identify potential signaling pathways leading to Akt activation in CRC cells by CAF-CM stimulation, a medium throughput cellular screening was performed. Therefore, starved HCT116 cells were treated with a kinase inhibitor library for one hour containing 378 different kinase inhibitors prior to the addition of CAF-CM for 15 minutes. Total Akt and p-Akt levels were detected performing an ICW assay. MFIs of p-Akt signals were normalized to total Akt levels detected by a total Akt antibody. Starved cells were used as control. Additionally, cells stimulated with CAF-CM served as positive control for Akt activation and cells treated with MK-2206 and stimulated with CAF-CM were used as positive control for Akt inhibition.

A heatmap of the normalized MFIs including all used inhibitors was generated to get a comprehensive overview of p-Akt levels in the cancer cells. Additionally, the heatmap shows the coherence within the triplicates which illustrates the precision of this method. Each row represents one inhibitor and the columns show the triplicates and their mean value. Green indicates high p-Akt values, which means no inhibition of Akt by the target kinase of the inhibitor. Yellow indicates mediocre p-Akt levels and red indicates low levels indicating the inhibitor either target Akt directly or upstream kinases of Akt. Starved cells and the positive control for Akt inhibition displayed low p-Akt levels whereas the positive control showed high p-Akt levels in HCT116 cells. Inhibitors, which were very abundant in the top hits meaning that they induced a decrease of p-Akt in HCT116 cells, were classified in inhibitor categories. Inhibitors targeting PI3K, mTOR and Akt are represented as grey lines on the left of the heatmap. This inhibitor category was the most abundant one in the top hits of the screen but it was excluded from further investigations as it directly interacts with Akt or kinases which phosphorylate Akt. Selective IGF-1-R/Ins-R inhibitors, meaning that they are exclusively targeting the IGF-1-R or Ins-R, are depicted in blue. This class of inhibitors was also very prominent in the top hits and lead to an effective p-Akt inhibition. Selective c-Met inhibitors, showed as yellow lines, could be found solely in the top 100 inhibitors leading to decreased p-Akt levels in HCT116 cells. Additionally, selective JAK inhibitors, depicted as red lines, could be found in the top hits but they were also spread over the whole heatmap (Figure 8).

We focused on the two most potent selective IGF-1-R/Ins-R inhibitors and c-Met inhibitors for further validation experiments. Therefore, the IGF-1-R/Ins-R inhibitors OSI-906 and NVP-ADW742 were chosen. As most potent selective c-Met inhibitors leading to Akt inhibition, SGX-523 and JNJ-38877605 were chosen (Figure 9).

A list of all results including all values can be found in the appendix.

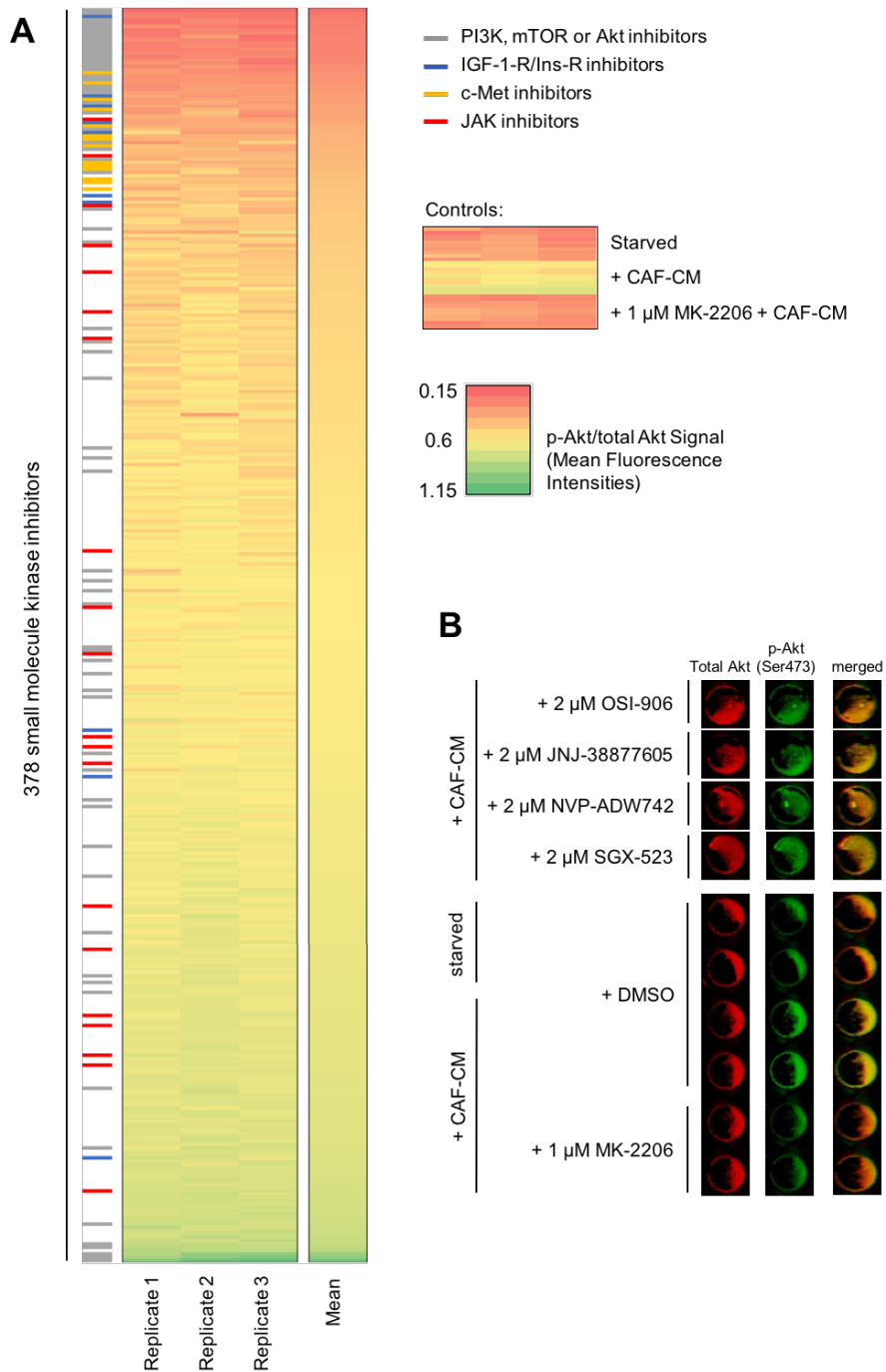


Fig. 8: Heatmap of the kinase inhibitor library screening results. HCT116 cells were starved for 24 hours and treated with kinase inhibitors at 2 μ M each for one hour prior to Akt activation with CAF-CM for 15 minutes. Starved cells were used as control and cells stimulated with CAF-CM served as positive control for Akt activation. Cells treated with MK-2206 were used as positive control for Akt inhibition. After cell treatment, an ICW assay was performed to detect total Akt and p-Akt (Ser473) levels. All inhibitors were tested in triplicates ($n = 3$). Controls were tested in duplicates per plate ($n = 30$). **A:** Heatmap of the screen depicting normalized MFIs of p-Akt levels (p-Akt/total Akt). Red indicates low p-Akt values (i.e. strong inhibition), yellow indicates mediocre values and green indicates high values. The columns show the replicates (1, 2, 3) and their mean. Each row represents an inhibitor. Colored lines show the distribution of selective inhibitors over the heatmap. Positive controls and starved cells are depicted in a separate heatmap. **B:** Representative ICW wells showing the inhibitors which were chosen for further validation and the controls of the plate.

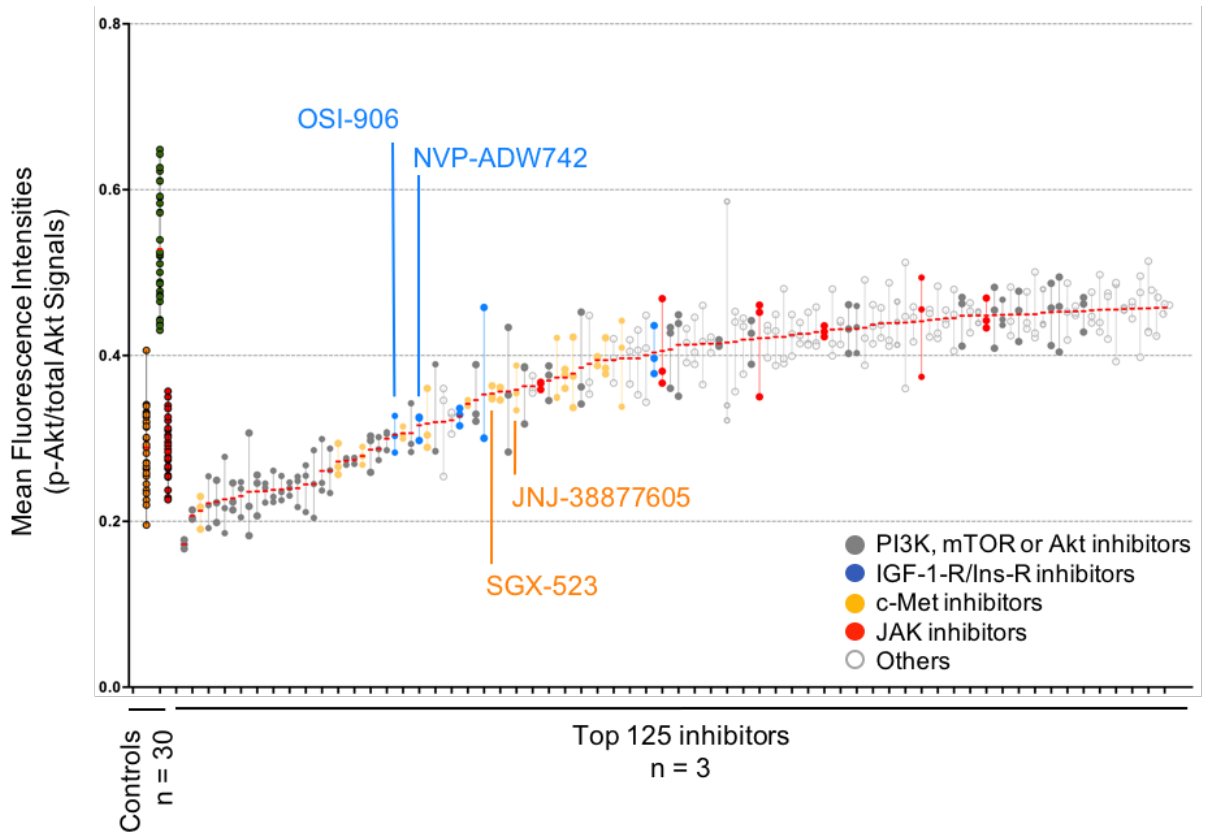


Fig. 9: Quantitative effects on p-Akt levels of the top 125 inhibitors of the kinase inhibitor library screen. HCT116 cells were starved for 24 hours and treated with kinase inhibitors at 2 μ M each for one hour prior to Akt activation with CAF-CM for 15 minutes. Starved cells were used as control (dark orange dots encircled in black). Cells stimulated with CAF-CM served as positive control for Akt activation (green dots encircled in black) and cells treated with MK-2206 were used as positive control for Akt inhibition (red dots encircled in black). After cell treatment, an ICW assay was performed to detect Total Akt and p-Akt (Ser473) levels. All inhibitors were tested in triplicates (n = 3). Controls were tested in duplicates per plate (n = 30). The y-axis shows the normalized MFIs of p-Akt levels (p-Akt/total Akt) and the x-axis depicts the controls and the top 125 inhibitors of the screen. The colored dots represent the triplicates of the inhibitor categories. PI3K, Akt and mTOR inhibitors are shown in dark grey, IGF-1-R/Ins-R inhibitors in blue, c-Met inhibitors in orange and JAK inhibitors in red. All other inhibitors are shown in light grey. The labelled inhibitors show those inhibitors which were chosen for further validation.

4.3. Validation of the kinase inhibitor screening in HCT116, DLD-1 and LS174T cells

To validate our chosen selective IGF-1-R/Ins-R inhibitors OSI-906 and NVP-ADW742 as well as the selective c-Met inhibitors SGX-523 and JNJ-38877605 the experimental setup used in the screen was repeated. To test the effect of the inhibitors on p-Akt levels, three different human colon cancer cell lines (HCT116, DLD-1 and LS174T) were treated. Cells were cultured in 6-well plates for 48 hours before they were starved using DMEM plain for 24 hours.

Afterwards, cells were treated with the selective inhibitors at 2 μ M each for one hour prior to the addition of CAF-CM for 15 minutes in order to activate the Akt signaling pathway. p-Akt (Ser473) and total Akt levels were detected by performing a near-infrared Western blot. MFIs of p-Akt signals were normalized to MFIs of total Akt. Starved cells were used as control. Cells stimulated with CAF-CM served as positive control for Akt activation and cells treated with MK-2206 and stimulated with CAF-CM were used as positive control for Akt inhibition.

HCT116 cells showed almost the same pattern of p-Akt inhibition as already seen in the medium throughput screen (Figure 8A). OSI-906, the most potent selective IGF-1-R/Ins-R inhibitor, decreased the phosphorylation of Akt to 60 % compared to CAF-CM controls. The other IGF-1-R/Ins-R inhibitor NVP-ADW742 was not as efficient as OSI-906, however, a slight decrease in p-Akt levels was detected in all cell lines (Figure 10A-C). In contrast to the screen, c-Met inhibitors showed different efficacies regarding p-Akt inhibition. HCT-119 and LS174T cells treated with the second strongest c-Met inhibitor JNJ-38877605 from the screen showed less p-Akt signals than the treatment with the other c-Met inhibitor SGX-523 (Figure 10A and 10C). However, this inhibition pattern was different in DLD-1 cells as SGX-523 downregulated p-Akt stronger than JNJ-38877605 (Figure 10B). In combination, the inhibitors worked best in HCT116 cells regarding p-Akt inhibition. In this cell line, the strongest inhibition was achieved when NVP-ADW742 and JNJ-38877605 were combined. The other inhibitor combinations in HCT116 cells had similar effects on Akt inhibition comparable to the MK-2206 control (Figure 10A). DLD-1 cells showed the strongest Akt inhibition when OSI-906 and JNJ-38877605 were combined, followed by the OSI-906 and SGX-523 combination. The other combinations were less effective regarding p-Akt levels but mostly more effective than the single inhibitor treatments. In DLD-1 cells, no inhibitor combination could downregulate p-Akt levels as efficiently as the MK-2206 control (Figure 10B). In LS174T cells p-Akt inhibition worked best when a combination treatment of OSI-906 and SGX-523 was used. Almost the same inhibition could be seen in NVP-ADW742 and SGX-523. The other combinations were slightly less effective regarding p-Akt levels (Figure 10C). Importantly, combination of all IGF-1-R/Ins-R and c-Met inhibitors did not result in lower p-Akt levels than the combination of one inhibitor in each category strongly suggesting that no off-target effects were observed (Figure 10A-C).

The IGF-1-R/Ins-R inhibitor OSI-906 and the c-Met inhibitor JNJ-38877605 were considered in further experiments as they showed the best overall outcome in single and combination treatments in all cell lines.

4.4. Determining the on-target specificity of OSI-906 and JNJ-38877605 in HCT116 cells

To test whether the inhibitors OSI-906 and JNJ-38877605 are on-target in our cellular system, they were tested for their effects on phosphorylation of the respective receptors. For this, HCT116 cells were cultured in 6-well plates for 48 hours until they reached a confluence of 80–90 % before they were starved for 24 hours with DMEM plain. After starvation, cells were treated with the inhibitors OSI-906 and JNJ-38877605 for one hour prior to the addition of CAF-CM for 15 minutes. A near-infrared Western blot was performed to detect p-IGF-1-R β (Tyr1131)/Ins-R β (Tyr1146) and p-Met (Tyr1234/1235) levels. GAPDH was used as a loading control. MFIs of p-IGF-1-R β /Insulin-R β and p-Met signals were normalized to MFIs of GAPDH. Cells stimulated with CAF-CM served as positive control for Akt activation and cells treated with MK-2206 and stimulated with CAF-CM were used as positive control for Akt inhibition.

Unfortunately, it turned out that the antibody against p-IGF-1-R β (Tyr1131)/Ins-R β (Tyr1146) did not work properly as there were no distinct bands detectable on the Western blot membrane (Figure 11A). Cells treated with JNJ-38877605 exhibited less c-Met phosphorylation in comparison to the positive control which showed the highest levels of p-Met. In addition, JNJ-38877605 treatment resulted in less p-Met signals compared to starved cells and cells treated with the Akt inhibitor MK-2206 (Figure 11B).

Taken together, we could demonstrate for c-Met that the inhibitor JNJ-38877605 led to an inhibition of c-Met activity in our cells, whereas for OSI-906 a direct involvement of the IGF-1-R could not be shown here due to lack of a suitable antibody. However, previous work of the group has already convincingly demonstrated the activation of the IGF-1-R/PI3K/Akt axis by CAF-derived IGF-2 (Unger et al. 2017).

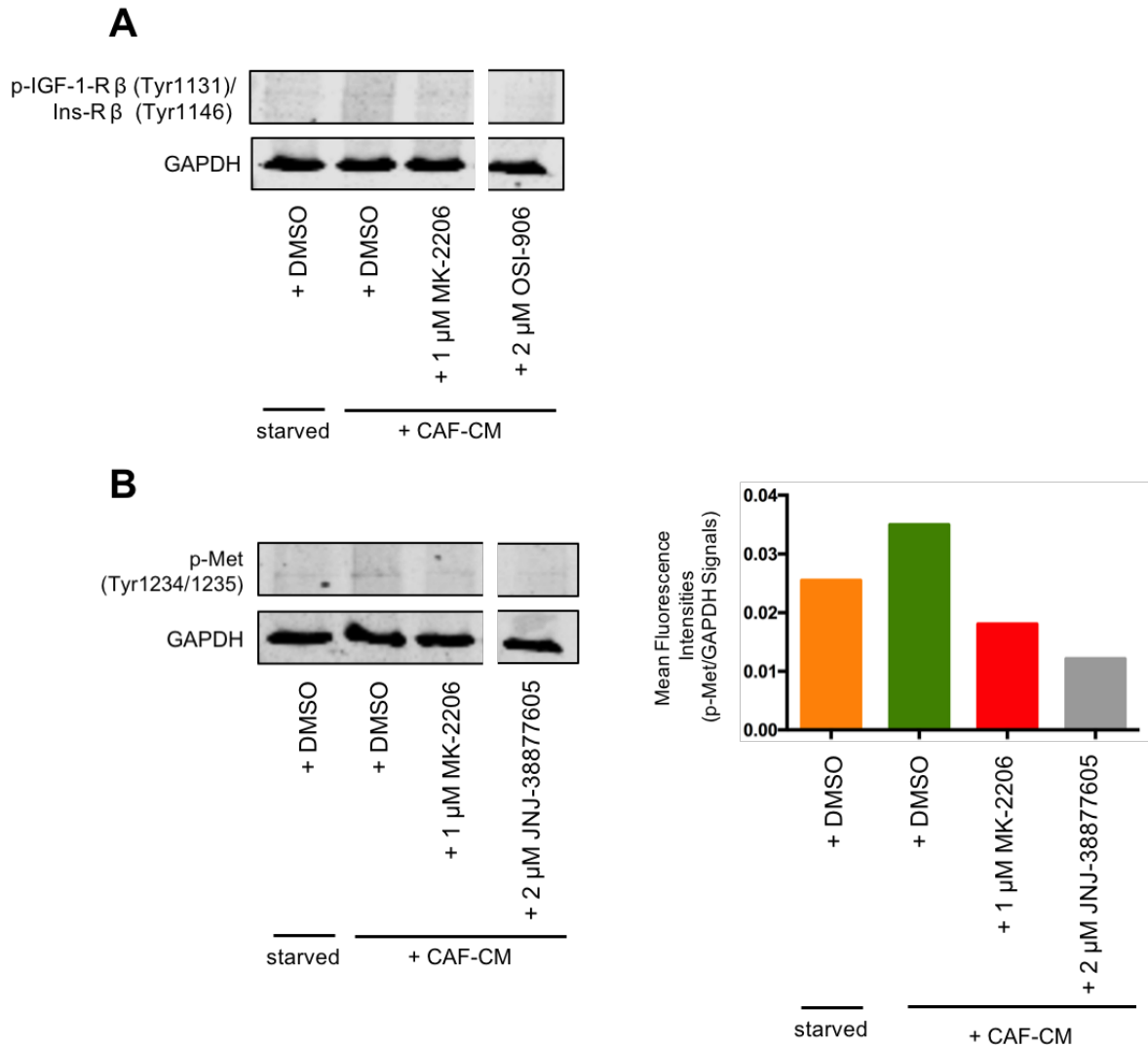


Fig. 11: Testing on-target specificity of OSI-906 and JNJ-38877605 in HCT116 cells. HCT116 cells were starved for 24 hours and treated with the inhibitors for one hour prior to the stimulation of p-Akt with CAF-CM for 15 minutes. Starved cells were used as control. Cells stimulated with CAF-CM served as positive control for Akt activation and cells treated with MK-2206 were used as positive control for Akt inhibition. A near-infrared Western blot was performed to detect protein levels. **A:** Western blot membranes showing GAPDH levels. p-IGF-1-R β (Tyr1131)/Insulin-R β (Tyr1146) levels couldn't be detected. **B:** Western blot membranes showing p-Met (Tyr1234/1235) and GAPDH protein levels. Bar charts represent the background corrected and normalized MFIs of p-Met (p-Met/GAPDH) of the near-infrared Western blot.

4.5. The impact of recombinant human IGF-2 and HGF on p-Akt levels in HCT116 cells

Next, HCT116 cells were stimulated with recombinant human (rh)IGF-2 or rhHGF to determine if the activation of the respective receptors by the specific ligands is leading to an activation of the PI3K/Akt signaling. Additionally, this experiment was carried out to validate if these growth factors show similar effects regarding Akt phosphorylation as cells stimulated with CAF-CM. Hence, HCT116 cells were cultured in 6-well plates for 48 hours and starved for 24 hours. After starvation, cells were treated with the inhibitors OSI-906 and JNJ-38877605 for one hour prior to the addition of CAF-CM or directly by rhIGF-2 and rhHGF addition for 15 minutes to the starvation medium. A near-infrared Western blot was performed to detect p-Akt (Ser473) levels. GAPDH was used as a loading control. MFIs of p-Akt signals were normalized to MFIs of GAPDH. Starved cells were used as control. Cells stimulated with CAF-CM served as positive control for Akt activation and cells treated with MK-2206 prior to the addition of CAF-CM were used as control for Akt inhibition.

In line with our previous results, p-Akt levels in HCT116 cells decreased by more than 50 % compared to the CAF-CM induced control when cells were treated with OSI-906 prior to the addition of CAF-CM. In starved cells and cells treated with MK-2206 almost no p-Akt signals were detectable. Cells stimulated with rhIGF-2 showed high p-Akt levels similar to the positive control for Akt activation (Figure 12A). Similar results were obtained in cells which were stimulated with rhHGF as they showed increased p-Akt levels comparable to cells stimulated with CAF-CM. p-Akt levels decreased when cells were treated with JNJ-388770605 prior to the addition of CAF-CM (Figure 12B).

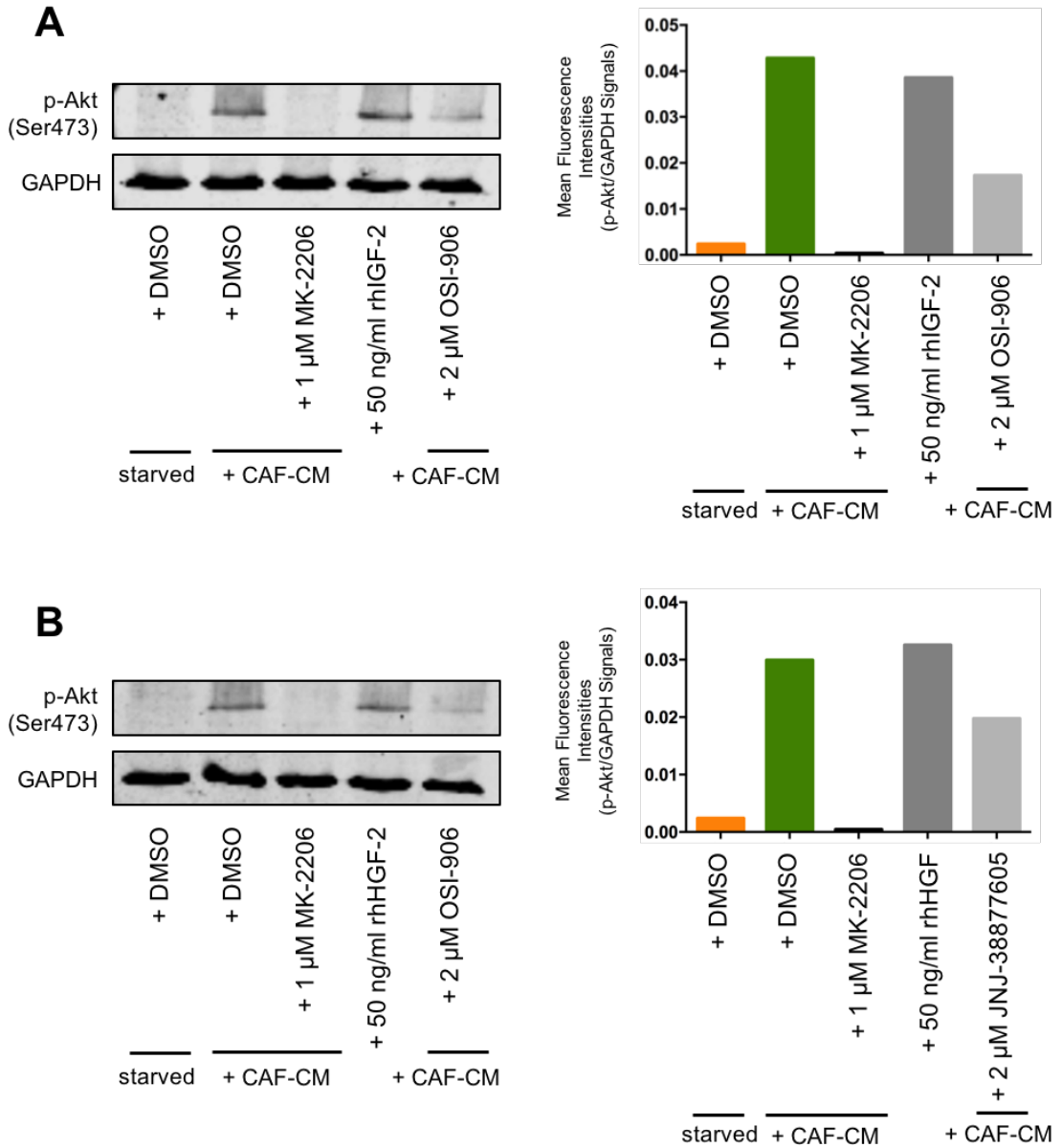


Fig. 12: Determination of the impact of rhIGF-2 and rhHGF on p-Akt levels in HCT116 cells. HCT116 cells were starved for 24 hours and treated with the inhibitors for one hour prior to the stimulation with CAF-CM for 15 minutes. In one approach, cells were stimulated with rhIGF-2 or rhHGF for 15 minutes without inhibitor treatment. Starved cells were used as control and cells stimulated with CAF-CM served as positive control for Akt activation. Cells treated with MK-2206 were used as positive control for Akt inhibition. A near-infrared Western blot was performed to detect p-Akt (Ser473) and GAPDH protein levels. **A:** Cells stimulated with rhIGF-2. Western blot membranes showing p-Akt (Ser473) and GAPDH levels. Bar charts represent the background corrected and normalized MFIs of p-Akt (p-Akt /GAPDH) of the near-infrared Western blot. **B:** Cells stimulated with rhHGF. Western blot membranes showing p-Akt (Ser473) and GAPDH levels. Bar charts represent the background corrected and normalized MFIs of p-Akt (p-Akt /GAPDH) of the near-infrared Western blot.

4.6. Determination of dose responses

In order to determine dose response of increasing inhibitor concentrations, different amounts of OSI-906 and JNJ-38877605 were tested. The aim of this experiment was to find the lowest concentration with the highest efficacy for inhibition of p-Akt levels in HCT116 cells without exceeding inhibitor concentrations above 1 μ M to avoid unspecific side effects. HCT116 cells were cultured in 96-well plates for 48 hours, starved for 24 hours and treated with inhibitor concentrations from 1,000 nM to 30 nM for one hour prior to the addition of CAF-CM for 15 minutes. Inhibitors OSI-906 and JNJ-38877605 were used as single treatments or in combination. In order to detect p-Akt and total Akt levels an ICW assay was performed. MFIs of p-Akt signals were normalized to MFIs of total Akt. Starved cells were used as control. In addition, cells stimulated with CAF-CM served as positive control for Akt activation and cells treated with MK-2206 and stimulated with CAF-CM were used as positive control for Akt inhibition.

Regardless of whether inhibitors were analyzed as single treatment or in combination with each other, a clear dose response curve could be observed indicating proper dose dependent inhibition. When 1,000 nM of the inhibitors were used, p-Akt levels significantly decreased compared to cells stimulated with CAF-CM. This could be seen when cells were treated with OSI-906 or JNJ-38877605 alone or when they were treated with both inhibitors in combination ($p = 0.0014$ for cells treated with OSI-906; $p = 0.0068$ for cells treated with JNJ-38877605; $p = 0.0001$ for cells treated with the combination of OSI-906 and JNJ-38877605). Inhibitor concentrations lower than 1,000 nM (300 nM to 10 nM) couldn't decrease p-Akt levels in HCT116 cells as effective as 1,000 nM (Figure 13).

Hence, further experiments were performed with a concentration of 1,000 nM for OSI-906 and JNJ-38877605.

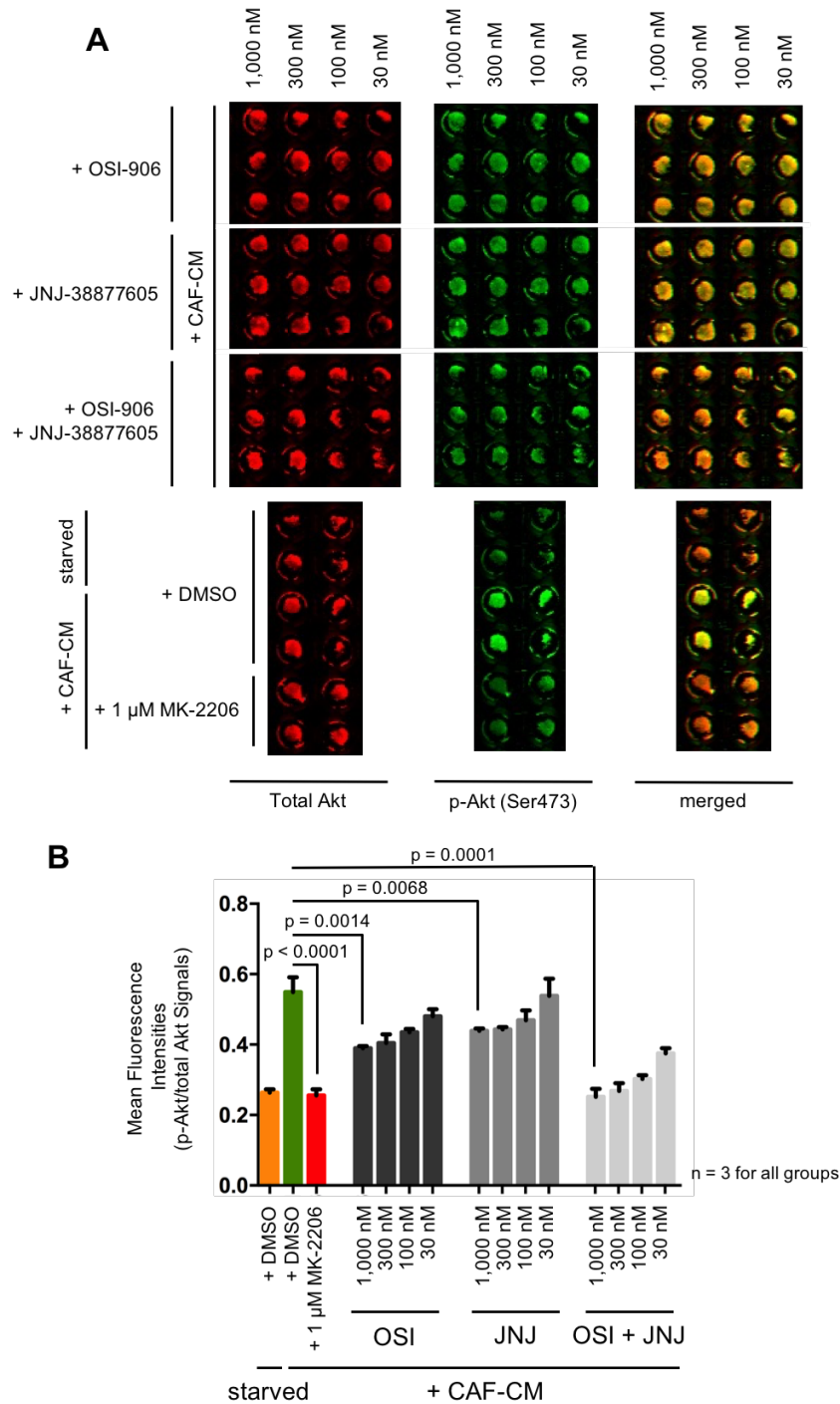


Fig. 13: Determination of dose responses of the selected inhibitors alone or in combination. HCT116 cells were starved for 24 hours and treated with different inhibitor concentrations for one hour prior to Akt activation with CAF-CM for 15 minutes in triplicates ($n = 3$). Subsequently, an ICW assay was performed detecting p-Akt (Ser473) and total Akt levels. Starved cells were used as control. Cells stimulated with CAF-CM served as positive control for Akt activation and cells treated with MK-2206 were used as control for efficient Akt inhibition. **A:** Representative wells of the ICW assay showing p-Akt (Ser473), total Akt and merged channels. **B:** Graphical illustration of the ICW assay. Bar graphs represent the normalized MFIs of p-Akt levels (p-Akt/total Akt) of the ICW assay, error bars display the standard error of the mean. p-values were calculated using a t-test for independent samples (two-tailed, unpaired).

4.7. Testing the impact of JAK inhibitors on p-Akt levels in HCT116 cells

As a substantial amount of JAK inhibitors were found in the top 125 hits of our screening assay, we decided to further analyze this inhibitor category. In HCT116 cells the combination of IGF-1-R/Ins-R and c-Met inhibitors themselves already decreased p-Akt almost to control levels induced by direct inhibition of Akt by MK-2206. Thus, we assumed that in our cellular system JAK signaling is probably downstream of one of the inhibitor targets. In order to test this assumption, HCT116 cells were cultured in a 96-well plate, starved for 24 hours and treated with the inhibitors for one hour prior to CAF-CM stimulation for 15 minutes. A combination of IGF-1-R/Ins-R or c-Met inhibitors and the best selective JAK2 inhibitor targeting wildtype JAK2 namely Fedratinib was used to find out in which of the two pathways JAK2 is presumably involved. Total Akt and p-Akt levels were determined using the ICW method. MFIs of p-Akt signals were normalized to MFIs of total Akt. Starved cells were used as control. Cells stimulated with CAF-CM served as positive control for Akt activation and cells treated with MK-2206 and stimulated with CAF-CM were used as control for efficient Akt inhibition.

In line with the previous experiments and the screening results, p-Akt levels were significantly decreased under all treatment conditions compared to the CAF-CM induced control ($p < 0.0078$ for cells treated with OSI-906 and cells treated with OSI-906 in combination with Fedratinib; $p < 0.0017$ for cells treated JNJ-38877605 and cells treated with JNJ-38877605 in combination with Fedratinib; $p = 0.0033$ for cells treated with Fedratinib; $p < 0.0001$ for cells treated with OSI-906 and JNJ-38877605 or OSI-906 and JNJ-38877605 in combination with Fedratinib). Moreover, a significant difference between cells treated with JNJ-38877605 alone or in combination with Fedratinib was detected ($p = 0.0256$). In contrast, cells which were treated with OSI-906 or OSI-906 and Fedratinib in combination did not show significant changes in Akt phosphorylation. These results would support the idea that JAK2 can be activated downstream of IGF-1-R signaling but not of c-Met signaling, since the inhibition of IGF-1-R signaling by OSI-906 would not lead to JAK2 activation any more and thus Fedratinib would be without effect (Figure 14).

However, a combination of all inhibitors resulted in the most efficient p-Akt inhibition comparable to the MK-2206 control, pointing to a more complex mode of regulation of Akt activity by CAFs in the tumor cells (Figure 14). Hence, we decided to include the JAK inhibitor Fedratinib in our further studies in a separate approach to figure out if a triple combination therapy including all inhibitors is more efficient than a double combination with OSI-906 and JNJ-38877605 regarding cancer cell proliferation, migration and invasion.

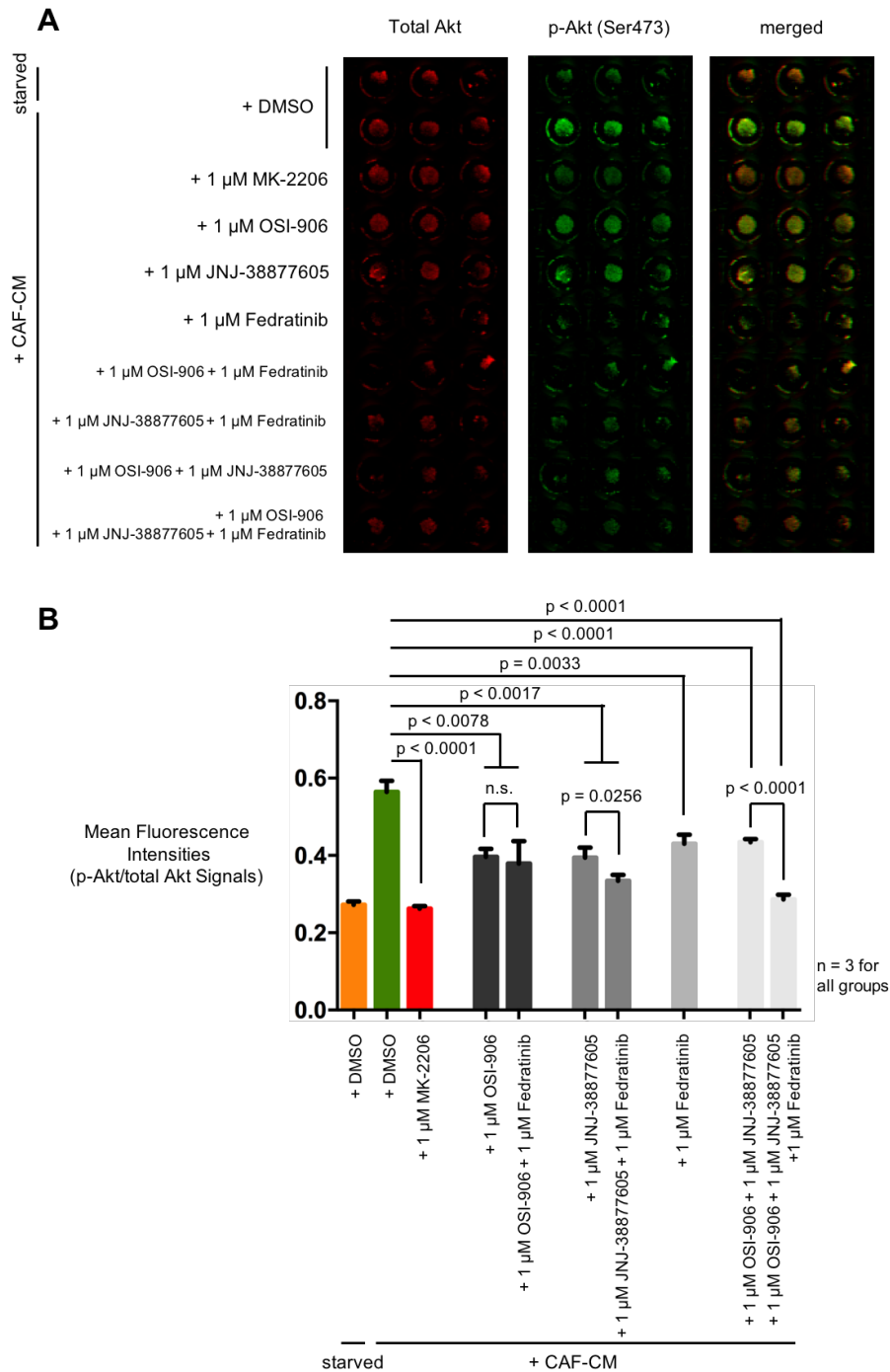


Fig. 14: Testing the impact of the JAK2 inhibitor Fedratinib on p-Akt levels. HCT116 cells were starved for 24 hours and treated with kinase inhibitors for one hour prior to Akt activation with CAF-CM for 15 minutes in triplicates (n = 3). Subsequently, an ICW assay was performed detecting total Akt and p-Akt levels. Starved cells were used as control. Cells stimulated with CAF-CM served as positive control for Akt activation and cells treated with MK-2206 were used as positive control for Akt inhibition. **A:** ICW plates showing p-Akt (Ser473), total Akt and merged channels. **B:** Graphical illustration of the ICW assay. Bar graphs represent the normalized MFIs of p-Akt (p-Akt /total Akt) of the ICW assay, error bars display the standard error of the mean. p-values were calculated using a t-test for independent samples (two-tailed, unpaired).

4.8. Impact of OSI-906, JNJ-38877605 and Fedratinib on cell proliferation in HCT116 cells

As we were interested if OSI-906, JNJ-38877605 and Fedratinib had an impact on cell proliferation, we performed a 7-AAD/Click-iT™ EdU proliferation assay to reliably determine the distribution of cell cycle phases. HCT116 were starved for 24 hours and treated with the inhibitors for another 24 hours in the presence of CAF-CM. Thereafter, cells were incubated with EdU for 30 minutes and harvested. The 7-AAD/1xClick-iT™ EdU proliferation assay was performed according to the manufacturer's instructions as described in chapter 3.5. Starved cells were used as control. Cells stimulated with CAF-CM served as positive control for Akt activation and cells treated with MK-2206 and stimulated with CAF-CM were used as control for efficient Akt inhibition.

In starved cells and cells treated with the Akt inhibitor MK-2206 the percentage of cells in S phase was reduced in contrast to cells stimulated with CAF-CM. These cells showed the highest percentage of cells in S phase. In contrast to that, the percentage of cells in S phase significantly decreased when cells were treated with OSI-906, JNJ-38877605 and Fedratinib in combination ($p = 0.002$). Cells treated with OSI-906 and JNJ-38877605 didn't show a significant decrease in percentage of cells in S phase compared to the positive control (Figure 15 and Figure 16).

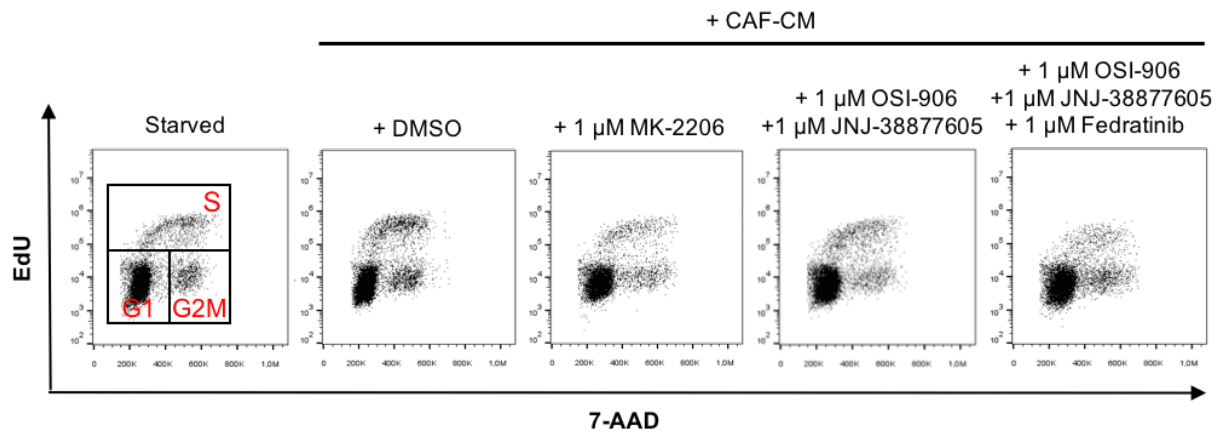


Fig. 15: Dot plot analysis of cells stained with 7-AAD and EdU by flow cytometry. HCT116 cells were starved for 24 hours and treated with OSI-906, JNJ-38877605 and Fedratinib for 24 hours in CAF-CM. EdU was added to the medium and cells were fixed after 30 minutes. Incorporated EdU was stained with the Click-iT™ reaction, total DNA was stained with 7-AAD and analyzed by flow cytometry. Starved cells were used as control. Cells stimulated with CAF-CM served as control for Akt activation and cells treated with MK-2206 were used as positive control for Akt inhibition. Flow cytometry plots show EdU plotted against the total DNA stained by 7-AAD. The first representative plot shows the gates for G1, S and G2M cell cycle phase.

A

		G1 phase			G2/M phase			S phase		
		Batch 1	Batch 2	Batch 3	Batch 1	Batch 2	Batch 3	Batch 1	Batch 2	Batch 3
starved	+ DMSO	80%	80.9 %	84.5 %	8.7 %	9.6 %	7%	11.3 %	9.5 %	8.5 %
	+ DMSO	76.6 %	80.5 %	80.5 %	9.6 %	5.7 %	8.4 %	13.8 %	13.8 %	11.1 %
+ CAF-CM	+ 1 μ M MK-2206	82.9 %	87.4 %	83.5 %	8.4 %	5.4 %	6.6 %	8.7 %	7.2 %	9.9 %
	+ 1 μ M OSI-906 + 1 μ M JNJ-38877605	82.2 %	82.7 %	85.4 %	7.1 %	5.2 %	6.7 %	10.7 %	12.1 %	7.9 %
	+ 1 μ M OSI-906 + 1 μ M JNJ-38877605 + 1 μ M Fedratinib	83.6 %	88.4 %	87.7 %	10.6 %	6%	5.6 %	5.8 %	5.6 %	6.7 %

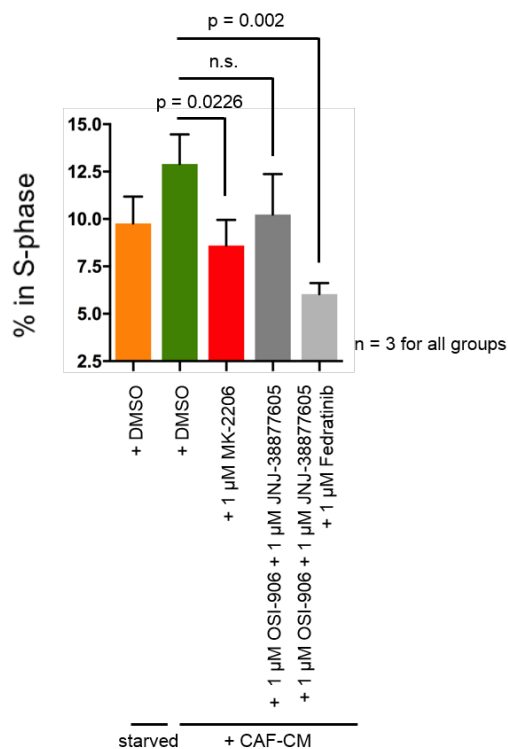
B

Fig. 16: Quantification of the percentage of G1, S and G2/M phase cells with the 7-AAD/EdU assay. The cells from Figure 15 were analyzed in triplicates ($n = 3$) and percentages of cells in G1, S and G2/M were determined. **A:** Percentage of cells in different cell cycle phases from three different batches. **B:** Graphical illustration of the 7-AAD/EdU proliferation assay results from A. Bar charts represent the percentage of cells in S phase, error bars display the standard error of the mean. p-values were calculated using a Mann-Whitney U test.

4.9. Impact of OSI-906, JNJ-38877605 and Fedratinib on cell migration in HCT116 cells

In a next step, we focused on the influence of the inhibitors OSI-906, JNJ-38877605 and Fedratinib on cell migration. Accordingly, a transwell migration assay was performed in duplicates to analyze the migration capacity of HCT116 colon cancer cells in the presence of the inhibitors. After 24 hours, non-migrated cells were removed and migrated cell nuclei were stained with DAPI, photographed (Figure 17) and migration capacities were quantified by determining DAPI fluorescence intensities per frame (Figure 18). Untreated cells were used as control and cells treated with MK-2206 were used as positive control for Akt inhibition.

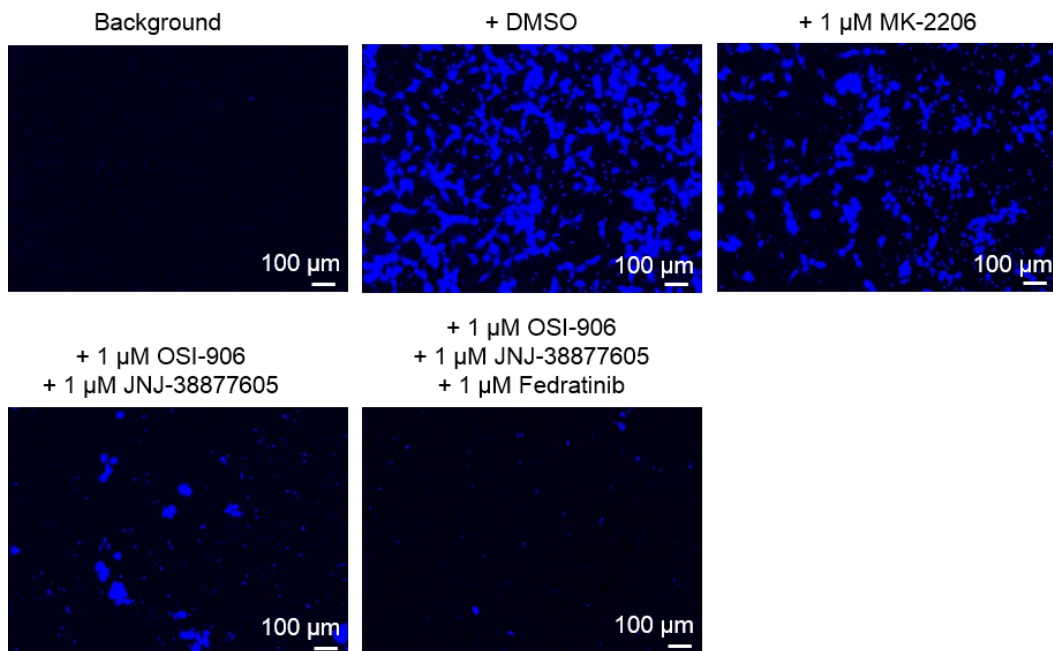


Fig. 17: Representative pictures of the transwell migration assay. HCT116 cells were seeded in transwell chambers using DMEM plain as culture medium. To induce cell migration from the transwell through the membrane CAF-CM was used in the bottom wells. Cells were treated with OSI-906, JNJ-38877605 and Fedratinib for 24 hours. Untreated cells were used as control. Cells treated with MK-2206 were used as positive control for Akt inhibition. Non-migrated cells were removed and migrated nuclei were stained with DAPI. Transwells without cells were used as background control.

Untreated cells stimulated to migrate through the transwell to the well containing CAF-CM displayed high migration capacity. In contrast to that, cells treated with the Akt inhibitor MK-2206 showed a significantly decreased migratory ability ($p < 0.0001$), resulting in a

reduction of migrated cells to less than half. Of note, the DAPI signal further decreased significantly when cells were treated with OSI-906 and JNJ-38877605 in combination compared to untreated cells ($p < 0.0001$) and to MK-2206 treated cells (< 0.0001). Combination of OSI-906, JNJ-38877605 and Fedratinib led to an even more pronounced suppression of migration of HCT116 cells compared to untreated cells ($p < 0.0001$) and MK-2206 treated cells ($p < 0.0001$). Migration capacities of cells treated with OSI-906 and JNJ-38877605 did not significantly differ from cells treated with the triple combination (Figure 18).

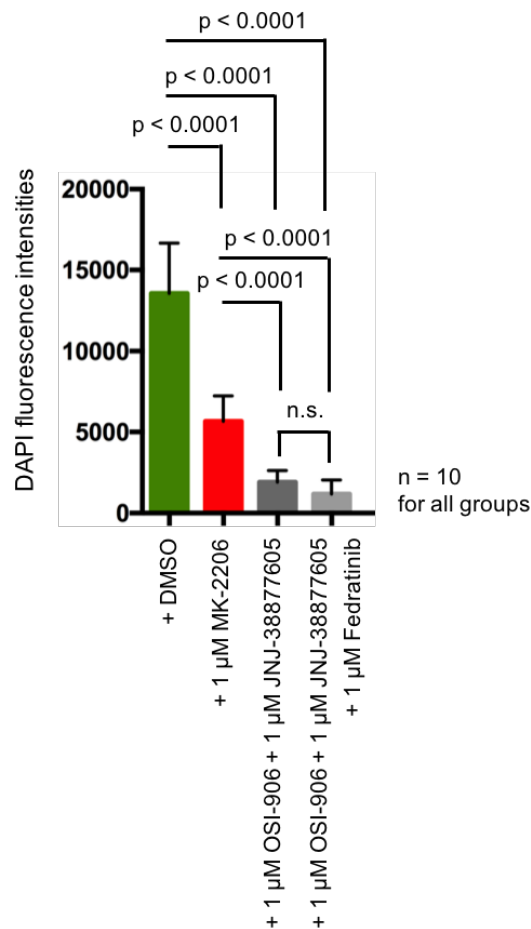


Fig. 18: Quantification of HCT116 cell transwell migration. HCT116 cells were seeded in transwells chambers using DMEM plain as culture medium. To induce cell migration from the transwell through the membrane CAF-CM was used in the lower chamber. Cells were treated with OSI-906, JNJ-38877605 and Fedratinib for 24 hours. Untreated cells were used as control. Cells treated with MK-2206 were used as positive control for Akt inhibition. Non-migrated cells were removed and migrated nuclei were stained with DAPI. Migration capacities were evaluated by determining DAPI fluorescence intensities per frame using ImageJ. Bar charts represent the fluorescence intensities of DAPI stained nuclei migrated through the transwell membrane. Error bars display the standard error of the mean. p-values were calculated using a t-test for independent samples (two-tailed, unpaired). Measured frames per condition: $n = 10$ in two biological replicates.

4.10. Impact of OSI-906, JNJ-38877605 and Fedratinib on cell invasion in HCT116 cells

Finally, we investigated the impact of the inhibitors OSI-906, JNJ-38877605 and Fedratinib on the outgrowth of spheroids in collagen I gels. HCT116 spheroids were embedded in collagen gels and cultured in CAF-CM and DMEM 5 % FCS in a ratio of 1:2 containing either a DMSO control or the inhibitor combinations. After 24 and 96 hours, pictures were taken to compare the outgrowth area of the spheroids. Untreated cells were used as controls and cells treated with MK-2206 were used as positive effective Akt inhibition.

After 24 hours of incubation with the inhibitors, the outgrowth areas of the spheroids appeared similar in each treatment condition as only initial small invasive structures could be observed (Figure 19A). Nevertheless, measuring and comparing the outgrowth area of the spheroids revealed less spreading capacity of spheroids treated with the inhibitor combinations. Spheroids treated with OSI-906 and JNJ-38877605 or OSI-906, JNJ-38877605 and Fedratinib in combination showed significantly smaller outgrowth areas than untreated spheroids ($p < 0.0001$ for both conditions) (Figure 19B). 96 hours after the treatment start, the difference in outgrowth capacity of the spheroids was already visible by eye (Figure 19A). Untreated spheroids showed the most prominent outgrowth, being almost two times larger than the mean area of spheroids treated with the Akt inhibitor MK-2206. When spheroids were treated with OSI-906 and JNJ-38877605 in combination, the invasive area was significantly smaller compared to the invasive areas of untreated cells ($p < 0.0001$). The best results were obtained when OSI-906, JNJ-38877605 and Fedratinib were used as triple treatment. This combination treatment almost lead to a complete inhibition of outgrowth areas, which were significantly smaller compared to untreated cells ($p < 0.0001$) and MK-2206 treated cells ($p < 0.0001$). Additionally, outgrowth areas of cells treated with OSI-906, JNJ-38877605 and Fedratinib were significantly reduced compared to the mean area of spheroids treated with double combination of OSI-906 and JNJ-38877605 ($p < 0.0001$) (Figure 19B).

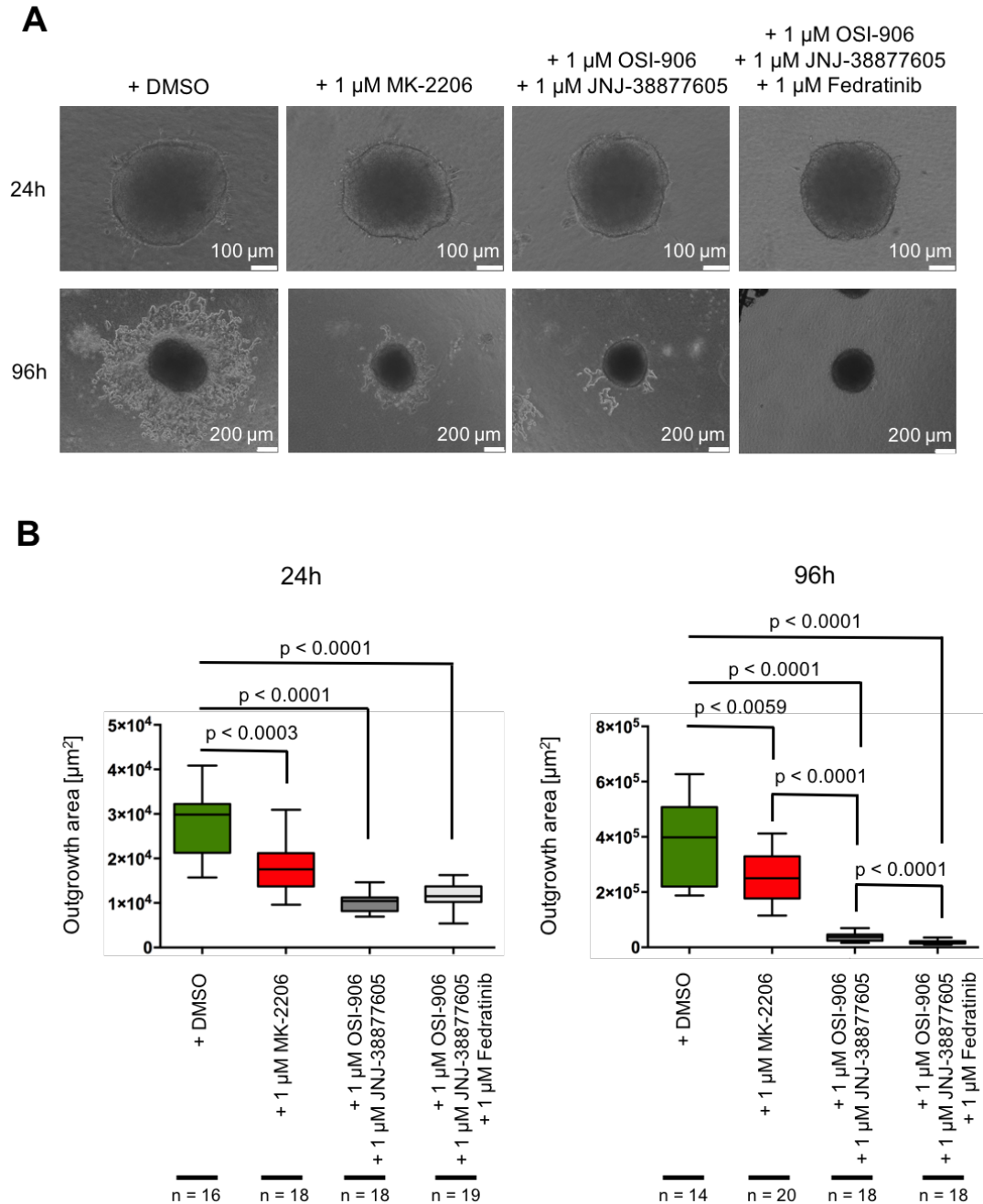


Fig. 19: Spheroid outgrowth assay in collagen I gels. HCT116 spheroids were embedded in collagen type I gels which were cultured in CAF-CM containing OSI-906, JNJ-38877605 and Fedratinib. Untreated spheroids were used as controls and spheroids treated with MK-2206 were used as positive control for Akt inhibition. Evaluation of the spheroid spreading was done after 24 and 96 hours and performed with ImageJ. **A:** Representative pictures of HCT116 spheroids in collagen gels after 24 and 96 hours of treatment. **B:** Quantification of the outgrowth areas. Box-plots represent the interquartile range of the outgrowth area in μm^2 and the end of the whiskers display the minimum and maximum of all data analyzed. p-values were calculated using a t-test for independent samples (two-tailed, unpaired). Total numbers of spheroids analyzed: 24h – no inhibitors (n = 16); + MK-2206 (n = 18); + OSI-906 + JNJ-38877605 (n = 18); + OSI-906 + JNJ-38877605 + Fedratinib (n = 19); 96h – no inhibitors (n = 14); + MK-2206 (n = 20); + OSI-906 + JNJ-38877605 (n = 18); + OSI-906 + JNJ-38877605 + Fedratinib (n = 18).

5. DISCUSSION

Over the last decades, the TME also named tumor stroma, has gained a lot of interest because of its pro-tumorigenic properties. CAFs are the most abundant cells of the tumor stroma. They are similar to normal fibroblasts during inflammation or wound healing but they are permanently activated (Fridman et al. 2019). They support tumor growth, stimulate angiogenesis and metastasis and induce chemoresistance by modulating the tumor stroma or acting on cancer cells directly (Tao et al. 2017). CAFs thereby secrete different growth factors and cytokines which positively influence cancer progression (LeBleu and Kalluri 2018).

In this study, we aimed to find CAF-derived factors or CAF-induced signaling pathways leading to an increased PI3K/Akt signaling in colon cancer cells which has been reported in 60–70 % of all CRC cases and is associated with bad prognosis (Malinowsky et al. 2014). In previous studies, we already showed that IGF-2 derived from CAFs is partially responsible for elevated p-Akt levels, which is commonly regarded as marker for increased PI3K/Akt signaling, in CRC cell lines. Nevertheless, remaining p-Akt levels indicated that there must be other CAF-induced signaling pathways besides IGF-1-R/Ins-R signaling leading to Akt activation in colon cancer cells (Unger et al. 2017). Thus, the research question of this study was: Which upstream signaling cascades other than IGF-1-R signaling activated by CAF-secreted factors lead to the activation of the PI3K/Akt pathway in colon cancer cells?

Therefore, we performed a medium throughput screening with a kinase inhibitor library containing 378 small molecule inhibitors which together target 60 different kinases. In order to activate the PI3K/Akt signaling pathway by CAF-derived factors, HCT116 human colon cancer cells were stimulated with CAF-CM. Subsequently, an ICW assay was accomplished to compare p-Akt levels of cells treated with different inhibitors.

In this screening approach, we anticipated to identify inhibitors directly targeting PI3K, mTOR or Akt as these inhibitors either inhibit Akt directly or prevent the immediate upstream phosphorylation of Akt. Thus, these inhibitors were used as internal quality control for the screen but excluded from further studies since we were interested in further upstream signaling. Indeed, the majority of top hits decreasing p-Akt levels in HCT116 cells are comprised of these inhibitors as 29 out of the top 50 hits were inhibitors targeting PI3K, mTOR or Akt directly. This indicates that the ICW readout is able to reliably identify Akt inhibition. By focusing on the most potent selective inhibitors besides PI3K, mTOR or Akt inhibitors, we found two promising IGF-1-R/Ins-R inhibitors (again validating our previous results on IGF-2

function), two c-Met inhibitors and two JAK inhibitors which downregulated p-Akt most efficiently (Unger et al. 2017) (see Figure 8 and 9).

We verified our primary hits in several validation experiments. In order to confirm their general applicability for CRC, three different human CRC cell lines were tested. Moreover, the technical readout of the ICW assay was verified by Western blotting using phospho specific Akt and total Akt antibodies. Although each cell line slightly differed comparing the inhibitors efficiency to downregulate p-Akt levels, the best overall outcome was achieved by the inhibitors OSI-906 targeting the IGF-1-R/Ins-R and JNJ-38877605 targeting the c-Met receptor (see Figure 10). Fedratinib was the most potent selective JAK2 inhibitor which was detected by implementing an ICW assay (Figure 10). Importantly, by performing a Western blot to validate the data obtained by the IGF-1-R/Ins-R and c-Met inhibitors, we could demonstrate that the ICW method fulfills the necessary quality requirements for our purposes (see Figure 10).

Subsequently, we determined dose response curves to show specific inhibition and to find the appropriate concentrations for OSI-906 and JNJ-38877605 for most efficient Akt inhibition. We could demonstrate that both inhibitors decreased p-Akt levels most efficiently at 1,000 nM whether they were administrated singularly or in combination. Of note, 300 nM of the inhibitors were almost as effective as 1,000 nM leaving the possibility to reduce drug concentrations without essential loss of inhibition (see Figure 13). However, we decided to use 1,000 nM of each drug to maximally inhibit Akt inhibition. Importantly, an evaluation study of the inhibitor OSI-906 reported a half maximal inhibitory concentration (IC₅₀) of 130 nM for the cellular inhibition of p-Akt (Mulvihill et al. 2009). Another study, which compared p-Akt levels in liver cancer cells under treatment with different concentrations of JNJ-38877605, revealed that a concentration of 1 μ M of the c-Met inhibitor was needed to fully inhibit p-Akt (Rebouissou et al. 2017). Hence, our findings regarding the appropriate inhibitor concentration for decreased p-Akt signaling in CRC cells coincides with the concentration determined in other studies. As we decided to include Fedratinib in our study at a later time point, we couldn't test its appropriate concentration regarding the decrease of p-Akt levels in our cellular system due to time restrictions. We followed the manufacturers' recommendations and guidelines regarding the biological activity of Fedratinib and decided to perform our further studies with the same concentration of 1,000 nM as we used for the inhibitors OSI-906 and JNJ-38877605.

After the inhibitor validation, we wanted to identify the actual molecules in CAF-CM leading to PI3K/Akt activation in HCT116 cells. Furthermore, we performed phenotypic assays to evaluate the impact of OSI-906, JNJ-38877605 and Fedratinib on cancer cell proliferation, migration and invasion. These results are discussed in more detail in the next two chapters.

5.1. Activation of IGF-1-R, c-Met and JAK2 by cancer-associated fibroblast-derived factors are responsible for full Akt activation in HCT116 colon cancer cells

OSI-906, also called linsitinib, is a dual inhibitor of the IGF-1-R/Ins-R. IGF-1 and IGF-2 can bind to these receptors and activate the PI3K/Akt and MAPK pathways (Barata et al. 2018). As already mentioned above, we could show that IGF-2 is induced in stromal fibroblasts of colon cancer and can be found in elevated levels in CAF-CM (Unger et al. 2017). These findings can be further confirmed by two other studies which observed an overexpression of IGF-2 mRNA in the tumor stroma of human microdissected CRC samples (Nishida et al. 2012, Calon et al. 2015). Our previous results underline the fact that IGF-2 is among other factors responsible for an increased PI3K/Akt signaling. Indeed, we could demonstrate that HCT116 colon cancer cells responded to rhIGF-2 stimulation by increased p-Akt levels compared to starved cells. Furthermore, we could show that the treatment of CAF-CM stimulated HCT116 cells with the IGF-1-R/Ins-R inhibitor OSI-906 resulted in decreased p-Akt signals which again demonstrates the involvement of Ins-R/IGF-1-R signaling in the PI3K/Akt signaling pathway (see Figure 12A). Stroma-derived IGF-2 and its receptors are potential therapeutic targets in cancer and many strategies were developed to block IGF signaling (Osher and Macaulay 2019). OSI-906 was tested in many clinical studies in patients suffering from prostate cancer, adrenocortical carcinoma or advanced solid tumors with different outcomes (Fassnacht et al. 2015, Jones et al. 2015, Barata et al. 2018). Many molecular approaches with e.g. siRNA and agents to block the IGF-1-R or IGF ligands are currently tested in clinical studies. While preclinical data supported the development of drugs interfering in the IGF axis, no positive clinical trials were conducted in the last years. Nevertheless, exceptional responders to the IGF axis blockade reveal the need to better understand the contribution of the IGF-1-R/Ins-R signaling in cancer progression (Osher and Macaulay 2019).

Furthermore, we found c-Met activation by CAF-CM leading to Akt signaling in colon cancer cells. c-Met receptor activation is associated with increased cell motility, proliferation and morphogenesis in normal development and adult homeostasis. Several downstream molecules can be activated by this RTK such as PI3K (De Silva et al. 2017). Most likely, HGF derived from CAFs is responsible for the activation of c-Met in the tumor cells. In the past, studies already showed that the secretion of HGF is a characteristic feature of CAFs to support tumor cells in many different ways (Tyan et al. 2011, Jia et al. 2013, Suzuki et al. 2019). Indeed, we also found HGF secretion into the medium by CAFs using ELISA (Stadler, 2016). In

addition, elevated HGF mRNA levels could be found in the tumor stroma of CRC samples compared to the epithelial compartment (Nishida et al. 2012, Calon et al. 2015). In this context, it was shown that PI3K/Akt signaling induced by HGF plays a crucial role in several cancer types in regard to angiogenesis or therapy resistance (Ying et al. 2015, Ding et al. 2018b). We could confirm that HCT116 colon cancer cells indeed respond to rhHGF treatment by an upregulation of the PI3K/Akt pathway. Moreover, p-Akt levels decreased when cells were treated with the c-Met inhibitor JNJ-38877605 prior to the stimulation with CAF-CM (see Figure 12B). We compared p-Met levels with p-Akt levels in CRC cells after treatment with JNJ-38877605 and could see similar p-Akt inhibition patterns strongly supporting the notion that Akt is indeed involved in downstream signaling of c-Met in our cell system (see Figure 11B and 12B). Interestingly, the selective Akt inhibitor MK-2206 also downregulated p-Met indicating possible feedback mechanisms in the signaling cascade or off-target effects of this inhibitor (see Figure 11B). In contrast to our findings, Bian *et al.* claimed that Akt inhibition by MK-2206 in non-small lung cancer cells induces c-Met expression and activation as a compensatory response (Bian et al. 2018). These somewhat contradicting data show that further investigation is needed to fully understand the mechanism of action of MK-2206 and to assess the interaction of Akt and Met as compensatory mechanisms. The c-Met inhibitor JNJ-38877605 used for our experiments showed promising results in preclinical studies as oncogenic HGF/c-Met signaling could be blocked successfully (D'Amico et al. 2016, Gao et al. 2017). Unfortunately, a phase I dose-escalation study from 2015 revealed that JNJ-38877605 causes renal toxicity in patients which excluded this inhibitor from further studies (Lolkema et al. 2015). Nevertheless, c-Met inhibitors are promising therapeutic targets as c-Met is amplified in many cancer types (Bahrami et al. 2017). We show here that most likely HGF derived from CAFs can potentially activate the c-Met/Akt signaling axis in CRC cells. Thus, even without amplification of c-Met, strong activation of c-Met/PI3K/Akt signaling in cancer cells can be the result of high HGF levels secreted from CAFs. This opens the possibility that also patients with non-amplified Met in the carcinomas might benefit from a c-Met inhibitor therapy.

The last kinase inhibitor selected from the results of our screen leading to a downregulation of p-Akt in HCT116 cells was the selective JAK2 specific inhibitor Fedratinib. JAK2 is a non-receptor protein kinase and gets activated when cytokines bind to their receptors (Hubbard 2018). Two of these cytokines are IL-6 and IL-11 which can activate JAKs by binding to the IL-6 and IL-11 receptor (Lokau et al. 2017). Elevated IL-6 serum levels are associated with a higher mortality in CRC patients and the concentration of IL-6 in the serum can be used as an indicator for cancer recurrence (Lu et al. 2014). Knowledge on IL-11 is more scarce compared

to IL-6 but it also acts as a potent driver for CRC as inhibiting the IL-11 signaling resulted in a growth arrest of CRC cells and robust inhibition of tumor growth *in vivo* (Putoczki et al. 2013, Heichler et al. 2019). In this regard, CAFs are a widely accepted source of IL-6 and IL-11 (Nagasaki et al. 2014, Huynh et al. 2016, Ma et al. 2019). In addition, previous data from our group showed that IL-6 and IL-11 could be found in high concentrations in CAF-CM and stimulated STAT3, which is a downstream molecule of IL-6/JAK2 signaling, in colon cancer cells. In fact, IL-6 was the main inducer of STAT3 activation whereas IL-11 contributed to STAT3 activation by only 15–20 % (Neuhold, 2018). Thus, it is tempting to speculate that CAF-derived IL-6/IL-11 activates JAK2/STAT3 via IL-6 receptor signaling which obviously also results in Akt activation. These findings are in accordance with other studies which described decreased PI3K/Akt signaling after inhibition or knockdown of JAK2 (Li et al. 2012, Xu and Lv 2016). In this study, we could demonstrate that Fedratinib treated CRC cells, which were stimulated with CAF-CM, showed decreased p-Akt levels comparable to the inhibition with OSI-906 and JNJ-38877605 in contrast to untreated cells. As OSI-906 and JNJ-38877605 in combination already downregulated p-Akt levels similar to the Akt inhibitor MK-2206, we had to exclude that JAK2 is downstream of the IGF-1-R/Ins-R or c-Met. If JAK2 activation was downstream of IGF-1-R or c-Met, the additional inactivation of JAK2 in combination with the respective RTK inhibitors would lead to the same p-Akt levels. Due to time restrictions, we could not completely confirm this hypothesis. On the one hand, we could identify IGF-1-R signaling being potentially upstream of JAK2 in our cells. On the other hand, the strongest decrease of p-Akt levels in HCT116 cells was observed when all three inhibitors were combined, which also could be seen in the phenotypic assays (see below), indicating three distinct signaling routes (Figure 14). Next to its promising effect in our study, Fedratinib is a very encouraging therapeutic agent as it recently received its first approval in the US for the treatment of myelofibrosis patients (Blair 2019).

In conclusion, there is strong evidence generated by this and our previous studies that CAF-derived IGF-2, HGF, IL-6 and to a minor extent IL-11 are responsible for a strong Akt activation in HCT116 colon cancer cells. Nevertheless, further experiments are necessary to confirm the functional involvement and mode of action of these paracrine factors. This would include using neutralizing antibodies or performing knockdowns of the respective genes in CAFs.

5.2. Inhibition of the IGF-1-R/Ins-R, c-Met and JAK-2 in HCT116 colon cancer cells showed impaired proliferation, migration and invasion

After we revealed the signaling pathways leading to the activation of the PI3K/Akt pathway in HCT116 we wanted to analyze the cellular consequences of the inhibition of the pathways by OSI-906, JNJ-38877605 and Fedratinib. Hence, we treated CAF-CM-induced HCT116 cells with a combination of OSI-906 and JNJ-38877605 and compared them to an administration of all three inhibitors together in phenotypic analyses.

First we tested the impact of the inhibitors on cell proliferation by performing a 7-AAD/EdU assay. MK-2206 treatment resulted in a significant reduction of S phase cells, whereas when HCT116 cells were treated with OSI-906 and JNJ-38877605 the percentage of cells in S phase did not differ significantly from the DMSO control. However, a slight decrease was recognizable. Whether the observed drop in S phase is reliable and similar to MK-2206 treatment could only be determined by increasing the number of experiments to gain more statistical power. In contrast to that, cells in S phase were significantly reduced at higher statistical significance when cells were treated with OSI-906, JNJ-38877605 and Fedratinib (see Figure 15 and 16). These results show that a combination of all inhibitors is most efficiently affecting cell proliferation. Our findings correlate with other CRC studies as it was shown that a direct inhibition of the PI3K/Akt pathway by PI3K inhibitors or PI3K knockdown resulted in reduced cell proliferation in HCT116 cells (Yang et al. 2017). Additionally, we could observe that the proliferation abilities of cells treated with a combination of all three inhibitors dropped below those of cells which were treated with the Akt inhibitor MK-2206 (see Figure 15 and 16). As this could not be achieved by the administration of OSI-906 and JNJ-388776065 in combination, we concluded that the JAK2 inhibitor Fedratinib might have additional effects on CAF-CM-induced HCT116 cell proliferation acting on other pathways than PI3K/Akt. Important pathways, which are involved in cell proliferation next to PI3K/Akt, are the MAPK cascades which get activated by mitogens binding to their RTKs (Zhang and Liu 2002). Whereas some studies stated that JAK2 inhibitors also downregulate MAPK pathways in cells, nothing similar is reported for Fedratinib (De Vos et al. 2000, Koppikar et al. 2010). However, it is known that the JAK/STAT pathway interacts with the Ras/MAPK pathway at multiple levels which might explain the efficacy of Fedratinib to downregulate cell proliferation to a greater extent than the treatment with the Akt inhibitor MK-2206 can (Rawlings et al. 2004). Additionally, STAT3, which is constitutively activated in colon cancer, is associated with cancer cell proliferation. Hence,

inhibition of JAK2 and consequently blockage of STAT3 phosphorylation result in decreased CRC cell division (Corvinus et al. 2005, Lin et al. 2011).

After testing the effect of the inhibitors on cell proliferation, we wanted to know if cell migration is reduced by treating cells with OSI-906, JNJ-38877605 and Fedratinib. Indeed, we could demonstrate that cell migration significantly decreased when HCT116 cells were treated with OSI-906 and JNJ-38877605 or OSI-906, JNJ-38877605 and Fedratinib in combination compared to the positive control. The strongest inhibition was observed in the treatment approach using all inhibitors (Figure 18). It is widely accepted that the PI3K/Akt pathway is involved in migration of cancer cells (Fu et al. 2015, Luo et al. 2018, Zhou et al. 2019). Our results confirmed these findings but as already seen before in the proliferation assay, other pathways activated by CAF-CM and signaling via IGF-1-R, c-Met and JAK2 seem to be involved in cell migration since cells treated with MK-2206 showed less reduction in migration than the combination treatment including all three inhibitors. Next to the PI3K/Akt signaling pathway, Rho-family GTPases, which are linked to the MAPK signaling pathways, participate in cell motility (Zohrabian et al. 2009). OSI-906, JNJ-38877605 or Fedratinib might act on upstream kinases involved in these pathways and thereby inhibit cell migration.

Finally, a collagen gel assay was performed to investigate the influence of OSI-906, JNJ-38877605 and Fedratinib on tumor spheroid spreading. Cell invasion, which is involved as initial step in metastasis, is an important topic in cancer as many cancer related deaths are caused by the metastatic spread of tumor cells to vital organs (Justus et al. 2014). The involvement of the PI3K/Akt pathway in cancer cell invasion is already described in several research studies (Meng et al. 2006, Chen et al. 2016). In this study, we could show that the inhibition of the IGF-1-R/Ins-R, c-Met receptor and JAK2 significantly impaired the outgrowth of HCT116 colon cancer cells into the ECM regardless of whether they were treated with OSI-906, JNJ-38877605 in combination or with the triple inhibitor combination including Fedratinib. As these inhibitors lead to decreased p-Akt signals, we can confirm that the PI3K/Akt pathway has a crucial role in spheroid outgrowth. Nevertheless, cells treated with MK-2206, which represents the positive control for Akt inhibition, resulted in larger outgrowth areas compared to cells treated with the two or three inhibitor combinations which indicates that other pathways beside the PI3K/Akt signaling pathway are involved in outgrowth mechanisms in our cellular system (Figure 19). In invasion, similar molecules are involved as during cell migration such as GTPases of the Rho-family (Gerashchenko et al. 2019). Furthermore, an involvement of the MAPK pathways in the regulation of cell invasion and

metastasis has been observed in the past (Janda et al. 2002, Hsieh et al. 2010, Jung et al. 2013, Wang et al. 2013). It is reasonable that cancer cell invasion requires a remodeling of the ECM. Matrix-metalloproteinases (MMPs) play an essential role in metastasis by degrading matrix barriers. It was shown that Akt is involved in MMP expression by e.g. inhibiting their degradation (Park et al. 2001, Guan et al. 2018). These findings together with ours demonstrate the interplay of different pathways to regulate cancer cell invasion.

Although it is generally accepted that the PI3K/Akt pathway is involved in cell proliferation, migration and invasion we could show that the CAF-derived paracrine factors IGF-2, HGF and IL6/11 are most likely responsible for the activation of this pathway. As far as we know, we are the first who demonstrated the parallel involvement of three signal routes induced by these factors in the PI3K/Akt signaling in CRC cells. Thus, with this Master thesis I clarified that IGF-2/IGF-1-R, HGF/c-Met and IL-6/IL-11/JAK2 are the most prominent signaling routes leading to Akt activation in colon cancer cells. Moreover, we clearly demonstrated that the inhibition of downstream kinases of these factors impaired CRC progression *in vitro*.

6. CONCLUSION

In this study, we could show that the inhibitors OSI-906 targeting the IGF-1-R/Ins-R, JNJ-38877605 targeting the c-Met receptor and Fedratinib targeting JAK2 were sufficient to completely block the phosphorylation of Akt at Ser473 in HCT116 colon cancer cells and thereby the pro-tumorigenic effects of Akt signaling. Additionally, we could demonstrate the effectiveness of combined treatments of these inhibitors in reducing cancer cell proliferation, migration and invasion *in vitro*. Based on previous studies from our group or findings of others we conclude that CAF-derived IGF-2, HGF, IL-6 and IL-11 are responsible for the activation of the PI3K/Akt signaling pathway in CRC cells.

We found promising therapeutic targets to perturb the crosstalk between the TME and cancer cells. A combinatory inhibition of the IGF-1-R/Ins-R, c-Met and JAK2 signaling is a possible future treatment approach for cancer therapy. Nevertheless, further research is needed to proof our findings in patient-derived organoids to reveal intertumoral differences regarding the inhibitor treatments and to enable the development of personalized health plans. In addition, analysis *in vivo* need to be conducted by testing the inhibition of the PI3K/Akt signaling pathway in patient-derived xenograft mouse models in order to detect potential side effects when intervening in the tumor/stroma crosstalk by targeting stromal IGF-2, HGF, IL-6 and IL-11 or downstream molecules of these CAF-derived factors.

BIBLIOGRAPHY

- Ahmed Farag AF, Elbarmelgi MY, Azim HA, Abozeid AA, Mashhour AN. 2016. TNMF versus TNM in staging of colorectal cancer. *International Journal of Surgery*, 27:147–150.
- Akhtar M, Haider A, Rashid S, Al-Nabet ADMH. 2019. Paget's „Seed and Soil“ Theory of Cancer Metastasis: An Idea Whose Time has Come. *Advances in Anatomic Pathology*, 26(1):69–74.
- Alguacil-Núñez C, Ferrer-Ortiz I, García-Verdú E, López-Pirez P, Llorente-Cortijo IM, Sainz B. 2018. Current perspectives on the crosstalk between lung cancer stem cells and cancer-associated fibroblasts. *Critical Reviews in Oncology/Hematology*, 125:102–110.
- Alkasalias T, Moyano-Galceran L, Arsenian-Henriksson M, Lehti K. 2018. Fibroblasts in the Tumor Microenvironment: Shield or Spear? *International Journal of Molecular Sciences*, 19(5).
- Arnold M, Sierra MS, Laversanne M, Soerjomataram I, Jemal A, Bray F. 2017. Global patterns and trends in colorectal cancer incidence and mortality. *Gut*, 66(4):683–691.
- Auerbach R, Arensman R, Kubai L, Folkman J. 1975. Tumor-induced angiogenesis: lack of inhibition by irradiation. *International Journal of Cancer*, 15(2):241–245.
- Augsten M. 2014. Cancer-Associated Fibroblasts as Another Polarized Cell Type of the Tumor Microenvironment. *Frontiers in Oncology*, 4.
- Avagliano A, Granato G, Ruocco MR, Romano V, Belviso I, Carfora A, Montagnani S, Arcucci A. 2018. Metabolic Reprogramming of Cancer Associated Fibroblasts: The Slavery of Stromal Fibroblasts. *BioMed Research International*, 2018:1–12.
- Awaji M, Futakuchi M, Heavican T, Iqbal J, Singh RK. 2019. Cancer-Associated Fibroblasts Enhance Survival and Progression of the Aggressive Pancreatic Tumor Via FGF-2 and CXCL8. *Cancer Microenvironment*, 12(1):37–46.
- Bahrami A, Shahidsales S, Khazaei M, Ghayour-Mobarhan M, Maftouh M, Hassanian SM, Avan A. 2017. C-Met as a potential target for the treatment of gastrointestinal cancer: Current status and future perspectives: c-Met in gastrointestinal cancers. *Journal of Cellular Physiology*, 232(10):2657–2673.
- Bainbridge P. 2013. Wound healing and the role of fibroblasts. *Journal of Wound Care*, 22(8):407–408, 410–412.
- Barata P, Cooney M, Tyler A, Wright J, Dreicer R, Garcia JA. 2018. A phase 2 study of OSI-906 (linsitinib, an insulin-like growth factor receptor-1 inhibitor) in patients with asymptomatic or mildly symptomatic (non-opioid requiring) metastatic castrate resistant prostate cancer (CRPC). *Investigational New Drugs*, 36(3):451–457.
- Bartoschek M, Oskolkov N, Bocci M, Lövrot J, Larsson C, Sommarin M, Madsen CD, Lindgren D, Pekar G, Karlsson G, et al. 2018a. Spatially and functionally distinct subclasses of breast cancer-associated fibroblasts revealed by single cell RNA sequencing. *Nature Communications*, 9(1):5150.
- Bartoschek M, Oskolkov N, Bocci M, Lövrot J, Larsson C, Sommarin M, Madsen CD, Lindgren D, Pekar G, Karlsson G, et al. 2018b. Spatially and functionally distinct subclasses of breast cancer-associated fibroblasts revealed by single cell RNA sequencing. *Nature Communications*, 9(1):5150.

- Bergman D, Halje M, Nordin M, Engström W. 2013. Insulin-Like Growth Factor 2 in Development and Disease: A Mini-Review. *Gerontology*, 59(3):240–249.
- Bian C, Liu Z, Li D, Zhen L. 2018. PI3K/AKT inhibition induces compensatory activation of the MET/STAT3 pathway in non-small cell lung cancer. *Oncology Letters*, 15(6):9655–9662.
- Binefa G, Rodríguez-Moranta F, Teule À, Medina-Hayas M. 2014. Colorectal cancer: From prevention to personalized medicine. *World Journal of Gastroenterology : WJG*, 20(22):6786–6808.
- Björk P, Källberg E, Wellmar U, Riva M, Olsson A, He Z, Törngren M, Liberg D, Ivars F, Leanderson T. 2013. Common interactions between S100A4 and S100A9 defined by a novel chemical probe. *PloS One*, 8(5):e63012.
- Blair HA. 2019. Fedratinib: First Approval. 107010 Bytes.
- Bochet L, Lehuédé C, Dauvillier S, Wang YY, Dirat B, Laurent V, Dray C, Guiet R, Maridonneau-Parini I, Le Gonidec S, et al. 2013. Adipocyte-derived fibroblasts promote tumor progression and contribute to the desmoplastic reaction in breast cancer. *Cancer Research*, 73(18):5657–5668.
- Bousoik E, Montazeri Aliabadi H. 2018. “Do We Know Jack” About JAK? A Closer Look at JAK/STAT Signaling Pathway. *Frontiers in Oncology*, 8:287.
- Boussios S, Ozturk MA, Moschetta M, Karathanasi A, Zakynthinakis-Kyriakou N, Katsanos KH, Christodoulou DK, Pavlidis N. 2019. The Developing Story of Predictive Biomarkers in Colorectal Cancer. *Journal of Personalized Medicine*, 9(1).
- Bradbury KE, Murphy N, Key TJ. 2019. Diet and colorectal cancer in UK Biobank: a prospective study. *International Journal of Epidemiology*.
- Bray F, Ferlay J, Soerjomataram I, Siegel RL, Torre LA, Jemal A. 2018. Global cancer statistics 2018: GLOBOCAN estimates of incidence and mortality worldwide for 36 cancers in 185 countries. *CA: a cancer journal for clinicians*, 68(6):394–424.
- Brouwer-Visser J, Huang GS. 2015. IGF2 signaling and regulation in cancer. *Cytokine & Growth Factor Reviews*, 26(3):371–377.
- Bu L, Baba H, Yoshida N, Miyake K, Yasuda T, Uchihara T, Tan P, Ishimoto T. 2019. Biological heterogeneity and versatility of cancer-associated fibroblasts in the tumor microenvironment. *Oncogene*, 38(25):4887–4901.
- Buskermolen M, Cenin DR, Helsingen LM, Guyatt G, Vandvik PO, Haug U, Bretthauer M, Lansdorp-Vogelaar I. 2019. Colorectal cancer screening with faecal immunochemical testing, sigmoidoscopy or colonoscopy: a microsimulation modelling study. *The BMJ*, 367.
- Calon A, Lonardo E, Berenguer-Llargo A, Espinet E, Hernando-Momblona X, Iglesias M, Sevillano M, Palomo-Ponce S, Tauriello DVF, Byrom D, et al. 2015. Stromal gene expression defines poor-prognosis subtypes in colorectal cancer. *Nature Genetics*, 47(4):320–329.
- Campbell I, Polyak K, Haviv I, Eng C, Leone G, Orloff MS, Ostrowski MC. 2009. Clonal Mutations in the Cancer-Associated Fibroblasts: The Case against Genetic Coevolution. *Cancer Research*, 69(17):6765–6769.
- Chen H, Zhou L, Wu X, Li R, Wen J, Sha J, Wen X. 2016. The PI3K/AKT pathway in the pathogenesis of prostate cancer. *Frontiers in Bioscience (Landmark Edition)*, 21:1084–1091.
- Chen X, Song E. 2019. Turning foes to friends: targeting cancer-associated fibroblasts. *Nature Reviews Drug Discovery*, 18(2):99–115.

- Colak S, ten Dijke P. 2017. Targeting TGF- β Signaling in Cancer. *Trends in Cancer*, 3(1):56–71.
- Corvinus FM, Orth C, Moriggl R, Tsareva SA, Wagner S, Pfitzner EB, Baus D, Kaufman R, Huber LA, Zatloukal K, et al. 2005. Persistent STAT3 Activation in Colon Cancer Is Associated with Enhanced Cell Proliferation and Tumor Growth. *Neoplasia*, 7(6):545–555.
- Costa A, Kieffer Y, Scholer-Dahirel A, Pelon F, Bourachot B, Cardon M, Sirven P, Magagna I, Fuhrmann L, Bernard C, et al. 2018. Fibroblast Heterogeneity and Immunosuppressive Environment in Human Breast Cancer. *Cancer Cell*, 33(3):463–479.e10.
- D'Amico L, Belisario D, Migliardi G, Grange C, Bussolati B, D'Amelio P, Perera T, Dalmaso E, Carbonare LD, Godio L, et al. 2016. C-met inhibition blocks bone metastasis development induced by renal cancer stem cells. *Oncotarget*, 7(29):45525–45537.
- Danielsen SA, Eide PW, Nesbakken A, Guren T, Leithe E, Lothe RA. 2015. Portrait of the PI3K/AKT pathway in colorectal cancer. *Biochimica et Biophysica Acta (BBA) - Reviews on Cancer*, 1855(1):104–121.
- DE ROSA M, PACE U, REGA D, COSTABILE V, DURATURO F, IZZO P, DELRIO P. 2015. Genetics, diagnosis and management of colorectal cancer (Review). *Oncology Reports*, 34(3):1087–1096.
- De Silva DM, Roy A, Kato T, Cecchi F, Lee YH, Matsumoto K, Bottaro DP. 2017. Targeting the hepatocyte growth factor/Met pathway in cancer. *Biochemical Society Transactions*, 45(4):855–870.
- De Vos J, Jourdan M, Tarte K, Jasmin C, Klein B. 2000. JAK2 tyrosine kinase inhibitor tyrphostin AG490 downregulates the mitogen-activated protein kinase (MAPK) and signal transducer and activator of transcription (STAT) pathways and induces apoptosis in myeloma cells. *British Journal of Haematology*, 109(4):823–828.
- De Wever O, Demetter P, Mareel M, Bracke M. 2008. Stromal myofibroblasts are drivers of invasive cancer growth. *International Journal of Cancer*, 123(10):2229–2238.
- Delinassios JG. 1987. Cytocidal effects of human fibroblasts on HeLa cells in vitro. *Biology of the Cell*, 59(1):69–77.
- Delinassios JG, Kottaridis SD, Garas J. 1983. Uncontrolled growth of tumour stromal fibroblasts in vitro. *Experimental Cell Biology*, 51(4):201–209.
- Devroede GJ, Taylor WF, Sauer WG, Jackman RJ, Stickler GB. 1971. Cancer risk and life expectancy of children with ulcerative colitis. *The New England Journal of Medicine*, 285(1):17–21.
- Ding X, Ji J, Jiang J, Cai Q, Wang C, Shi M, Yu Y, Zhu Z, Zhang J. 2018a. HGF-mediated crosstalk between cancer-associated fibroblasts and MET-unamplified gastric cancer cells activates coordinated tumorigenesis and metastasis. *Cell Death & Disease*, 9(9):867.
- Ding X, Xi W, Ji J, Cai Q, Jiang J, Shi M, Yu Y, Zhu Z, Zhang J. 2018b. HGF derived from cancer-associated fibroblasts promotes vascularization in gastric cancer via PI3K/AKT and ERK1/2 signaling. *Oncology Reports*, 40(2):1185–1195.
- Dongre A, Weinberg RA. 2019. New insights into the mechanisms of epithelial–mesenchymal transition and implications for cancer. *Nature Reviews Molecular Cell Biology*, 20(2):69–84.

- Dvořánková B, Smetana K, Říhová B, Kučera J, Mateu R, Szabo P. 2015. Cancer-associated fibroblasts are not formed from cancer cells by epithelial-to-mesenchymal transition in nu/nu mice. *Histochemistry and Cell Biology*, 143(5):463–469.
- Ellis MJ, Singer C, Hornby A, Rasmussen A, Cullen KJ. 1994. Insulin-like growth factor mediated stromal-epithelial interactions in human breast cancer. *Breast Cancer Research and Treatment*, 31(2–3):249–261.
- Elyada E, Bolisetty M, Laise P, Flynn WF, Courtois ET, Burkhart RA, Teinor JA, Belleau P, Biffi G, Lucito MS, et al. 2019. Cross-Species Single-Cell Analysis of Pancreatic Ductal Adenocarcinoma Reveals Antigen-Presenting Cancer-Associated Fibroblasts. *Cancer Discovery*, 9(8):1102–1123.
- Fassnacht M, Berruti A, Baudin E, Demeure MJ, Gilbert J, Haak H, Kroiss M, Quinn DI, Hesseltine E, Ronchi CL, et al. 2015. Linsitinib (OSI-906) versus placebo for patients with locally advanced or metastatic adrenocortical carcinoma: a double-blind, randomised, phase 3 study. *The Lancet Oncology*, 16(4):426–435.
- Fearon ER. 2011. Molecular Genetics of Colorectal Cancer. *Annual Review of Pathology: Mechanisms of Disease*, 6(1):479–507.
- Fridman WH, Miller I, Sautès-Fridman C, Byrne AT. 2019. Therapeutic Targeting of the Colorectal Tumor Stroma. *Gastroenterology*, S001650851941442X.
- Fu Q-F, Liu Y, Fan Y, Hua S-N, Qu H-Y, Dong S-W, Li R-L, Zhao M-Y, Zhen Y, Yu X-L, et al. 2015. Alpha-enolase promotes cell glycolysis, growth, migration, and invasion in non-small cell lung cancer through FAK-mediated PI3K/AKT pathway. *Journal of Hematology & Oncology*, 8(1):22.
- Funa K, Sasahara M. 2014. The roles of PDGF in development and during neurogenesis in the normal and diseased nervous system. *Journal of Neuroimmune Pharmacology: The Official Journal of the Society on NeuroImmune Pharmacology*, 9(2):168–181.
- Gao P, Li C, Chang Z, Wang X, Xuan M. 2017. Carcinoma associated fibroblasts derived from oral squamous cell carcinoma promote lymphangiogenesis via c-Met/PI3K/AKT in *in vitro*. *Oncology Letters*.
- Garamszegi N, Garamszegi SP, Samavarchi-Tehrani P, Walford E, Schneiderbauer MM, Wrana JL, Scully SP. 2010. Extracellular matrix-induced transforming growth factor- β receptor signaling dynamics. *Oncogene*, 29(16):2368–2380.
- Gerashchenko TS, Novikov NM, Krakhmal NV, Zolotaryova SY, Zavyalova MV, Cherdyntseva NV, Denisov EV, Perelmuter VM. 2019. Markers of Cancer Cell Invasion: Are They Good Enough? *Journal of Clinical Medicine*, 8(8).
- Guan B, Yan R, Huang J-W, Li F-L, Zhong Y-X, Chen Y, Liu F-N, Hu B, Huang S-B, Yin L-H. 2018. Activation of G protein coupled estrogen receptor (GPER) promotes the migration of renal cell carcinoma via the PI3K/AKT/MMP-9 signals. *Cell Adhesion & Migration*, 12(2):109–117.
- Hawinkels LJAC, Paauwe M, Verspaget HW, Wiercinska E, van der Zon JM, van der Ploeg K, Koelink PJ, Lindeman JHN, Mesker W, ten Dijke P, et al. 2014. Interaction with colon cancer cells hyperactivates TGF- β signaling in cancer-associated fibroblasts. *Oncogene*, 33(1):97–107.

- Heichler C, Scheibe K, Schmied A, Geppert CI, Schmid B, Wirtz S, Thoma O-M, Kramer V, Waldner MJ, Büttner C, et al. 2019. STAT3 activation through IL-6/IL-11 in cancer-associated fibroblasts promotes colorectal tumour development and correlates with poor prognosis. *Gut*, gutjnl-2019-319200.
- Hemmings BA, Restuccia DF. 2012. PI3K-PKB/Akt Pathway. *Cold Spring Harbor Perspectives in Biology*, 4(9).
- Holohan C, Van Schaeybroeck S, Longley DB, Johnston PG. 2013. Cancer drug resistance: an evolving paradigm. *Nature Reviews Cancer*, 13(10):714–726.
- Hossen MdN, Rao G, Dey A, Robertson JD, Bhattacharya R, Mukherjee P. 2019. Gold Nanoparticle Transforms Activated Cancer-Associated Fibroblasts to Quiescence. *ACS Applied Materials & Interfaces*, 11(29):26060–26068.
- Hoxhaj G, Manning BD. 2019. The PI3K–AKT network at the interface of oncogenic signalling and cancer metabolism. *Nature Reviews Cancer*.
- Hsieh M-J, Chen K-S, Chiou H-L, Hsieh Y-S. 2010. Carbonic anhydrase XII promotes invasion and migration ability of MDA-MB-231 breast cancer cells through the p38 MAPK signaling pathway. *European Journal of Cell Biology*, 89(8):598–606.
- Huang H, Hagopian M, Du W, Zhang Y, Driscoll KE, Brekken RA. 2018. Abstract B68: Targeted inhibition of Tgfr2 reduces IL-6 production from cancer-associated fibroblasts, suppresses Stat3 activation in pancreatic cancer cells and reverses immunosuppression. *Tumor Microenvironment*. B68–B68, American Association for Cancer Research;
- Hubbard SR. 2018. Mechanistic Insights into Regulation of JAK2 Tyrosine Kinase. *Frontiers in Endocrinology*, 8:361.
- Hughes LAE, Simons CCJM, van den Brandt PA, van Engeland M, Weijnenberg MP. 2017. Lifestyle, Diet, and Colorectal Cancer Risk According to (Epi)genetic Instability: Current Evidence and Future Directions of Molecular Pathological Epidemiology. *Current Colorectal Cancer Reports*, 13(6):455–469.
- Huynh PT, Beswick EJ, Coronado YA, Johnson P, O'Connell MR, Watts T, Singh P, Qiu S, Morris K, Powell DW, et al. 2016. CD90+ stromal cells are the major source of IL-6 which supports cancer stem-like cells and inflammation in colorectal cancer. *International journal of cancer*, 138(8):1971–1981.
- Imada K, Leonard WJ. 2000. The Jak-STAT pathway. *Molecular Immunology*, 37(1–2):1–11.
- Iwano M, Plieth D, Danoff TM, Xue C, Okada H, Neilson EG. 2002. Evidence that fibroblasts derive from epithelium during tissue fibrosis. *The Journal of Clinical Investigation*, 110(3):341–350.
- Jain RK, Lahdenranta J, Fukumura D. 2008. Targeting PDGF Signaling in Carcinoma-Associated Fibroblasts Controls Cervical Cancer in Mouse Model. *PLoS Medicine*, 5(1):e24.
- Janda E, Lehmann K, Killisch I, Jechlinger M, Herzig M, Downward J, Beug H, Grünert S. 2002. Ras and TGF[β] cooperatively regulate epithelial cell plasticity and metastasis: dissection of Ras signaling pathways. *The Journal of Cell Biology*, 156(2):299–313.
- Jia C-C, Wang T-T, Liu W, Fu B-S, Hua X, Wang G-Y, Li T-J, Li X, Wu X-Y, Tai Y, et al. 2013. Cancer-associated fibroblasts from hepatocellular carcinoma promote malignant cell proliferation by HGF secretion. *PLoS One*, 8(5):e63243.

- Johnson DE, O'Keefe RA, Grandis JR. 2018. Targeting the IL-6/JAK/STAT3 signalling axis in cancer. *Nature reviews. Clinical oncology*, 15(4):234–248.
- Jones RL, Kim ES, Nava-Parada P, Alam S, Johnson FM, Stephens AW, Simantov R, Poondru S, Gedrich R, Lippman SM, et al. 2015. Phase I Study of Intermittent Oral Dosing of the Insulin-like Growth Factor-1 and Insulin Receptors Inhibitor OSI-906 in Patients With Advanced Solid Tumors. *Clinical Cancer Research*, 21(4):693–700.
- Jung MK, Houh YK, Ha S, Yang Y, Kim D, Kim TS, Yoon SR, Bang SI, Cho BJ, Lee WJ, et al. 2013. Recombinant Erdr1 suppresses the migration and invasion ability of human gastric cancer cells, SNU-216, through the JNK pathway. *Immunology Letters*, 150(1–2):145–151.
- Justus CR, Leffler N, Ruiz-Echevarria M, Yang LV. 2014. In vitro Cell Migration and Invasion Assays. *Journal of Visualized Experiments : JoVE*, (88).
- Kadel D, Zhang Y, Sun H-R, Zhao Y, Dong Q-Z, Qin L. 2019. Current perspectives of cancer-associated fibroblast in therapeutic resistance: potential mechanism and future strategy. *Cell Biology and Toxicology*.
- Kahounová Z, Kurfürstová D, Bouchal J, Kharaishvili G, Navrátil J, Remšík J, Šimečková Š, Študent V, Kozubík A, Souček K. 2018. The fibroblast surface markers FAP, anti-fibroblast, and FSP are expressed by cells of epithelial origin and may be altered during epithelial-to-mesenchymal transition. *Cytometry. Part A: The Journal of the International Society for Analytical Cytology*, 93(9):941–951.
- Kasprzak, Adamek. 2019. Insulin-Like Growth Factor 2 (IGF2) Signaling in Colorectal Cancer—from Basic Research to Potential Clinical Applications. *International Journal of Molecular Sciences*, 20(19):4915.
- Keum N, Giovannucci E. 2019. Global burden of colorectal cancer: emerging trends, risk factors and prevention strategies. *Nature Reviews. Gastroenterology & Hepatology*.
- Kim JH. 2015. Chemotherapy for colorectal cancer in the elderly. *World Journal of Gastroenterology : WJG*, 21(17):5158–5166.
- Klemm F, Joyce JA. 2015. Microenvironmental regulation of therapeutic response in cancer. *Trends in Cell Biology*, 25(4):198–213.
- Kolligs FT. 2016. Diagnostics and Epidemiology of Colorectal Cancer. *Visceral Medicine*, 32(3):158–164.
- Konstorum A, Lowengrub JS. 2018. Activation of the HGF/c-Met axis in the tumor microenvironment: a multispecies model. *Journal of theoretical biology*, 439:86–99.
- Koppikar P, Abdel-Wahab O, Hedvat C, Marubayashi S, Patel J, Goel A, Kucine N, Gardner JR, Combs AP, Vaddi K, et al. 2010. Efficacy of the JAK2 inhibitor INCB16562 in a murine model of MPLW515L-induced thrombocytosis and myelofibrosis. *Blood*, 115(14):2919–2927.
- Kuipers EJ, Grady WM, Lieberman D, Seufferlein T, Sung JJ, Boelens PG, van de Velde CJH, Watanabe T. 2015. Colorectal cancer. *Nature Reviews Disease Primers*, 1(1).
- Kuzet S-E, Gaggioli C. 2016. Fibroblast activation in cancer: when seed fertilizes soil. *Cell and Tissue Research*, 365(3):607–619.
- Lambrechts D, Wauters E, Boeckx B, Aibar S, Nittner D, Burton O, Bassez A, Decaluwé H, Pircher A, Van den Eynde K, et al. 2018. Phenotype molding of stromal cells in the lung tumor microenvironment. *Nature Medicine*, 24(8):1277–1289.

- Langer R, Conn H, Vacanti J, Haudenschild C, Folkman J. 1980. Control of tumor growth in animals by infusion of an angiogenesis inhibitor. *Proceedings of the National Academy of Sciences of the United States of America*, 77(7):4331–4335.
- LeBleu VS, Kalluri R. 2018. A peek into cancer-associated fibroblasts: origins, functions and translational impact. *Disease Models & Mechanisms*, 11(4):dmm029447.
- Lee M, Rhee I. 2017. Cytokine Signaling in Tumor Progression. *Immune Network*, 17(4):214.
- Li B, Zhang G, Li C, He D, Li X, Zhang C, Tang F, Deng X, Lu J, Tang Y, et al. 2012. Identification of JAK2 as a Mediator of FIP1L1-PDGFR α -Induced Eosinophil Growth and Function in CEL. *PLoS ONE*, 7(4):e34912.
- Li H, Courtois ET, Sengupta D, Tan Y, Chen KH, Goh JLL, Kong SL, Chua C, Hon LK, Tan WS, et al. 2017. Reference component analysis of single-cell transcriptomes elucidates cellular heterogeneity in human colorectal tumors. *Nature Genetics*, 49(5):708–718.
- Liao Z, Tan ZW, Zhu P, Tan NS. 2019. Cancer-associated fibroblasts in tumor microenvironment - Accomplices in tumor malignancy. *Cellular Immunology*, 343:103729.
- Lin L, Liu A, Peng Z, Lin H-J, Li P-K, Li C, Lin J. 2011. STAT3 Is Necessary for Proliferation and Survival in Colon Cancer-Initiating Cells. *Cancer Research*, 71(23):7226–7237.
- Liu T, Han C, Wang S, Fang P, Ma Z, Xu L, Yin R. 2019. Cancer-associated fibroblasts: an emerging target of anti-cancer immunotherapy. *Journal of Hematology & Oncology*, 12(1).
- Lo A, Wang L-CS, Scholler J, Monslow J, Avery D, Newick K, O'Brien S, Evans RA, Bajor DJ, Clendenin C, et al. 2015. Tumor-Promoting Desmoplasia Is Disrupted by Depleting FAP-Expressing Stromal Cells. *Cancer Research*, 75(14):2800–2810.
- Lokau J, Agthe M, Flynn CM, Garbers C. 2017. Proteolytic control of Interleukin-11 and Interleukin-6 biology. *Biochimica et Biophysica Acta (BBA) - Molecular Cell Research*, 1864(11):2105–2117.
- Lolkema MP, Bohets HH, Arkenau H-T, Lampo A, Barale E, de Jonge MJA, van Doorn L, Helleman P, de Bono JS, Eskens FALM. 2015. The c-Met Tyrosine Kinase Inhibitor JNJ-38877605 Causes Renal Toxicity through Species-Specific Insoluble Metabolite Formation. *Clinical Cancer Research*, 21(10):2297–2304.
- Lu C-C, Kuo H-C, Wang F-S, Jou M-H, Lee K-C, Chuang J-H. 2014. Upregulation of TLRs and IL-6 as a Marker in Human Colorectal Cancer. *International Journal of Molecular Sciences*, 16(1):159–177.
- Lu P, Takai K, Weaver VM, Werb Z. 2011. Extracellular Matrix Degradation and Remodeling in Development and Disease. *Cold Spring Harbor Perspectives in Biology*, 3(12).
- Luo K-W, Lung W-Y, Chun-Xie, Luo X-L, Huang W-R. 2018. EGCG inhibited bladder cancer T24 and 5637 cell proliferation and migration via PI3K/AKT pathway. *Oncotarget*, 9(15):12261–12272.
- Ma J, Song X, Xu X, Mou Y. 2019. Cancer-Associated Fibroblasts Promote the Chemoresistance in Gastric Cancer through Secreting IL-11 Targeting JAK/STAT3/Bcl2 Pathway. *Cancer Research and Treatment: Official Journal of Korean Cancer Association*, 51(1):194–210.
- Malinowsky K, Nitsche U, Janssen K-P, Bader FG, Späth C, Drecoll E, Keller G, Höfler H, Slotta-Huspenina J, Becker K-F. 2014. Activation of the PI3K/AKT pathway correlates with prognosis in stage II colon cancer. *British Journal of Cancer*, 110(8):2081–2089.

- Maman S, Witz IP. 2018. A history of exploring cancer in context. *Nature Reviews. Cancer*, 18(6):359–376.
- Marley AR, Nan H. 2016. Epidemiology of colorectal cancer. *International Journal of Molecular Epidemiology and Genetics*, 7(3):105–114.
- Mármol I, Sánchez-de-Diego C, Pradilla Dieste A, Cerrada E, Rodríguez Yoldi MJ. 2017. Colorectal Carcinoma: A General Overview and Future Perspectives in Colorectal Cancer. *International Journal of Molecular Sciences*, 18(1).
- McDonald LT, Russell DL, Kelly RR, Xiong Y, Motamarry A, Patel RK, Jones JA, Watson PM, Turner DP, Watson DK, et al. 2015. Hematopoietic Stem Cell–Derived Cancer–Associated Fibroblasts Are Novel Contributors to the Pro-Tumorigenic Microenvironment. *Neoplasia (New York, N.Y.)*, 17(5):434–448.
- Meng Q, Xia C, Fang J, Rojanasakul Y, Jiang B-H. 2006. Role of PI3K and AKT specific isoforms in ovarian cancer cell migration, invasion and proliferation through the p70S6K1 pathway. *Cellular Signalling*, 18(12):2262–2271.
- Miao L, Liu Q, Lin CM, Luo C, Wang Y, Liu L, Yin W, Hu S, Kim WY, Huang L. 2017. Targeting Tumor-associated Fibroblasts for Therapeutic Delivery in Desmoplastic Tumors. *Cancer research*, 77(3):719–731.
- Micallef L, Vedrenne N, Billet F, Coulomb B, Darby IA, Desmoulière A. 2012. The myofibroblast, multiple origins for major roles in normal and pathological tissue repair. *Fibrogenesis & Tissue Repair*, 5(Suppl 1):S5.
- Mishra PJ, Mishra PJ, Humeniuk R, Medina DJ, Alexe G, Mesirov JP, Ganesan S, Glod JW, Banerjee D. 2008. Carcinoma Associated Fibroblast Like Differentiation of Human Mesenchymal Stem Cells. *Cancer research*, 68(11):4331–4339.
- Mitra AK, Zillhardt M, Hua Y, Tiwari P, Murmann AE, Peter ME, Lengyel E. 2012. MicroRNAs Reprogram Normal Fibroblasts into Cancer Associated Fibroblasts in Ovarian Cancer. *Cancer discovery*, 2(12):1100–1108.
- Monteiro Araujo A, Abaurrea A, Lawrie C, Caffarel M. 2018. PO-290 Oncostatin M signalling mediates the crosstalk between cancer cells and tumour microenvironment and promotes breast cancer progression. *Tumour Microenvironment*. A341.1-A341, BMJ Publishing Group Ltd;
- Mpekris F, Papageorgis P, Polydorou C, Voutouri C, Kalli M, Pirentis AP, Stylianopoulos T. 2017. Sonic-hedgehog pathway inhibition normalizes desmoplastic tumor microenvironment to improve chemo- and nanotherapy. *Journal of Controlled Release*, 261:105–112.
- Mulvihill MJ, Cooke A, Rosenfeld-Franklin M, Buck E, Foreman K, Landfair D, O'Connor M, Pirritt C, Sun Y, Yao Y, et al. 2009. Discovery of OSI-906: a selective and orally efficacious dual inhibitor of the IGF-1 receptor and insulin receptor. *Future Medicinal Chemistry*, 1(6):1153–1171.
- Nagasaki T, Hara M, Nakanishi H, Takahashi H, Sato M, Takeyama H. 2014. Interleukin-6 released by colon cancer-associated fibroblasts is critical for tumour angiogenesis: anti-interleukin-6 receptor antibody suppressed angiogenesis and inhibited tumour–stroma interaction. *British Journal of Cancer*, 110(2):469–478.

- Neuhold P. 2018. Interaction dependent changes of signaling pathways in cancer-associated fibroblasts and colon carcinoma cells. Master Thesis, University of Applied Sciences FH Campus Vienna.
- Nishida N, Nagahara M, Sato T, Mimori K, Sudo T, Tanaka F, Shibata K, Ishii H, Sugihara K, Doki Y, et al. 2012. Microarray analysis of colorectal cancer stromal tissue reveals upregulation of two oncogenic miRNA clusters. *Clinical Cancer Research: An Official Journal of the American Association for Cancer Research*, 18(11):3054–3070.
- Nurmik M, Ullmann P, Rodriguez F, Haan S, Letellier E. 2019. In search of definitions: Cancer-associated fibroblasts and their markers. *International Journal of Cancer*.
- Öhlund D, Handly-Santana A, Biffi G, Elyada E, Almeida AS, Ponz-Sarvise M, Corbo V, Oni TE, Hearn SA, Lee EJ, et al. 2017. Distinct populations of inflammatory fibroblasts and myofibroblasts in pancreatic cancer. *The Journal of Experimental Medicine*, 214(3):579–596.
- Okumura T, Ohuchida K, Kibe S, Iwamoto C, Ando Y, Takesue S, Nakayama H, Abe T, Endo S, Koikawa K, et al. 2019. Adipose tissue-derived stromal cells are sources of cancer-associated fibroblasts and enhance tumor progression by dense collagen matrix. *International Journal of Cancer*, 144(6):1401–1413.
- Oruç Z, Kaplan MA. 2019. Effect of exercise on colorectal cancer prevention and treatment. *World Journal of Gastrointestinal Oncology*, 11(5):348–366.
- Osher E, Macaulay VM. 2019. Therapeutic Targeting of the IGF Axis. *Cells*, 8(8).
- Österreicher CH, Penz-Österreicher M, Grivennikov SI, Guma M, Koltsova EK, Datz C, Sasik R, Hardiman G, Karin M, Brenner DA. 2011. Fibroblast-specific protein 1 identifies an inflammatory subpopulation of macrophages in the liver. *Proceedings of the National Academy of Sciences of the United States of America*, 108(1):308–313.
- Özdemir BC, Pentcheva-Hoang T, Carstens JL, Zheng X, Wu C-C, Simpson T, Laklai H, Sugimoto H, Kahlert C, Novitskiy SV, et al. 2014. Depletion of Carcinoma-Associated Fibroblasts and Fibrosis Induces Immunosuppression and Accelerates Pancreas Cancer with Diminished Survival. *Cancer cell*, 25(6):719–734.
- Park BK, Zeng X, Glazer RI. 2001. Akt1 induces extracellular matrix invasion and matrix metalloproteinase-2 activity in mouse mammary epithelial cells. *Cancer Research*, 61(20):7647–7653.
- Pavrides S, Whitaker-Menezes D, Castello-Cros R, Flomenberg N, Witkiewicz AK, Frank PG, Casimiro MC, Wang C, Fortina P, Addya S, et al. 2009. The reverse Warburg effect: Aerobic glycolysis in cancer associated fibroblasts and the tumor stroma. *Cell Cycle*, 8(23):3984–4001.
- Pezzella F, Tavassoli M, Kerr DJ. 2019. *Oxford Textbook of Cancer Biology*. Oxford University Press.
- Poltavets V, Kochetkova M, Pitson SM, Samuel MS. 2018. The Role of the Extracellular Matrix and Its Molecular and Cellular Regulators in Cancer Cell Plasticity. *Frontiers in Oncology*, 8.
- Prakash J. 2016. Cancer-Associated Fibroblasts: Perspectives in Cancer Therapy. *Trends in Cancer*, 2(6):277–279.
- Punt CJA, Koopman M, Vermeulen L. 2017. From tumour heterogeneity to advances in precision treatment of colorectal cancer. *Nature Reviews Clinical Oncology*, 14(4):235–246.
- Puré E, Blomberg R. 2018. Pro-tumorigenic roles of fibroblast activation protein in cancer: back to the basics. *Oncogene*, 37(32):4343–4357.

- Putoczki TL, Thiem S, Loving A, Busuttill RA, Wilson NJ, Ziegler PK, Nguyen PM, Preaudet A, Farid R, Edwards KM, et al. 2013. Interleukin-11 is the dominant IL-6 family cytokine during gastrointestinal tumorigenesis and can be targeted therapeutically. *Cancer Cell*, 24(2):257–271.
- Quante M, Tu SP, Tomita H, Gonda T, Wang SSW, Takashi S, Baik GH, Shibata W, DiPrete B, Betz KS, et al. 2011. Bone Marrow-Derived Myofibroblasts Contribute to the Mesenchymal Stem Cell Niche and Promote Tumor Growth. *Cancer Cell*, 19(2):257–272.
- Rawlings JS, Rosler KM, Harrison DA. 2004. The JAK/STAT signaling pathway. *Journal of Cell Science*, 117(8):1281–1283.
- Rebouissou S, La Bella T, Rekik S, Imbeaud S, Calatayud A-L, Rohr-Udilova N, Martin Y, Couchy G, Bioulac-Sage P, Grasl-Kraupp B, et al. 2017. Proliferation Markers Are Associated with MET Expression in Hepatocellular Carcinoma and Predict Tivantinib Sensitivity In Vitro. *Clinical Cancer Research: An Official Journal of the American Association for Cancer Research*, 23(15):4364–4375.
- Revathidevi S, Munirajan AK. 2019. Akt in cancer: Mediator and more. *Seminars in Cancer Biology*.
- Ritchie KE, Nör JE. 2013. Perivascular stem cell niche in head and neck cancer. *Cancer Letters*, 338(1):41–46.
- Roberts EW, Deonarine A, Jones JO, Denton AE, Feig C, Lyons SK, Espeli M, Kraman M, McKenna B, Wells RJB, et al. 2013. Depletion of stromal cells expressing fibroblast activation protein- α from skeletal muscle and bone marrow results in cachexia and anemia. *The Journal of Experimental Medicine*, 210(6):1137–1151.
- Sagaert X, Vanstapel A, Verbeek S. 2018. Tumor Heterogeneity in Colorectal Cancer: What Do We Know So Far? *Pathobiology: Journal of Immunopathology, Molecular and Cellular Biology*, 85(1–2):72–84.
- Sandberg TP, Stuart MPME, Oosting J, Tollenaar RAEM, Sier CFM, Mesker WE. 2019. Increased expression of cancer-associated fibroblast markers at the invasive front and its association with tumor-stroma ratio in colorectal cancer. *BMC Cancer*, 19.
- Sangaletti S, Chiodoni C, Tripodo C, Colombo MP. 2017. The good and bad of targeting cancer-associated extracellular matrix. *Current Opinion in Pharmacology*, 35:75–82.
- Santi A, Kugeratski FG, Zanivan S. 2018. Cancer Associated Fibroblasts: The Architects of Stroma Remodeling. *Proteomics*, 18(5–6).
- Schmidt A, Weber OF. 2006. In memoriam of Rudolf Virchow: a historical retrospective including aspects of inflammation, infection and neoplasia. *Contributions to Microbiology*, 13:1–15.
- Sherman MH, Yu RT, Engle DD, Ding N, Atkins AR, Tiriack H, Collisson EA, Connor F, Van Dyke T, Kozlov S, et al. 2014. Vitamin D Receptor-Mediated Stromal Reprogramming Suppresses Pancreatitis and Enhances Pancreatic Cancer Therapy. *Cell*, 159(1):80–93.
- Slattery ML, Lundgreen A, Kadlubar SA, Bondurant KL, Wolff RK. 2013. JAK/STAT/SOCS-signaling pathway and colon and rectal cancer. *Molecular Carcinogenesis*, 52(2):155–166.
- Son GM, Kwon M-S, Shin D-H, Shin N, Ryu D, Kang C-D. 2019. Comparisons of cancer-associated fibroblasts in the intratumoral stroma and invasive front in colorectal cancer. *Medicine*, 98(18).

- Sperr E. 2016. PubMed by Year [Internet]. Available from <http://esperr.github.io/pubmed-by-year/>.
- Stadler M. 2016. Tumor Cell-Fibroblast Interaction Influences Macrophage Recruitment and Polarization in Colon Cancer. Master Thesis, University of Vienna.
- Suzuki E, Yamazaki S, Naito T, Hashimoto H, Okubo S, Udagawa H, Goto K, Tsuboi M, Ochiai A, Ishii G. 2019. Secretion of high amounts of hepatocyte growth factor is a characteristic feature of cancer-associated fibroblasts with EGFR-TKI resistance-promoting phenotype: A study of 18 cases of cancer-associated fibroblasts. *Pathology International*, 69(8):472–480.
- Tao L, Huang G, Song H, Chen Y, Chen L. 2017. Cancer associated fibroblasts: An essential role in the tumor microenvironment. *Oncology Letters*, 14(3):2611–2620.
- Tian F, Tang Z, Song G, Pan Y, He B, Bao Q, Wang S. 2012. Loss of imprinting of IGF2 correlates with hypomethylation of the H19 differentially methylated region in the tumor tissue of colorectal cancer patients. *Molecular Medicine Reports*, 5(6):1536–1540.
- Tsujino T, Seshimo I, Yamamoto H, Ngan CY, Ezumi K, Takemasa I, Ikeda M, Sekimoto M, Matsuura N, Monden M. 2007. Stromal myofibroblasts predict disease recurrence for colorectal cancer. *Clinical Cancer Research: An Official Journal of the American Association for Cancer Research*, 13(7):2082–2090.
- Tyan S-W, Kuo W-H, Huang C-K, Pan C-C, Shew J-Y, Chang K-J, Lee EY-HP, Lee W-H. 2011. Breast Cancer Cells Induce Cancer-Associated Fibroblasts to Secrete Hepatocyte Growth Factor to Enhance Breast Tumorigenesis. *PLoS ONE*, 6(1):e15313.
- Unger C, Kramer N, Unterleuthner D, Scherzer M, Burian A, Rudisch A, Stadler M, Schleder M, Lenhardt D, Riedl A, et al. 2017. Stromal-derived IGF2 promotes colon cancer progression via paracrine and autocrine mechanisms. *Oncogene*, 36(38):5341–5355.
- Valenti G, Quinn HM, Heynen GJJE, Lan L, Holland JD, Vogel R, Wulf-Goldenberg A, Birchmeier W. 2017. Cancer Stem Cells Regulate Cancer-Associated Fibroblasts via Activation of Hedgehog Signaling in Mammary Gland Tumors. *Cancer Research*, 77(8):2134–2147.
- Valkenburg KC, de Groot AE, Pienta KC. 2018. Targeting the tumour stroma to improve cancer therapy. *Nature reviews. Clinical oncology*, 15(6):366–381.
- Walker C, Mojares E, del Río Hernández A. 2018. Role of Extracellular Matrix in Development and Cancer Progression. *International Journal of Molecular Sciences*, 19(10).
- Wang H, An H, Wang B, Liao Q, Li W, Jin X, Cui S, Zhang Y, Ding Y, Zhao L. 2013. miR-133a represses tumour growth and metastasis in colorectal cancer by targeting LIM and SH3 protein 1 and inhibiting the MAPK pathway. *European Journal of Cancer*, 49(18):3924–3935.
- Wang J, Li D, Cang H, Guo B. 2019. Crosstalk between cancer and immune cells: Role of tumor-associated macrophages in the tumor microenvironment. *Cancer Medicine*, 8(10):4709–4721.
- Wang M, Wu C-P, Pan J-Y, Zheng W-W, Cao X-J, Fan G-K. 2015a. Cancer-associated fibroblasts in a human HEP-2 established laryngeal xenografted tumor are not derived from cancer cells through epithelial-mesenchymal transition, phenotypically activated but karyotypically normal. *PloS One*, 10(2):e0117405.
- Wang M, Zhao J, Zhang L, Wei F, Lian Y, Wu Y, Gong Z, Zhang S, Zhou J, Cao K, et al. 2017. Role of tumor microenvironment in tumorigenesis. *Journal of Cancer*, 8(5):761–773.

- Wang Y, Duan H, Yang H, Lin J. 2015b. A pooled analysis of alcohol intake and colorectal cancer. *International Journal of Clinical and Experimental Medicine*, 8(5):6878–6889.
- Watanabe S, Noma K, Ohara T, Kashima H, Sato H, Kato T, Urano S, Katsube R, Hashimoto Y, Tazawa H, et al. 2019. Photoimmunotherapy for cancer-associated fibroblasts targeting fibroblast activation protein in human esophageal squamous cell carcinoma. *Cancer Biology & Therapy*, 20(9):1234–1248.
- William Petersen O, Lind Nielsen H, Gudjonsson T, Villadsen R, Rønnev-Jessen L, Bissell MJ. 2001. The plasticity of human breast carcinoma cells is more than epithelial to mesenchymal conversion. *Breast Cancer Research : BCR*, 3(4):213–217.
- Xu WW, Li B, Guan XY, Chung SK, Wang Y, Yip YL, Law SYK, Chan KT, Lee NPY, Chan KW, et al. 2017. Cancer cell-secreted IGF2 instigates fibroblasts and bone marrow-derived vascular progenitor cells to promote cancer progression. *Nature Communications*, 8.
- Xu Y, Lv S-X. 2016. The effect of JAK2 knockout on inhibition of liver tumor growth by inducing apoptosis, autophagy and anti-proliferation via STATs and PI3K/AKT signaling pathways. *Biomedicine & Pharmacotherapy*, 84:1202–1212.
- Yamagishi H, Kuroda H, Imai Y, Hiraishi H. 2016. Molecular pathogenesis of sporadic colorectal cancers. *Chinese Journal of Cancer*, 35(1):4.
- Yamauchi M, Barker TH, Gibbons DL, Kurie JM. 2018. The fibrotic tumor stroma. *The Journal of Clinical Investigation*, 128(1):16–25.
- Yan G, Fukabori Y, McBride G, Nikolaropolous S, McKeenan WL. 1993. Exon switching and activation of stromal and embryonic fibroblast growth factor (FGF)-FGF receptor genes in prostate epithelial cells accompany stromal independence and malignancy. *Molecular and Cellular Biology*, 13(8):4513–4522.
- Yang F, Gao J-Y, Chen H, Du Z-H, Zhang X-Q, Gao W. 2017. Targeted inhibition of the phosphoinositide 3-kinase impairs cell proliferation, survival, and invasion in colon cancer. *OncoTargets and therapy*, 10:4413–4422.
- Ying L, Zhu Z, Xu Z, He T, Li E, Guo Z, Liu F, Jiang C, Wang Q. 2015. Cancer Associated Fibroblast-Derived Hepatocyte Growth Factor Inhibits the Paclitaxel-Induced Apoptosis of Lung Cancer A549 Cells by Up-Regulating the PI3K/Akt and GRP78 Signaling on a Microfluidic Platform. *PloS One*, 10(6):e0129593.
- Yu M, Tannock IF. 2012. Targeting Tumor Architecture to Favor Drug Penetration: A New Weapon to Combat Chemoresistance in Pancreatic Cancer? *Cancer Cell*, 21(3):327–329.
- Zhang W, Liu HT. 2002. MAPK signal pathways in the regulation of cell proliferation in mammalian cells. *Cell Research*, 12(1):9–18.
- Zhong H, Fazenbaker C, Chen C, Breen S, Huang J, Yao X, Ren P, Yao Y, Herbst R, Hollingsworth RE. 2017. Overproduction of IGF-2 drives a subset of colorectal cancer cells, which specifically respond to an anti-IGF therapeutic antibody and combination therapies. *Oncogene*, 36(6):797–806.
- Zhou W-M, Wu G-L, Huang J, Li J-G, Hao C, He Q-M, Chen X-D, Wang G-X, Tu X-H. 2019. Low expression of PDK1 inhibits renal cell carcinoma cell proliferation, migration, invasion and epithelial mesenchymal transition through inhibition of the PI3K-PDK1-Akt pathway. *Cellular Signalling*, 56:1–14.

Zohrabian VM, Forzani B, Chau Z, Murali R, Jhanwar-Uniyal M. 2009. Rho/ROCK and MAPK signaling pathways are involved in glioblastoma cell migration and proliferation. *Anticancer Research*, 29(1):119–123.

LIST OF FIGURES

Fig. 1:	<i>Schematic illustration of the PI3K/Akt pathway</i>	3
Fig. 2:	<i>Schematic illustration of the JAK/STAT pathway</i>	4
Fig. 3:	<i>Potential origins of cancer-associated fibroblasts</i>	10
Fig. 4:	<i>Markers of cancer-associated fibroblasts</i>	11
Fig. 5:	<i>Workflow In-Cell Western Assay</i>	24
Fig. 6:	<i>Scheme for the determination of the outgrowth area of spheroids used in the spheroid outgrowth assay</i>	33
Fig. 7:	<i>The impact of CAF-CM and DMEM 1 % FCS on p-Akt levels in HCT116 colon cancer cells</i>	35
Fig. 8:	<i>Heatmap of the kinase inhibitor library screening results</i>	37
Fig. 9:	<i>Quantitative effects on p-Akt levels of the top 125 inhibitors of the kinase inhibitor library screen</i>	38
Fig. 10:	<i>Validation of the top hits from the kinase inhibitor library screen by near-infrared Western blot analysis</i>	40
Fig. 11:	<i>Testing on-target specificity of OSI-906 and JNJ-38877605 in HCT116 cells</i>	42
Fig. 12:	<i>Determination of the impact of rhIGF-2 and rhHGF on p-Akt levels in HCT116 cells</i>	44
Fig. 13:	<i>Determination of dose responses of the selected inhibitors alone or in combination</i>	46
Fig. 14:	<i>Testing the impact of the JAK2 inhibitor Fedratinib on p-Akt levels</i>	48
Fig. 15:	<i>Dot plot analysis of cells stained with 7-AAD and EdU by flow cytometry</i>	49
Fig. 16:	<i>Quantification of the percentage of G1, S and G2/M phase cells with the 7-AAD/EdU assay</i>	50
Fig. 17:	<i>Representative pictures of the transwell migration assay</i>	51
Fig. 18:	<i>Quantification of HCT116 cell transwell migration</i>	52
Fig. 19:	<i>Spheroid outgrowth assay in collagen I gels</i>	54

APPENDIX

Tab. 1S: Results In-Cell Western assay. The table shows the entire list of results gained through ICW assay. Normalization was done by dividing the MFI of p-Akt results by the MFI of total Akt. Afterwards, the mean value of each well of the triplicates was calculated. A heatmap was used to create a better overview of the results. Red indicates low p-Akt values, which means a strong p-Akt inhibition proceeded, yellow indicates mediocre values and green indicates high values. The columns show the replicates (1, 2, 3) and their mean. Each row represents an inhibitor. The inhibitors are ordered according to mean value. Control wells can be found in a separate table.

Inhibitor number	Inhibitor name	Targets	Triplicate 1	Triplicate 2	Triplicate 3	Mean
1	GSK1059615	PI3K,mTOR	0,1669	0,1722	0,1777	0,1723
2	GDC-0941	PI3K	0,2138	0,2040	0,2027	0,2068
3	BMS-754807	IGF-1R,Trkreceptor,c-Met	0,2300	0,2172	0,1906	0,2126
4	Torin2	ATM/ATR,mTOR	0,1918	0,2544	0,2194	0,2219
5	INK128(MLN0128)	mTOR	0,1985	0,2495	0,2225	0,2235
6	MK-22062HCI	Akt	0,2779	0,2160	0,1857	0,2265
7	VS-5584(SB2343)	PI3K	0,2137	0,2463	0,2233	0,2278
8	WYE-125132(WYE-132)	mTOR	0,2049	0,2394	0,2474	0,2305
9	AZD8055	mTOR	0,2180	0,3065	0,1828	0,2358
10	BYL719	PI3K	0,2558	0,2461	0,2065	0,2361
11	AZD6482	PI3K	0,2227	0,2456	0,2404	0,2363
12	HS-173	PI3K	0,2296	0,2611	0,2234	0,2380
13	CH5132799	mTOR,PI3K	0,2256	0,2352	0,2548	0,2385
14	Triciribine	Akt	0,2469	0,2401	0,2310	0,2393
15	ETP-46464	mTOR,ATM/ATR	0,2171	0,2539	0,2488	0,2399
16	BGT226(NVP-BGT226)	PI3K,mTOR	0,2549	0,2676	0,2111	0,2446
17	PIK-75	PI3K,DNA-PK	0,2859	0,2451	0,2042	0,2451
18	GDC-0349	mTOR	0,2372	0,2993	0,2463	0,2609
19	GSK2126458(GSK458)	PI3K,mTOR	0,2876	0,2615	0,2341	0,2611
20	Foretinib(GSK1363089)	VEGFR,c-Met	0,2941	0,2565	0,2657	0,2721
21	GDC-0980(RG7422)	mTOR,PI3K	0,2743	0,2762	0,2683	0,2729
22	ZSTK474	PI3K	0,2693	0,2768	0,2761	0,2741
23	BMS-794833	VEGFR,c-Met	0,2784	0,2900	0,2681	0,2788
24	KU-0063794	mTOR	0,2590	0,3030	0,2974	0,2865
25	WYE-354	mTOR	0,2739	0,3016	0,2869	0,2875
26	AZD2014	mTOR	0,3075	0,3054	0,2859	0,2996
27	OSI-906(Linsitinib)	IGF-1R	0,3273	0,2829	0,3029	0,3044
28	Crizotinib(PF-02341066)	c-Met,ALK	0,2997	0,3144	0,3047	0,3062
29	PF-04691502	Akt,mTOR,PI3K	0,2933	0,3424	0,2836	0,3064
30	NVP-ADW742	IGF-1R	0,3247	0,2976	0,3257	0,3160
31	BMS-777607	Axl,c-Met	0,2893	0,3604	0,3039	0,3179
32	PP242	mTOR,Autophagy	0,2849	0,3894	0,2843	0,3195

33	TAE226(NVP-TAE226)	FAK	0,3458	0,3603	0,2541	0,3201
34	AT9283	JAK,AuroraKinase,Bcr-Abl	0,3292	0,3317	0,3054	0,3221
35	NVP-AEW541	IGF-1R	0,3154	0,3363	0,3288	0,3268
36	MGCD-265	Tie-2,VEGFR,c-Met	0,3395	0,3392	0,3464	0,3417
37	PI-103	PI3K,Autophagy,DNA-PK,mTOR	0,3891	0,3207	0,3293	0,3464
38	BMS-536924	IGF-1R	0,4581	0,3006	0,3002	0,3530
39	SGX-523	c-Met	0,3634	0,3477	0,3512	0,3541
40	Cabozantinib(XL184,BMS-907351)	FLT3,Tie-2,c-Kit,c-Met,VEGFR,Axl	0,3464	0,3618	0,3614	0,3565
41	A66	PI3K	0,2836	0,3523	0,4341	0,3566
42	JNJ-38877605	c-Met	0,3879	0,3544	0,3340	0,3588
43	PP121	DNA-PK,PDGFR,mTOR	0,3854	0,3864	0,3174	0,3631
44	SB202190(FHPI)	p38MAPK	0,3756	0,3589	0,3547	0,3631
45	LY2784544	JAK	0,3679	0,3590	0,3662	0,3643
46	CUDC-907	PI3K,HDAC	0,3457	0,3876	0,3762	0,3698
47	PF-04217903	c-Met	0,4213	0,3500	0,3488	0,3734
48	Golvatinib(E7050)	VEGFR,c-Met	0,3603	0,3765	0,3835	0,3734
49	AMG-458	c-Met	0,3752	0,4221	0,3373	0,3782
50	OSI-027	mTOR	0,3415	0,4523	0,3622	0,3853
51	BMS-265246	CDK	0,4483	0,3679	0,3535	0,3899
52	PHA-665752	c-Met	0,3973	0,3986	0,3877	0,3945
53	SU11274	c-Met	0,4213	0,3847	0,3777	0,3945
54	SP600125	JNK	0,3669	0,4203	0,3969	0,3947
55	NVP-BVU972	c-Met	0,3383	0,4420	0,4093	0,3965
56	PF-573228	FAK	0,4190	0,4051	0,3656	0,3966
57	AZD3463	ALK	0,4307	0,4064	0,3526	0,3966
58	VX-745	p38MAPK	0,3437	0,4090	0,4485	0,4004
59	GSK1838705A	IGF-1R,ALK	0,4361	0,3966	0,3782	0,4037
60	AZD1480	JAK	0,3668	0,4686	0,3810	0,4055
61	YM201636	PI3K	0,4273	0,4339	0,3605	0,4072
62	TWS119	GSK-3	0,4387	0,4491	0,3509	0,4129
63	ENMD-2076	AuroraKinase,FLT3,VEGFR	0,3915	0,4323	0,4153	0,4130
64	SB203580	p38MAPK	0,4462	0,3895	0,4041	0,4132
65	Telatinib	VEGFR,PDGFR,c-Kit	0,4605	0,3650	0,4169	0,4141
66	AZD7762	Chk	0,4172	0,4033	0,4223	0,4143
67	PIK-93	PI3K	0,4190	0,4112	0,4133	0,4145
68	DCC-2036(Rebastinib)	Bcr-Abl	0,3399	0,3219	0,5857	0,4158
69	Fasudil(HA-1077)HCl	ROCK,Autophagy	0,4531	0,4405	0,3565	0,4167
70	LY2228820	p38MAPK	0,3775	0,4351	0,4450	0,4192
71	PIK-293	PI3K	0,4421	0,3896	0,4269	0,4195
72	AZ960	JAK	0,4609	0,4521	0,3501	0,4210

73	TSU-68(SU6668,Orantinib)	VEGFR,PDGFR,FGFR	0,3973	0,4362	0,4300	0,4212
74	AST-1306	EGFR	0,4496	0,4296	0,3881	0,4224
75	AT7519	CDK	0,4806	0,3905	0,3964	0,4225
76	R406(freebase)	Syk	0,4493	0,4258	0,3993	0,4248
77	KW-2449	AuroraKinase,Bcr-Abl,FLT3	0,4145	0,4398	0,4241	0,4261
78	Nintedanib(BIBF1120)	VEGFR,PDGFR,FGFR	0,4143	0,4522	0,4128	0,4265
79	VX-680(Tozasertib,MK-0457)	AuroraKinase	0,4586	0,4150	0,4117	0,4284
80	Ruxolitinib(INCB018424)	JAK	0,4227	0,4287	0,4359	0,4291
81	AC480(BMS-599626)	HER2,EGFR	0,3996	0,4802	0,4144	0,4314
82	Roscovitine(Seliciclib,CYC202)	CDK	0,4401	0,4133	0,4421	0,4318
83	BX-795	IκB/IKK,PDK-1	0,4024	0,4613	0,4319	0,4319
84	GSK2334470	PDK-1	0,4343	0,4597	0,4029	0,4323
85	Lapatinib(GW-572016)Ditosylate	HER2,EGFR	0,4209	0,3881	0,4913	0,4334
86	CYC116	AuroraKinase,VEGFR	0,4613	0,4143	0,4353	0,4370
87	BS-181HCI	CDK	0,4213	0,4576	0,4372	0,4387
88	CO-1686(AVL-301)	EGFR	0,4114	0,4877	0,4183	0,4392
89	BIX02189	MEK	0,4405	0,4650	0,4128	0,4394
90	AZD8330	MEK	0,3601	0,5123	0,4471	0,4398
91	KU-60019	ATM/ATR	0,4165	0,4586	0,4461	0,4404
92	CYT387	JAK	0,4556	0,4940	0,3743	0,4413
93	GSK461364	PLK	0,4554	0,4224	0,4506	0,4428
94	PD173074	VEGFR,FGFR	0,4208	0,4835	0,4270	0,4438
95	Rigosertib(ON-01910)	PLK	0,4421	0,4375	0,4548	0,4448
96	Genistein	Topoisomerase,EGFR	0,4055	0,4797	0,4495	0,4449
97	PHT-427	PDK-1,Akt	0,4625	0,4702	0,4113	0,4480
98	BIX02188	MEK	0,4274	0,4534	0,4634	0,4481
99	SGI-1776freebase	Pim	0,4533	0,4391	0,4524	0,4483
100	TG101348(SAR302503)	JAK	0,4421	0,4694	0,4334	0,4483
101	AS-604850	PI3K	0,4089	0,4823	0,4548	0,4486
102	AP26113	ALK	0,4674	0,4434	0,4368	0,4492
103	Vemurafenib(PLX4032,RG7204)	Raf	0,4239	0,4826	0,4413	0,4493
104	WAY-600	mTOR	0,4543	0,4169	0,4775	0,4496
105	Ki8751	PDGFR,c-Kit,VEGFR	0,4323	0,4770	0,4395	0,4496
106	KU-55933(ATMKinaseInhibitor)	ATM/ATR	0,4216	0,5008	0,4270	0,4498
107	KRN633	PDGFR,VEGFR	0,4383	0,4799	0,4373	0,4518
108	Acadesine	AMPK	0,4871	0,4574	0,4120	0,4522
109	BX-912	PDK-1	0,4043	0,4948	0,4591	0,4527
110	Cabozantinimalate(XL184)	VEGFR	0,4187	0,4873	0,4525	0,4528
111	CCT129202	AuroraKinase	0,4485	0,4515	0,4598	0,4533
112	TG100-115	PI3K	0,4701	0,4284	0,4622	0,4536

113	MLN8054	AuroraKinase	0,4474	0,4765	0,4394	0,4544
114	OSI-930	c-Kit,CSF-1R,VEGFR	0,4285	0,4975	0,4399	0,4553
115	Pimasertib(AS-703026)	MEK	0,4199	0,4751	0,4713	0,4555
116	Hesperadin	AuroraKinase	0,4859	0,4880	0,3927	0,4555
117	Afatinib(BIBW2992)	EGFR,HER2	0,4548	0,4575	0,4557	0,4560
118	BI2536	PLK	0,4606	0,4649	0,4443	0,4566
119	JNJ-7706621	CDK,AuroraKinase	0,3980	0,4958	0,4761	0,4566
120	Tie2kinaseinhibitor	Tie-2	0,4290	0,5138	0,4280	0,4569
121	Lenvatinib(E7080)	VEGFR	0,4789	0,4701	0,4235	0,4575
122	SNS-032(BMS-387032)	CDK	0,4502	0,4609	0,4622	0,4578
123	Degrasyn(WP1130)	DUB,Bcr-Abl	0,5159	0,3104	0,5473	0,4578
124	AZD8931(Sapitinib)	HER2,EGFR	0,4546	0,4580	0,4626	0,4584
125	BrivanibAlaninate(BMS-582664)	VEGFR,FGFR	0,4696	0,5025	0,4053	0,4591
126	Quizartinib(AC220)	FLT3	0,4838	0,4480	0,4530	0,4616
127	PazopanibHCl(GW786034HCl)	VEGFR,PDGFR,c-Kit	0,4579	0,4826	0,4450	0,4618
128	TAK-901	AuroraKinase	0,4692	0,4630	0,4549	0,4624
129	R406	Syk,FLT3	0,4378	0,5014	0,4485	0,4626
130	AuroraAlnhibitorI	AuroraKinase	0,4228	0,5063	0,4610	0,4634
131	WZ3146	EGFR	0,4885	0,4520	0,4517	0,4640
132	Brivanib(BMS-540215)	FGFR,VEGFR	0,5077	0,4369	0,4489	0,4645
133	LY294002	Autophagy,PI3K	0,4895	0,4658	0,4421	0,4658
134	WZ8040	EGFR	0,5127	0,4508	0,4339	0,4658
135	Apatinib	VEGFR	0,4651	0,4591	0,4762	0,4668
136	PIK-294	PI3K	0,4621	0,5037	0,4350	0,4670
137	Linifanib(ABT-869)	CSF-1R,PDGFR,VEGFR	0,5000	0,4614	0,4473	0,4696
138	AEE788(NVP-AEE788)	HER2,VEGFR,EGFR	0,4063	0,5313	0,4732	0,4703
139	Dasatinib	Bcr-Abl,c-Kit,Src	0,4950	0,5017	0,4158	0,4708
140	CAL-101(Idelalisib,GS-1101)	PI3K	0,5001	0,4840	0,4287	0,4709
141	Mubritinib(TAK165)	HER2	0,4682	0,5298	0,4186	0,4722
142	Gefitinib(ZD1839)	EGFR	0,5034	0,4797	0,4360	0,4730
143	PH-797804	p38MAPK	0,4532	0,4776	0,4901	0,4737
144	PD98059	MEK	0,4939	0,4612	0,4662	0,4738
145	GSK429286A	ROCK	0,4514	0,4814	0,4893	0,4740
146	PD318088	MEK	0,4777	0,4814	0,4632	0,4741
147	OSI-420	EGFR	0,5015	0,4765	0,4466	0,4749
148	Semaxanib(SU5416)	VEGFR	0,4478	0,4595	0,5212	0,4762
149	Vandetanib(ZD6474)	VEGFR	0,4680	0,5086	0,4544	0,4770
150	Vatalanib(PTK787)2HCl	c-Kit,VEGFR	0,4872	0,5012	0,4462	0,4782
151	SNS-314Mesylate	AuroraKinase	0,5133	0,4628	0,4599	0,4787
152	PHA-793887	CDK	0,4588	0,5220	0,4571	0,4793
153	PHA-680632	AuroraKinase	0,4804	0,4969	0,4620	0,4798

154	Refametinib(RDEA119,Bay86-9766)	MEK	0,4743	0,4825	0,4826	0,4798
155	BIRB796(Doramapimod)	p38MAPK	0,4350	0,5658	0,4393	0,4800
156	HMN-214	PLK	0,4689	0,5075	0,4642	0,4802
157	MotesanibDiphosphate(AMG-706)	VEGFR,PDGFR,c-Kit	0,5112	0,4561	0,4756	0,4810
158	Thiazovivin	ROCK	0,4276	0,5191	0,4980	0,4816
159	PD184352(CI-1040)	MEK	0,4880	0,5175	0,4413	0,4823
160	PF-4708671	S6Kinase	0,4549	0,5300	0,4622	0,4824
161	Ponatinib(AP24534)	PDGFR,FGFR,VEGFR,Bcr-Abl	0,4896	0,4835	0,4782	0,4838
162	SL-327	MEK	0,4817	0,5037	0,4686	0,4847
163	Regorafenib(BAY73-4506)	c-RET,VEGFR	0,5062	0,4833	0,4669	0,4855
164	TG101209	JAK,FLT3,c-RET	0,4724	0,4982	0,4873	0,4860
165	CNX-2006	EGFR	0,4979	0,5420	0,4229	0,4876
166	PHA-767491	CDK	0,4769	0,5152	0,4765	0,4895
167	WZ4002	EGFR	0,4764	0,4725	0,5207	0,4899
168	SorafenibTosylate	PDGFR,Raf,VEGFR	0,4998	0,5317	0,4398	0,4904
169	PLX-4720	Raf	0,4811	0,5075	0,4827	0,4904
170	Wortmannin	Autophagy,ATM/ATR,PI3K	0,4001	0,5368	0,5416	0,4929
171	ZM336372	Raf	0,4402	0,5176	0,5212	0,4930
172	Palbociclib(PD-0332991)HCl	CDK	0,5055	0,4998	0,4754	0,4936
173	SAR245409(XL765)	PI3K,mTOR	0,4889	0,4967	0,4989	0,4948
174	AZD4547	FGFR	0,4803	0,5045	0,5019	0,4956
175	Barasertib(AZD1152-HQPA)	AuroraKinase	0,4972	0,4934	0,4963	0,4956
176	Quercetin	PKC,Src,PI3K,Sirtuin	0,4065	0,5644	0,5166	0,4958
177	SB590885	Raf	0,5134	0,4955	0,4804	0,4964
178	AG-1478(TyrphostinAG-1478)	EGFR	0,4721	0,4747	0,5500	0,4989
179	Tandutinib(MLN518)	FLT3	0,4693	0,5150	0,5153	0,4999
180	IPI-145(INK1197)	PI3K	0,5354	0,5140	0,4514	0,5003
181	WP1066	JAK	0,5535	0,4745	0,4731	0,5003
182	Saracatinib(AZD0530)	Src,Bcr-Abl	0,5099	0,4511	0,5418	0,5009
183	ErlotinibHCl(OSI-744)	Autophagy,EGFR	0,5087	0,5202	0,4768	0,5019
184	Dacomitinib(PF299804,PF299)	EGFR	0,4742	0,5026	0,5314	0,5027
185	KX2-391	Src	0,5003	0,4985	0,5097	0,5029
186	PD0325901	MEK	0,5104	0,4710	0,5283	0,5032
187	Danuserib(PHA-739358)	c-RET,FGFR,Bcr-Abl,AuroraKinase	0,4992	0,4575	0,5565	0,5044
188	Selumetinib(AZD6244)	MEK	0,4592	0,5312	0,5245	0,5050
189	Alisertib(MLN8237)	AuroraKinase	0,4805	0,5339	0,5007	0,5050
190	SB216763	GSK-3	0,5515	0,5012	0,4628	0,5052
191	Pelitinib(EKB-569)	EGFR	0,4605	0,5462	0,5099	0,5055
192	TPCA-1	IκB/IKK	0,5071	0,5102	0,4999	0,5057

193	TGX-221	PI3K	0,5263	0,4919	0,4991	0,5058
194	NU7441(KU-57788)	DNA-PK,PI3K	0,4734	0,5197	0,5281	0,5071
195	AG-490(TyrphostinB42)	JAK,EGFR	0,4869	0,5157	0,5221	0,5083
196	SunitinibMalate	VEGFR,PDGFR,c-Kit	0,5113	0,5407	0,4730	0,5084
197	3-Methyladenine	Autophagy,PI3K	0,5319	0,4952	0,4987	0,5086
198	U0126-EtOH	MEK	0,4873	0,5322	0,5065	0,5087
199	TAK-285	EGFR,HER2	0,4430	0,5281	0,5569	0,5093
200	ZM447439	AuroraKinase	0,4865	0,5347	0,5073	0,5095
201	XL147	PI3K	0,5028	0,5261	0,5007	0,5099
202	Y-276322HCl	Autophagy,ROCK	0,5084	0,5076	0,5137	0,5099
203	GDC-0879	Raf	0,5182	0,5075	0,5046	0,5101
204	Dinaciclib(SCH727965)	CDK	0,5016	0,5150	0,5158	0,5108
205	CP-673451	PDGFR	0,4356	0,5546	0,5422	0,5108
206	CAY10505	PI3K	0,4624	0,5641	0,5071	0,5112
207	CP-724714	EGFR,HER2	0,5968	0,4936	0,4434	0,5113
208	AS-252424	PI3K	0,5205	0,5248	0,4897	0,5116
209	FlavopiridolHCl	CDK	0,4632	0,5366	0,5353	0,5117
210	AZ20	ATM/ATR	0,5168	0,5405	0,4802	0,5125
211	H892HCl	PKA	0,5407	0,5172	0,4815	0,5131
212	BI-D1870	S6Kinase	0,4884	0,5451	0,5073	0,5136
213	Tivozanib(AV-951)	VEGFR,PDGFR,c-Kit	0,4999	0,5076	0,5342	0,5139
214	Volasertib(BI6727)	PLK	0,5351	0,4892	0,5198	0,5147
215	Cediranib(AZD2171)	VEGFR	0,6348	0,4522	0,4576	0,5149
216	Ro3280	PLK	0,4507	0,5660	0,5282	0,5150
217	Amuvatinib(MP-470)	FLT3,c-RET,PDGFR,c-Kit	0,5140	0,5201	0,5200	0,5180
218	GSK1904529A	IGF-1R	0,5420	0,5489	0,4647	0,5185
219	PF-00562271	FAK	0,5520	0,5132	0,4910	0,5187
220	Tofacitinib(CP-690550,Tasocitinib)	JAK	0,4732	0,5304	0,5532	0,5189
221	ImatinibMesylate(STI571)	c-Kit,Bcr-Abl,PDGFR	0,5289	0,5043	0,5263	0,5198
222	OSU-03012(AR-12)	PDK-1	0,5611	0,5211	0,4785	0,5202
223	NVP-BSK8052HCl	JAK	0,5667	0,4498	0,5482	0,5216
224	SB415286	GSK-3	0,5206	0,5082	0,5421	0,5237
225	ChrysophanicAcid	mTOR,EGFR	0,5638	0,5176	0,4937	0,5250
226	MK-2461	c-Met,PDGFR,FGFR	0,5235	0,5127	0,5405	0,5256
227	A-769662	AMPK	0,5302	0,4919	0,5588	0,5270
228	Pacritinib(SB1518)	JAK	0,5230	0,5210	0,5370	0,5270
229	RAF265(CHIR-265)	VEGFR,Raf	0,5107	0,5654	0,5058	0,5273
230	Honokiol	MEK,Akt	0,4206	0,5886	0,5731	0,5274
231	Crenolanib(CP-868596)	PDGFR	0,5397	0,5339	0,5123	0,5286
232	AG-1024	IGF-1R	0,5075	0,5535	0,5294	0,5301
233	ZM306416	VEGFR	0,5398	0,5433	0,5156	0,5329

234	CUDC-101	HDAC,HER2,EGFR	0,5245	0,5620	0,5133	0,5333
235	Masitinib(AB1010)	PDGFR,c-Kit	0,5326	0,5638	0,5077	0,5347
236	Trametinib(GSK1120212)	MEK	0,5133	0,5375	0,5615	0,5374
237	Dovitinib(TKI-258,CHIR-258)	FGFR,FLT3,c-Kit,VEGFR,PDGFR	0,5602	0,5325	0,5202	0,5377
238	Fostamatinib(R788)	Syk	0,5782	0,5311	0,5136	0,5410
239	Ridaforolimus(Deforolimus,MK-8669)	mTOR	0,5509	0,5683	0,5099	0,5430
240	PF-562271	FAK	0,5697	0,5582	0,5022	0,5434
241	BKM120(NVP-BKM120,Buparlisib)	PI3K	0,5256	0,5389	0,5667	0,5437
242	GSK650394	Others	0,5330	0,5666	0,5384	0,5460
243	Indirubin	GSK-3	0,4828	0,5953	0,5605	0,5462
244	CCT137690	AuroraKinase	0,5902	0,5688	0,4821	0,5470
245	Nilotinib(AMN-107)	Bcr-Abl	0,5361	0,5412	0,5703	0,5492
246	NU6027	CDK	0,5597	0,5985	0,4900	0,5494
247	AsiaticAcid	p38MAPK	0,5569	0,5689	0,5232	0,5496
248	NVP-BHG712	Raf,Src,Bcr-Abl,VEGFR,Ephrinreceptor	0,6007	0,5265	0,5225	0,5499
249	LDC000067	CDK	0,5215	0,5774	0,5527	0,5505
250	Varlitinib	EGFR	0,5428	0,5565	0,5572	0,5521
251	Bosutinib(SKI-606)	Src	0,5852	0,4875	0,5865	0,5531
252	PhenforminHCl	AMPK	0,5256	0,5809	0,5583	0,5549
253	Everolimus(RAD001)	mTOR	0,5579	0,5613	0,5475	0,5556
254	SSR128129E	FGFR	0,5060	0,6217	0,5400	0,5559
255	RKI-1447	ROCK	0,5974	0,5258	0,5461	0,5564
256	SAR131675	VEGFR	0,5370	0,5828	0,5499	0,5566
257	HER2-Inhibitor-1	HER2,EGFR	0,5976	0,5386	0,5336	0,5566
258	LY2835219	CDK	0,5503	0,6094	0,5114	0,5570
259	Losmapimod(GW856553X)	p38MAPK	0,5588	0,5710	0,5429	0,5576
260	PRT062607(P505-15,BIB057)HCl	Syk	0,5545	0,5574	0,5669	0,5596
261	LY2603618	Chk	0,5771	0,5477	0,5566	0,5605
262	Temsirolimus(CCI-779,NSC683864)	mTOR	0,5620	0,5937	0,5257	0,5605
263	TAK-733	MEK	0,5700	0,5621	0,5567	0,5629
264	PP1	Src	0,5230	0,6229	0,5434	0,5631
265	AZ628	Raf	0,5461	0,6169	0,5304	0,5645
266	Imatinib(STI571)	PDGFR	0,5431	0,5313	0,6234	0,5660
267	AZD5438	CDK	0,5204	0,5943	0,5851	0,5666
268	TyrphostinAG879	HER2	0,5347	0,5774	0,5923	0,5681
269	AZD1208	Pim	0,5712	0,6278	0,5138	0,5709
270	VE-822	ATM/ATR	0,5239	0,6187	0,5713	0,5713
271	WHI-P154	JAK,EGFR	0,5669	0,5585	0,5890	0,5715
272	TAK-715	p38MAPK	0,5913	0,5764	0,5506	0,5728

273	LDK378	ALK	0,6148	0,5629	0,5418	0,5732
274	PD173955	BCR-ABL	0,4978	0,6598	0,5637	0,5737
275	AVL-292	BTK	0,5663	0,6098	0,5459	0,5740
276	EHT1864	Rho	0,5508	0,5823	0,5902	0,5744
277	VX-702	p38MAPK	0,5981	0,5959	0,5421	0,5787
278	K-Ras(G12C)inhibitor9	Rho	0,5517	0,6154	0,5721	0,5797
279	Palomid529(P529)	mTOR	0,5324	0,6111	0,5966	0,5801
280	Sotrastaurin	PKC	0,5680	0,6134	0,5607	0,5807
281	JNKInhibitorIX	JNK	0,5892	0,6074	0,5462	0,5810
282	Ibrutinib(PCI-32765)	BTK	0,5248	0,5924	0,6257	0,5810
283	Skepinone-L	p38MAPK	0,5755	0,6158	0,5516	0,5810
284	XL019	JAK	0,5829	0,5866	0,5774	0,5823
285	Enzastaurin(LY317615)	PKC	0,6205	0,5732	0,5550	0,5829
286	PD168393	EGFR	0,5966	0,6092	0,5431	0,5829
287	Milciclib(PHA-848125)	CDK	0,5755	0,5852	0,5906	0,5838
288	R547	CDK	0,5911	0,5777	0,5836	0,5841
289	Dabrafenib(GSK2118436)	Raf	0,5602	0,6230	0,5714	0,5849
290	PP2	Src	0,5823	0,6069	0,5711	0,5868
291	GNE-9605	LRRK2	0,5374	0,6388	0,5862	0,5875
292	GSK2636771	PI3K	0,6010	0,6227	0,5411	0,5883
293	JNK-IN-8	JNK	0,6020	0,6215	0,5545	0,5927
294	TIC10	Akt	0,5413	0,6642	0,5728	0,5928
295	Axitinib	c-Kit,VEGFR,PDGFR	0,6019	0,5927	0,5851	0,5932
296	Piceatannol	Syk	0,6011	0,5785	0,6018	0,5938
297	Rapamycin(Sirolimus)	Autophagy,mTOR	0,6113	0,5746	0,5998	0,5952
298	MK-5108(VX-689)	AuroraKinase	0,5818	0,6234	0,5823	0,5958
299	6H05	Rho	0,5888	0,6210	0,5779	0,5959
300	IKK-16(IKKInhibitorVII)	IkB/IKK	0,6152	0,6007	0,5725	0,5961
301	AR-A014418	GSK-3	0,5995	0,6244	0,5727	0,5989
302	IPA-3	PAK	0,6012	0,6286	0,5682	0,5993
303	MK-8745	AuroraKinase	0,5611	0,6412	0,5988	0,6004
304	CEP-33779	JAK	0,5454	0,6192	0,6408	0,6018
305	PF-543	S1PRReceptor	0,5778	0,6218	0,6061	0,6019
306	CGK733	ATM/ATR	0,6167	0,6130	0,5767	0,6021
307	Filgotinib(GLPG0634)	JAK	0,6020	0,6424	0,5639	0,6028
308	GW5074	Raf	0,5824	0,6142	0,6166	0,6044
309	SC-514	IkB/IKK	0,6107	0,6157	0,5898	0,6054
310	SKIII	S1PRReceptor	0,6239	0,6077	0,5911	0,6076
311	GNF-5	Bcr-Abl	0,5880	0,6279	0,6083	0,6081
312	GNE-0877	LRRK2	0,6001	0,6180	0,6087	0,6089
313	IM-12	GSK-3	0,5999	0,6349	0,5943	0,6097

314	AZD9291	EGFR	0,5838	0,6576	0,5886	0,6100
315	ZCL278	Rac	0,5953	0,6182	0,6183	0,6106
316	S-Ruxolitinib(INCB018424)	JAK	0,6467	0,5994	0,5861	0,6107
317	10058-F4	c-Myc	0,5947	0,6488	0,5888	0,6108
318	Pazopanib	PDGFR,c-Kit,VEGFR	0,6024	0,6146	0,6169	0,6113
319	Tofacitinib(CP-690550)Citrate	JAK	0,5944	0,6476	0,5920	0,6114
320	CX-6258HCl	Pim	0,6059	0,6103	0,6246	0,6136
321	WZ4003	AMPK	0,5752	0,6427	0,6281	0,6154
322	Icotinib	EGFR	0,6215	0,6226	0,6034	0,6158
323	ZM323881HCl	VEGFR	0,6386	0,6049	0,6041	0,6159
324	AZD1080	GSK-3	0,6318	0,6301	0,5896	0,6172
325	BAY11-7082	I κ B/IKK,E2conjugating	0,6275	0,6401	0,5951	0,6209
326	CZC24832	PI3K	0,6051	0,6677	0,5921	0,6216
327	PFK15	Others	0,5749	0,7017	0,5929	0,6232
328	GNF-2	Bcr-Abl	0,6004	0,6462	0,6247	0,6237
329	Sorafenib	Raf	0,6239	0,6435	0,6041	0,6238
330	AMG-900	AuroraKinase	0,5905	0,6356	0,6477	0,6246
331	PF-3758309	PAK	0,5860	0,6390	0,6530	0,6260
332	P276-00	CDK	0,6736	0,5497	0,6560	0,6265
333	TG003	CDK	0,6340	0,6597	0,5863	0,6267
334	Fingolimod(FTY720)HCl	S1PReceptor	0,6100	0,6620	0,6097	0,6272
335	KN-93Phosphate	Others	0,6347	0,6261	0,6215	0,6274
336	Dovitinib(TKI-258)DilacticAcid	PDGFR,FGFR,c-Kit,FLT3,VEGFR	0,6038	0,6117	0,6688	0,6281
337	TAK-632	Raf	0,6522	0,6415	0,6052	0,6330
338	CGI1746	BTK	0,6450	0,6150	0,6396	0,6332
339	TCS359	FLT3	0,6433	0,6014	0,6596	0,6348
340	BIO	GSK-3	0,6372	0,6514	0,6159	0,6348
341	CHIR-99021(CT99021)HCl	GSK-3	0,6029	0,6760	0,6299	0,6363
342	EHop-016	Rac	0,6318	0,6832	0,5987	0,6379
343	GNE-7915	LRRK2	0,6308	0,6094	0,6823	0,6409
344	TG100713	PI3K	0,5784	0,6972	0,6629	0,6462
345	BMS-345541	I κ B/IKK	0,6247	0,6583	0,6573	0,6467
346	MEK162(ARRY-162,ARRY-438162)	MEK	0,6472	0,6707	0,6320	0,6500
347	PQ401	IGF-1R	0,6885	0,6782	0,5847	0,6505
348	MK-8776(SCH900776)	CDK,Chk	0,6344	0,6397	0,6788	0,6509
349	CHIR-124	Chk	0,6885	0,5988	0,6773	0,6548
350	NMS-P937(NMS1286937)	PLK	0,6622	0,6596	0,6436	0,6551
351	Butein	EGFR	0,6581	0,6556	0,6527	0,6555
352	VE-821	ATM/ATR	0,6437	0,6671	0,6589	0,6566
353	AG-18	EGFR	0,6330	0,6818	0,6614	0,6587

354	CNX-774	BTK	0,6500	0,6948	0,6377	0,6608
355	TyrphostinAG1296	FGFR,c-Kit,PDGFR	0,6873	0,6359	0,6615	0,6616
356	KN-62	Others	0,6850	0,6804	0,6531	0,6728
357	ZM39923HCl	JAK	0,6567	0,6637	0,6993	0,6732
358	AT7867	S6Kinase,Akt	0,6707	0,7118	0,6438	0,6754
359	WH-4-023	Src	0,6781	0,6934	0,6596	0,6770
360	GZD824	Bcr-Abl	0,6632	0,6982	0,6747	0,6787
361	AZD2858	GSK-3	0,6864	0,6943	0,6570	0,6793
362	SMI-4a	Pim	0,6790	0,6636	0,7022	0,6816
363	GF109203X	PKC	0,6631	0,7081	0,6863	0,6858
364	NSC23766	Rac	0,6534	0,6811	0,7332	0,6892
365	PF-477736	Chk	0,7024	0,6808	0,6961	0,6931
366	Go6983	PKC	0,7112	0,7126	0,6810	0,7016
367	Zotanolimus(ABT-578)	mTOR	0,7079	0,7243	0,6788	0,7037
368	XMD8-92	ERK	0,7882	0,6693	0,6543	0,7039
369	IMD0354	IkB/IKK	0,7038	0,6764	0,7484	0,7095
370	CEP-32496	CSF-1R,Raf	0,6867	0,7153	0,7337	0,7119
371	Ro31-8220Mesylate	PKC	0,6894	0,7790	0,7018	0,7234
372	BardoxoloneMethyl	IkB/IKK	0,7378	0,6857	0,7792	0,7342
373	GSK690693	Akt	0,7433	0,7590	0,7131	0,7385
374	A-674563	PKA,CDK,Akt	0,7793	0,7744	0,7409	0,7649
375	Tyrphostin9	EGFR	0,8142	0,7746	0,7724	0,7870
376	CCT128930	Akt	0,8060	0,9652	0,9735	0,9149
377	GDC-0068	Akt	0,8727	0,9820	1,0378	0,9641
378	AZD5363	Akt	1,0127	1,1239	1,1738	1,1035

Controls:

Condition	Triplicate 1	Triplicate 2	Triplicate 3	Mean
Starved	0,3408	0,2631	0,2257	0,2765
Starved	0,1955	0,2645	0,2376	0,2325
Starved	0,2450	0,3191	0,2579	0,2740
Starved	0,2545	0,3200	0,2196	0,2647
Starved	0,3262	0,3316	0,2661	0,3080
Starved	0,3002	0,3138	0,2338	0,2826
Starved	0,2893	0,3389	0,3011	0,3098
Starved	0,3262	0,3302	0,2708	0,3091
Starved	0,4061	0,3147	0,2923	0,3377
Starved	0,2701	0,3285	0,2821	0,2935

+ CAF-CM	0,5200	0,4776	0,4887	0,4954
+ CAF-CM	0,5003	0,4864	0,4867	0,4912
+ CAF-CM	0,4382	0,4730	0,4432	0,4515
+ CAF-CM	0,4652	0,4711	0,4304	0,4556
+ CAF-CM	0,5728	0,5238	0,5248	0,5404
+ CAF-CM	0,4423	0,5220	0,5396	0,5013
+ CAF-CM	0,4361	0,5108	0,5910	0,5126
+ CAF-CM	0,5721	0,5837	0,5922	0,5827
+ CAF-CM	0,6224	0,6269	0,6485	0,6326
+ CAF-CM	0,6107	0,6102	0,6428	0,6212
+ 1 μ M MK-2206	0,2741	0,2376	0,2554	0,2557
+ 1 μ M MK-2206	0,2535	0,2285	0,2536	0,2452
+ 1 μ M MK-2206	0,2777	0,3037	0,2666	0,2827
+ 1 μ M MK-2206	0,3102	0,2956	0,2638	0,2899
+ 1 μ M MK-2206	0,3500	0,3216	0,2916	0,3211
+ 1 μ M MK-2206	0,3570	0,3260	0,2872	0,3234
+ 1 μ M MK-2206	0,3397	0,3123	0,2656	0,3059
+ 1 μ M MK-2206	0,3359	0,3014	0,2640	0,3004
+ 1 μ M MK-2206	0,2262	0,2661	0,2541	0,2488
+ 1 μ M MK-2206	0,2540	0,2837	0,2760	0,2712

Buffers and Solutions

Cell culture:

0.25 % Trypsin-EDTA for 250 ml:

- 245 ml 1xPBS
- 1 g Trypsin (2.2 U/mg)
- 5 ml NaEDTA 1 % pH 7,4

Methylcellulose for spheroids for 1 l:

- 15 g Methylcellulose
- 500 ml DMEM
- 500 ml DMEM containing 10 ml L-glutamin

In-Cell Western:**Blocking buffer:**

- 1xPBS
- 1 % BSA

Tween washing solution:

- 1xPBS
- 0.1 % Tween-20

Near-infrared Western blot:**Lysis buffer:**

- RIPA buffer
 - dH₂O
 - 50 mM Tris base
 - 150 mM Sodium chloride
 - 1 % Triton X-100
 - 0.1 % Sodium dodecyl sulfate
 - 0.5 % Sodium deoxycolate
- 1 % Phenylmethylsulfonyl fluoride 100mM
- 2 % Protease inhibitor mix
 - 200 µg/ml Leupeptin
 - 200 µg/ml Aprotinin
 - 30 µg/ml Benzamidin hydrochloride
 - 1,000 µg/ml Trypsin inhibitor

10 % Running gel for 12 ml:

- 5 ml dH₂O
- 4 ml Acrylamide 30 %
- 3 ml Buffer B (pH 8.8)
 - 1.5 M Tris base
 - 0.4 % Sodium dodecyl sulfate

- dH₂O
- HCl for pH adjustment
- 120 µl Amoniumpersulfate 10 %
- 10 µl Tetramethylethylenediamin

5 % Stack gel for 3 ml:

- 0.5 ml Acryl amide
- 0.75 ml Buffer c (pH 6.8)
 - 0.5 M Tris base
 - 0.4 % Sodium dodecyl sulfate
 - dH₂O
 - HCl for pH adjustment
- 1.75 ml dH₂O
- 30 µl Amoniumpersulfate 10 %
- 2.5 µl Tetramethylethylenediamin

Sample loading buffer:

- dH₂O
- 200 mM Tris base pH 6.8
- 400 mM Dithiothreitol
- 8 % Sodium dodecyl sulfate
- 0.4 % Bromphenol blue
- 40 % Glycerol

Electrophoresis buffer for 2 l:

- 1,990 ml dH₂O
- 100 ml Sodium dodecyl sulfate 20 %
- 60.6 g Tris base
- 292 g Glycine

Harlow buffer for 5 l:

- 4 l H₂O
- 1 l Methanol
- 25 ml Sodium dodecyl sulfate 20 %

- 145 g Glycine
- 29 g Tris base

7AAD/EdU assay:

FACS buffer:

- 1xPBS
- 1 % BSA

List of reagents

Product name	Company	Article No.
Bromphenol blue	Sigma-Aldrich, St. Louis, MO, USA	B0126
2-Propanol (Isopropanol)	Carl Roth, Karlsruhe, Germany	6.752
10xDPBS	Lonza Group AG, Basel, Swiss	BE17-515F
Acrylamide/Bis-acrylamide, 30%	Sigma-Aldrich, St. Louis, MO, USA	A3699-100ml
Akt pan (40D0) mouse monoclonal antibody	Cell Signaling Technology, Danvers, MA, USA	2920
Amonium persulfate	Sigma-Aldrich, St. Louis, MO, USA	A3678
Aprotinin	Sigma-Aldrich, St. Louis, MO, USA	A1153
Benzamidine hydrochloride	Sigma-Aldrich, St. Louis, MO, USA	63226
Bradford reagent, Protein Assay Dye Reagent Concentrate	Bio-Rad Laboratoies, Inc., Hercules, CA, USA	500-0006
BSA, Albumin Fraction V	AppliChem GmbH, Darmstadt, Germany	A1391,0100
Collagen I, Rat Tail, 100mG	Corning Incorporated, Corning, NY, USA	354236
DAPI	Thermo Fisher Scientific™, Waltham, MA, USA	D1308
Dithiothreitol	Bio-Rad Laboratoies, Inc., Hercules, CA, USA	161-0611
DMEM	Thermo Fisher Scientific™, Waltham, MA, USA	21969035
DMSO	Sigma-Aldrich, St. Louis, MO, USA	D5879-M
DPBS	Thermo Fisher Scientific™, Waltham, MA, USA	14190-094
Endothelial Cell Growth Medium MV2	PromoCell GmbH, Heidelberg, Germany	C-22022
Ethanol 70%	VWR International, Radnor, PA, USA	85.825.360
Ethylenediaminetetraacetic acid disodium salt solution (EDTA)	Sigma-Aldrich, St. Louis, MO, USA	E7889
Fetal calv serum	Thermo Fisher Scientific™, Waltham, MA, USA	10500-056

GAPDH rabbit polyclonal antibody	Trevigen®, Gaithersburg, MD, USA	2275-PC-100
Glycerol	Sigma-Aldrich, St. Louis, MO, USA	G5516
Glycine	VWR International, Radnor, PA, USA	444495D
Hydrochlorid acid 37%	Carl Roth, Karlsruhe, Germany	9.277
IRDye® 680 RD goat anti-mouse IgG (H+L)	LI-COR Biosciences, Lincoln, NE, USA	629-68070
IRDye® 800 CW goat anti-rabbit IgG (H+L)	LI-COR Biosciences, Lincoln, NE, USA	926-32211
Kinase Inhibitor Library (378 inhibitors)	Selleckchem, Houston, TX, USA	L1200
L-Glutamine (200mM)	Thermo Fisher Scientific™, Waltham, MA, USA	25030081
Leupeptin	Sigma-Aldrich, St. Louis, MO, USA	L2023
Methanol ≥99,8%	VWR International, Radnor, PA, USA	20.847.307
Methylcellulose	Sigma-Aldrich, St. Louis, MO, USA	M0512
MK-2206	Selleckchem, Houston, TX, USA	S1078
Mouse IgG1	Santa Cruz Biotechnology, Dallas, TX, USA	sc-3877
Sodium chloride	VWR International, Radnor, PA, USA	443827W
Odyssey® Blocking Buffer (TBS)	LI-COR Biosciences, Lincoln, NE, USA	927-50000
OSI-906	Selleckchem, Houston, TX, USA	S1091
PageRuler™ Prestained Protein Ladder, 10 to 180 kDa	Thermo Fisher Scientific™, Waltham, MA, USA	26616
Phenylmethylsulfonyl fluoride	Sigma-Aldrich, St. Louis, MO, USA	P7626
Phospho-Akt (Ser473) (D9E) XP® rabbit monoclonal antibody	Cell Signaling Technology, Danvers, MA, USA	4060
Phospho-IGF-I Receptor beta (Tyr1135/1136)/Insulin Receptor beta (Tyr1150/1151) (19H7) rabbit monoclonal antibody	Cell Signaling Technology, Danvers, MA, USA	3024
Phospho-Met (Tyr1234/123d) (D26) XP® rabbit monoclonal antibody	Cell Signaling Technology, Danvers, MA, USA	3077
Phospho-STAT3 (Tyr705) (D3A7) XP® rabbit mAb	Cell Signaling Technology, Danvers, MA, USA	9145
Ponceau S	Sigma-Aldrich, St. Louis, MO, USA	P3504
Rabbit IgG	Santa Cruz Biotechnology, Dallas, TX, USA	sc-3888
Recombinant human IGF-2 (rhIGF-2)	PeproTech Austria, Vienna, Austria	100-12
Roti®-Histofix	Carl Roth, Karlsruhe, Germany	P087.5
Sodium deoxycolate	Sigma-Aldrich, St. Louis, MO, USA	30970-25G
Sodium dodecyl sulfate	Sigma-Aldrich, St. Louis, MO, USA	L3771-500G
STAT-3 mouse antibody, clone 84/Stat3 (RUO)	BD Bioscience, Franklin Lakes, NJ, USA	610189
Tetramethylethylenediamin (Temed)	Merck, Darmstadt, Germany	1.10732.0100

Tris base, Trizma® base	Sigma-Aldrich, St. Louis, MO, USA	T1503-1KG
Triton X-100	Sigma-Aldrich, St. Louis, MO, USA	X100-500ML
Trypsin 1:250 from bovine pancreas	Serva Electrophoresis GmbH, Heidelberg, Germany	37289.02
Tween® 20 Biochemica	AppliChem GmbH, Darmstadt, Germany	A1389,1000